

https://dspace.org/

# Non-oxidative conversion of methane into aromatic hydrocarbons over molybdenum modified H-ZSM-5 zeolite catalysts

**Tshabalala, Themba Emmanuel**

**2014-07-02**
http://hdl.handle.net10539/14856

Downloaded from a DSpace repository. https://dspace.org/

# Non-Oxidative Conversion of Methane into Aromatic Hydrocarbons over Molybdenum Modified H-ZSM-5 Zeolite Catalysts

**Themba E. Tshabalala**

*A thesis submitted to the Faculty of Science, University of the Witwatersrand, Johannesburg, in fulfillment of the requirements for the degree of Doctor of Philosophy*

CATOMMAT
MOLECULAR SCIENCES INSTITUTE
School of CHEMISTRY
University of the Witwatersrand

**Supervisors:**

**Prof. Neil Coville**

**Prof. Mike Scurrell**

**2/28/2013**

# *Declaration*

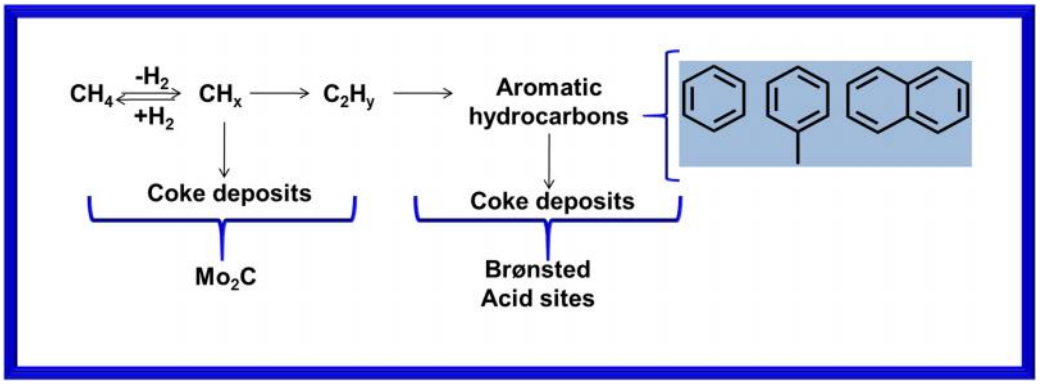
I declare that this thesis is my own, unaided work. It is being submitted for the Degree of Doctor of Philosophy in the University of the Witwatersrand, Johannesburg. It has not been submitted before for any degree or examination in any other University.

_____

(Signature of candidate)

**28th February 2013**

# Abstract




Dehydroaromatization of methane (MDA) reaction was investigated over platinum modified Mo/H-ZSM-5 catalysts which were pre-carbided at 750 $^{o}$C. The influence of platinum on the catalytic performance and product selectivity of Mo/H-ZSM-5 catalysts for the MDA reaction at 700 $^{o}$C was studied. The presence of platinum led to a slight decrease in methane conversion. As the platinum loading increased, the methane conversion decreased further and the catalytic stability increased with time-on-stream (TOS) during the MDA reaction. Aromatic selectivities above 90% were obtained with catalysts containing low platinum loadings (0.5 and 1.0 wt.%), with benzene being the most prominent product. A decrease in coke selectivity and coke deposits was noted with the platinum modified Mo/H-ZSM-5 zeolite catalysts.

A comparative study was performed to compare platinum, palladium and ruthenium promoted Mo/H-ZSM-5 zeolite catalysts with un-promoted Mo/H-ZSM-5. The ruthenium promoted catalyst proved to be superior in catalytic performance, with a higher methane conversion obtained than found for platinum promoted and palladium promoted Mo/H-ZSM-5 catalysts. Benzene selectivity of about 60% was obtained for ruthenium and palladium promoted Mo/H-ZSM-5 catalysts and the total aromatic selectivity was maintained at 90%. TGA results showed a total reduction of 50% by weight of carbon deposited on the promoted Mo/H-ZSM-5 catalyst.

Dehydroaromatization of methane was studied over tin modified Pt/Mo/HZSM-5 catalysts and compared to Pt/Mo/H-ZSM-5 catalyst at 700 $^{o}$C. Addition of tin decreased the activity towards methane aromatization. However, the formation of aromatic compounds was favoured. The CO FT-IR adsorption and CO chemisorption techniques showed that the catalyst preparation method had an effect on the catalytic performance of tin modified Pt/Mo/H-ZSM-5 catalysts. High aromatic selectivity and low coke selectivity were obtained with co-impregnated and sequentially impregnated Pt/Sn catalysts. While a decrease in the formation rate of carbonaceous deposits is mainly dependent on the availability of platinum sites for the hydrogenation of carbon. The order of sequentially loading platinum and tin has an effect on the electronic and structural properties of platinum as shown by XPS and FT-IR studies. CO chemisorption and the FT-IR adsorption studies showed that addition of tin decreased the adsorption capacity of the platinum surface atoms. Catalyst preparation methods and successive calcination treatments affected the location of both tin and platinum atoms in the catalyst. Catalysts prepared by the co-impregnation method showed a good platinum dispersion, better than found for the sequentially impregnated catalysts.

The MDA reaction was carried out at 800 $^{o}$C over manganese modified H-ZSM-5 zeolite catalysts prepared by the incipient wetness impregnation method. The effect of a number of parameters on the catalytic performance and product selectivity was investigated, such as reaction temperature, manganese precursor-type, tungsten as promoter, manganese loading and use of noble metals. The study of the effect of reaction temperature showed that the methane conversion increased linearly with increase in reaction temperature from 700 to 850 $^{o}$C. The selectivity towards aromatic compounds (of about 65%) was attained for the reactions performed at 750 and 800 $^{o}$C. Formation rate of carbonaceous deposits increased linearly with increase in reaction temperature. The use of different manganese precursors to prepare Mn/H-ZSM-5 catalysts had an effect on both the catalytic behaviour and the product distribution. High catalytic activities were obtained for the catalysts prepared from $Mn(NO_3)_2$ and $MnCl_2$ salts. However, the product distribution was significantly different, with the $Mn(NO_3)_2$ catalyst being more selective towards aromatic compounds while the $MnCl_2$ catalyst was more selective toward coke. The effect of manganese loading was studied at 800 $^{o}$C and an optimum catalyst activity

was obtained at 2 and 4 wt.% manganese loadings. The aromatic selectivity above 70% and coke selectivity of 20% were obtained for a 2 wt.% loaded catalyst.

Addition of tungsten as a promoter onto the 2 wt.% loaded catalyst (2Mn/H-ZSM-5) lowered the catalytic activity but the catalyst remained fairly stable with increase in TOS. Tungsten modified catalysts favoured the formation of carbonaceous deposits over aromatic compounds. TGA results showed a coke deposit of 164 mg/g.cat, an 88% increase in coke deposit when tungsten was used a promoter. Noble metals were added to reduce the total amount of coke on the tungsten modified Mn/H-ZSM-5 catalysts. The presence of a noble metal favoured the formation of aromatic compounds and suppressed the formation of coke. Platinum and ruthenium promoted catalysts were the active catalysts and aromatic selectivity increased from 12% to 55% and 46% respectively. A reduction in the total amount of coke deposit on the platinum promoted catalyst (42%) and the ruthenium promoted catalyst (31%) was noted.

# Acknowledgements

I would like to thank my supervisors, Prof. Neil Coville and Prof. Mike Scurrell for their guidance, support and enthusiasm over the last *mmmmh* years of my PhD. Much appreciated.

I will forever be grateful for having met Prof James Anderson and Dr. Richard Wells. Your understanding and specialty of FT-IR spectroscopy has added few colours on this thesis. Thank you very much for being the wonderful hosts in Aberdeen.

Basil Chassoulas (Gaileo Glilei of CATOMAT) for technical assistance he provided throughout the duration of the project. At last we detected ammonia using the old TPD.

I would also like to thanks Mr. David Moloto and Mr. Elias Baloyi. for being patient with me when we requested cylinders and other miscellaneous chemicals.

CATOMAT memebers, who always provided a friendly working environment with proper noise. Thank you guys for your *Clownish* behaviour.

Surface and Catalysis group in University of Aberdeen for being wonderful people.

Manoko Maubane, Zikhona Tetana, Sibongle Dube and Thobeka Kente (GaN) your assistance has added few pages. George Bepete, William Dlamini, Victor Baloyi, Isaac Beas, Ahmed (Msholozi) Shaikjee, Tumelo Phaahla', David (FatBoy) Kumi and Neo Phao; you've been a good company. I have never felt stressed in our research environment.

Nthabiseng Ntholeng and Mahalieo Kao thanks for everything. *Have a koinyas!*

To the Mshengu's, the Donga's Family, thank you for being there always.

University of the Witwatersrand for providing the facilities and financial assistance

School of Chemistry

NRF and for financial assistance

RSC for financing my UK trips.

# Presentations

## CONFERENCE PRESENTATIONS

### Oral Presentations

Themba Tshabalala, Neil Coville James Anderson and Richard Wells and Mike Scurrell, ***Dehydroaromatization of Methane over Sn-Pt Modified Mo/H-ZSM-5 Zeolite Catalysts: Effect of Preparation Method***, Natural Gas Conversion Conference, Doha, Qatar, 2-7 March 2013.

Themba Tshabalala, Neil Coville and Mike Scurrell***, Dehydroaromatization of Methane over Sn Doped Pt/Mo/H-ZSM-5 Zeolite Catalysts***, Catalysis Society of South Africa Conference, Honeydew, Gauteng November 2011.

Themba Tshabalala, James Anderson, Richard Wells and Mike Scurrell, ***Methane Dehydroaromatization on Platinum Loaded Mo/H-ZSM-5 Catalysts,*** 40th South African Chemical Institute Conference, University of the Witwatersrand, Johannesburg, Gauteng, January 2011.

### Poster Presentations

Themba Tshabalala, James Anderson, Richard Wells and Mike Scurrell, ***FT-IR Studies on CO Adsorption on Platinum-Molybdenum H-ZSM-5 Zeolite Systems,*** Catalysis Society of South Africa Conference, Cape Town, Western Cape, 8-11 November 2009.

# Table of Contents

Declaration i

Abstract ii

Acknowledgements v

Presentations vii

Table of Contents viii

List of Figures xiii

List of Tables xviii

List of Abbreviations xx

**Chapter 1**
**Introduction**

1.1. Background 1

1.2. An Overview on Utilization of Methane 3

1.3. Aims and Objectives of the Study 5

1.4. Thesis Outline 6

1.5. Reference List 6

**Chapter 2**
**Literature Review**

2.1. Background on the Production of Aromatic Hydrocarbons 8

2.2. Dehydroaromatization of Methane 9

2.3. Formation and Nature of Active Sites 10

2.4. Induction Period of MDA Reaction 12

2.5. Reaction Mechanisms of Methane Aromatization 13

2.6. The Role of Brønsted Acid Sites 15

2.7. Catalyst Deactivation 17

*2.7.1. Formation of Coke* 17

2.8. Summary 19

2.9. Reference List 20

**Chapter 3**
**Experimental**

3.1. Material Used 24

3.2. Synthesis of H-ZSM-5 Zeolite Catalyst 24

3.3. Catalysts Characterization 25

*3.3.1. Nitrogen Adsorption (BET) Analysis* 25

*3.3.2. Ammonia Temperature Programmed Desorption ($NH_3$-TPD)* 25

*3.3.3. Hydrogen Temperature Programmed Reduction ($H_2$-TPR)* 26

*3.3.4. Carbon Monoxide Adsorption: Fourier Transform Infrared (FT-IR) Spectroscopy* 26

*3.3.5. Pulse Carbon Monoxide Chemisorption* 26

*3.3.6. X-ray Photoelectron Spectroscopy (XPS) Analysis* 27

*3.3.7. Powder X-Ray Diffraction (XRD) Analysis* 27

*3.3.8. Thermogravimetric Analysis (TGA) Measurements* 27

3.4. Catalytic Evaluation of the MDA Reaction 28

*3.4.1. Calculations* 28

3.5. Reference List 28

**Chapter 4**
**Dehydroaromatization of Methane over Noble Metal loaded Mo/H-ZSM-5 Zeolite Catalysts**

4.1. Introduction 29

4.2. Experimental 31

4.2.1. Catalysts Preparation 31

4.3. Results and Discussion 32

4.3.1. Characterization Results 32

4.3.2. Catalytic Results 38

*4.3.2.1. Effect of Platinum Loading on the MDA Reaction* 38

*4.3.2.2. Comparison Study of the Effect of Noble Metals (i.e. Pt, Pd and Ru) on the MDA reaction* 45

4.4. Summary 48

4.5. Reference List 49

**Chapter 5**
**Dehydroaromatization of Methane over Sn Doped Pt/Mo/H-ZSM-5 Zeolite Catalysts**

5.1. Introduction 53

5.2. Experimental 54

5.2.1. Catalyst Preparation 53

5.3. Results and Discussion 55

5.3.1. Catalyst Characterization 55

5.3.2. Catalytic Results of MDA Reaction 61

5.4. Summary 68

5.5. Reference List 68

**Chapter 6**
**Dehydroaromatization of Methane over Sn-Pt Modified Mo/H-ZSM-5 Zeolite Catalysts: Effect of Preparation Method**

6.1. Introduction 70

6.2. Experimental 71

6.2.1. Catalysts Preparation 71

6.3. Results and Discussion 72

*6.3.1. Characterization Results* 72

*6.3.2. Catalytic Results of MDA Reaction* 81

6.4. Summary 86

6.5. Reference List 87

**Chapter 7**
**Dehydroaromatization of Methane over Mn/H-ZSM-5 Zeolite Catalysts**

7.1. Introduction 89

7.2. Experimental 91

7.2.1. Catalysts Preparation 91

7.3 Results and Discussion 92

*7.3.1. Effect of Reaction Temperature* 92

*7.3.2. The Effect of Manganese Precursor* 98

*7.3.3. Effect of Manganese Loading* 102

*7.3.4. Effect of Tungsten on the MDA Reaction* 111

*7.3.5. Addition Effect of Noble Metals of the MDA Reaction over W/Mn/H-ZSM-5 Catalyst* 116

7.4. Summary 120

7.5. Reference List 121

**Chapter 8**
**General Conclusions**

8.1. Conclusions 123

8.2. Recommendations 126

# List of Figures

## Chapter 4


| | | |
|---|---|---|
| **Figure 4.1** | $NH_3$-TPD profiles of the parent H-ZSM-5, 2Mo/H-ZSM-5 and Pt/2Mo/H-ZSM-5 zeolite catalysts with various platinum loadings | 33 |
| **Figure 4.2** | Adsorption of CO on platinum loaded samples at different CO pressures. a) 2Pt/H-ZSM-5, b) 0.5Pt/2Mo/H-ZSM-5, c) 1Pt/2Mo/H-ZSM-5 and d) 2Pt/2Mo/H-ZSM-5. | 35 |
| **Figure 4.3** | FT-IR spectra of CO adsorption on 2Mo/H-ZSM-5 and Pt/Mo/H-ZSM-5 zeolite catalysts with various platinum loadings take at 5 Torr CO pressure. | 36 |
| **Figure 4.4** | FT-IR spectra of the CO adsorption on the 2%$Mo_2C$ reduced at 200 $^oC$ for 1 hour. (a) 0.5Pt/2MoC/H-ZSM-5, (b) 1Pt/2Mo/H-ZSM-5, (c) 2Pt/2Mo/H-ZSM-5 and (d) 2Pt/H-ZSM-5. | 37 |
| **Figure 4.5** | The effect of platinum loading on methane conversion at 700 $^oC$ at steady state after a time-on-stream of 245 minutes. | 38 |
| **Figure 4.6** | Effect of platinum loading on the catalytic conversion of methane versus time-on-stream taken a 700 $^oC$ for 6 hours on-stream. | 39 |
| **Figure 4.7** | Aromatic and coke selectivities of Mo/H-ZSM-5 and Pt/H-ZSM-5 with various platinum loadings (i.e. between 0.5 and 2 wt.%) plotted against time-on-stream. | 41 |
| **Figure 4.8** | Benzene selectivity of Mo/H-ZSM-5 and Pt/Mo/H-ZSM-5 with various platinum loadings (i.e. between 0.5 and 2 wt.%) plotted against time-on-stream. | 41 |
| **Figure 4.9** | TGA (a) and DTG (b) profiles of coked Mo/H-ZSM-5, Pt/Mo/H-ZSM-5 and Pt/H-ZSM-5 zeolite catalysts after MDA reactions at 700 $^oC$. | 43 |
| **Figure 4.10** | The catalytic conversion of methane as a function of time-on-stream over noble metal modified 2Mo/H-ZSM-5 zeolite catalysts with a of 0.5 wt.% loading of the noble metal | 45 |
| **Figure 4.11** | TGA (a) and DTG (b) profiles of coked Mo/H-ZSM-5, Pt/Mo/H-ZSM-5 Pd/Mo/H-ZSM-5 and Ru/Mo/H-ZSM-5 zeolite catalysts after MDA reactions for 6 hours at 700 $^oC$. | 47 |

# Chapter 5


| | | |
|---|---|---|
| **Figure 5.1** | XRD profiles of Mo/H-ZSM-5 and Sn doped Pt/Mo/H-ZSM-5 catalysts. | 56 |
| **Figure 5.2** | $NH_3$-TPD profiles of Mo/H-ZSM-5, Pt/Mo/H-ZSM-5 and Sn doped Pt/Mo/H-ZSM-5 zeolite catalysts. | 57 |
| **Figure 5.3** | Hydrogen TPR profiles of 5Sn/H-ZSM-5 and 0.5Pt/5Sn/H-ZSM-5 zeolite catalysts. | 58 |
| **Figure 5.4** | Hydrogen TPR profiles of Mo/H-ZSM-5 and Pt/Mo/H-ZSM-5 zeolite catalysts. | 59 |
| **Figure 5.5** | Hydrogen TPR profiles for the Sn-containing Pt/Mo/H-ZSM-5 zeolites catalysts with tin loadings between 0 and 0.2 wt.%. | 60 |
| **Figure 5.6** | The catalytic conversion of methane over Sn doped Pt/Mo/H-ZSM-5 catalysts with Sn loadings between 0.05 and 0.2 wt.% loadings. | 62 |
| **Figure 5.7** | The percentage aromatic selectivity as a function of time-on-stream of tin doped Pt/Mo/H-ZSM-5 catalysts. | 63 |
| **Figure 5.8** | The effect of tin loading on the $C_2$ species, aromatics and coke selectivity during methane aromatization at 700 $^oC$. Catalysts were compared at methane conversions of approximately 7%. | 64 |
| **Figure 5.9** | The effect of tin loading on the aromatic product distribution of MDA at 700 $^oC$ taken at a methane conversion of 7%. | 64 |
| **Figure 5.10** | TGA (a) and DTG (b) profiles of coked Pt/Mo/H-ZSM-5 and Sn-containing Pt/Mo/H-ZSM-5 zeolite catalysts after MDA at 700 $^oC$. | 65 |
| **Figure 5.11** | Schematic representation of the dehydroaromatization of methane with tin adding the dehydrogenation character to the reaction. | 67 |

# Chapter 6


| | | |
|---|---|---|
| **Figure 6.1** | Hydrogen TPR profiles of tin modified Pt/Mo/H-ZSM-5 zeolite catalysts prepared by sequential and co-impregnation methods, (a) co-impregnated 0.2Sn-0.5Pt/2Mo/H-ZSM-5, (b) sequentially impregnated 0.2Sn/0.5Pt/2Mo/H-ZSM-5 and (c) 0.5Pt/0.2Sn/2Mo/H-ZSM-5. | 73 |
| **Figure 6.2** | FT-IR spectra of CO adsorbed on uncalcined 0.5Pt/2Mo/H-ZSM-5 and co-impregnated 0.2Sn-0.5Pt/2Mo/H-ZSM-5 zeolite catalysts. | 74 |
| **Figure 6.3** | FT-IR spectra of CO adsorbed of calcined Sn modified Pt/Mo/H-ZSM-5 zeolite catalysts, taken at different CO pressure after 15 minutes adsorption intervals. (a) 0.5Pt/2Mo/H-ZSM-5, (b) co-impregnated 0.2Sn-0.5Pt/2Mo/H-ZSM-5, (c) sequentially impregnated 0.2Sn/0.5Pt/2Mo/H-ZSM-5 and (d) 0.5Pt/0.2Sn/2Mo/H-ZSM-5. | 77 |
| **Figure 6.4** | FTIR spectra of CO adsorbed of reduced Sn modified Pt/Mo/H-ZSM-5 zeolite catalysts, taken at 5 Torr CO pressure. (a) 0.5Pt/2Mo/H-ZSM-5, (b) Co impregnated 0.2Sn-0.5Pt/Mo/H-ZSM-5, (c) Sequentially impregnated 0.2Sn/0.5Pt/2Mo/H-ZSM-5.. | 78 |
| **Figure 6.5** | XPS spectra corresponding to the Pt 4f level of sequentially impregnated Sn/Pt/Mo/H-ZSM-5 catalyst; (a) calcined form and (b) reduced form. | 79 |
| **Figure 6.6** | XPS spectra corresponding to the Sn 3d level of sequentially impregnated Sn/Pt/Mo/H-ZSM-5 catalyst; (a) calcined form and (b) reduced form. | 79 |
| **Figure 6.7** | FT-IR spectra of CO adsorption on 0.2Sn/0.5Pt/2Mo/H-ZSM-5 zeolite catalyst which was reduced at 200 $^{o}$C and oxidized at different temperatures. (a) reduced, (b) oxidized 300 $^{o}$C, (c) 400 $^{o}$C and (d) 450 $^{o}$C. | 82 |
| **Figure 6.8** | The catalytic conversion of methane over Sn doped Pt/Mo/H-ZSM-5 catalysts prepared using different impregnation methods. | 84 |
| **Figure 6.9** | Percentage aromatic selectivity as a function of time-on-stream for tin doped Pt/Mo/H-ZSM-5 catalysts prepared using co-impregnation and sequential impregnation methods | 84 |
| **Figure 6.10** | The effect of preparation method on the $C_2$ species, aromatics and coke selectivity during methane aromatization at 700 $^{o}$C taken at a methane conversion of 7%. | 85 |

# Chapter 7


| | | |
|---|---|---|
| **Figure 7.1** | MDA catalytic activity of 2%Mn/H-ZSM-5zeolite catalyst taken at different reaction temperatures between 700 and 850 $^{o}$C for 6 hours on-stream | 94 |
| **Figure 7.2** | The catalytic conversion as the function of reaction temperature over the 2Mn/H-ZSM-5 catalysts at TOS of 5, 185 and 365 minutes. | 95 |
| **Figure 7.3** | Aromatic selectivity versus TOS plot of 2Mn/H-ZSM-5 catalyst taken at different reaction temperatures. | 95 |
| **Figure 7.4** | The effect of reaction temperature on the product distribution of methane aromatization over 2Mn/H-ZSM-5 catalyst at time-on-stream of 245 minutes. | 96 |
| **Figure 7.5** | TGA (a) and DTG (b) profiles of coked Mn/H-ZSM-5 catalysts after MDA reaction at different reaction temperatures. | 97 |
| **Figure 7.6** | TPR profiles of Mn/H-ZSM-5 catalysts impregnated with different manganese precursors (i.e. $Mn(NO_3)_2$, $MnCl_2$ and $KMnO_4$). | 99 |
| **Figure 7.7** | The catalytic conversion of methane of Mn/H-ZSM-5 zeolite catalysts impregnated with different manganese precursors (i.e. $Mn(NO_3)_2$, $MnCl_2$ and $KMnO_4$), taken at 800 $^{o}$C for 6 hours. | 101 |
| **Figure 7.8** | The effect manganese precursor on the aromatic selectivity of Mn/H-ZSM-5 zeolite catalysts. | 101 |
| **Figure 7.9** | The effect manganese precursor on the product distribution of Mn/H-ZSM-5 catalysts for methane conversion at 800 $^{o}$C after TOS of 245 minutes. | 102 |
| **Figure 7.10** | The XRD patterns of Mn/H-ZSM-5 zeolite catalysts of different manganese loadings. | 104 |
| **Figure 7.11** | TPR profiles of bulk $MnO_2$ and Mn/H-ZSM-5 zeolite catalysts with different manganese loadings prepared by incipient impregnation method. | 105 |

| | | |
|---|---|---|
| **Figure 7.12** | $NH_3$-TPD profiles of the parent H-ZSM-5 and Mn/H-ZSM-5 catalysts with different manganese loadings. | 106 |
| **Figure 7.13** | The effect of manganese loading on methane conversion over Mn/H-ZSM-5 catalyst at 800 $^oC$, taken at TOS of 125 min. | 107 |
| **Figure 7.14** | The catalytic conversion of methane of Mn/H-ZSM-5 zeolite catalysts with different manganese loading as the function of time-on-stream with reaction temperature set at 800 $^oC$. | 108 |
| **Figure 7.15** | The effect of manganese loading the C2s, aromatics and coke selectivity from MDA over Mn/H-ZSM-5 at 800 $^oC$ taken at isoconversion of 6%, for a TOS of 245 minutes. | 109 |
| **Figure 7.16** | TGA (a) and DTG (b) profiles of coked Mn/H-ZSM-5 zeolite catalysts with different manganese loadings that were used for MDA reaction at 800 $^oC$ for 6 hours on-stream. | 111 |
| **Figure 7.17** | The effect of tungsten on the catalytic conversion and stability of Mn/H-ZSM-5 zeolite catalysts for MDA reaction at 800 $^oC$. | 113 |
| **Figure 7.18** | The effect of tungsten loading on the catalysts product distribution of Mn/H-ZSM-5 for MDA reaction at 800 $^oC$ taken after 245 minutes on-stream. | 114 |
| **Figure 7.19** | TGA (a) and DTG (b) profiles of coked tungsten modified Mn/H-ZSM-5 zeolite catalysts with different tungsten loadings that were used for MDA reaction at 800 $^oC$ for 6 hours on-stream. | 115 |
| **Figure 7.20** | The catalytic conversion of methane as a function of time-on-stream over noble metal modified 2Mo/H-ZSM-5 zeolite catalysts with a of 0.5 wt.% loading of the noble metal. | 118 |
| **Figure 7.21** | TGA (a) and DTG (b) profiles of coked tungsten modified Mn/H-ZSM-5 zeolite catalysts with various tungsten loadings after for the MDA reaction at 800 $^oC$ for 6 hours on-stream. | 119 |

# List of Tables

## Chapter 4


| Table No. | | Page No. |
|---|---|---|
| **Table 4.1** | Nitrogen adsorption (BET) results of Pt loaded Mo/H-ZSM-5 zeolite catalysts | 32 |
| **Table 4.2** | CO Chemisorption on Pt/Mo/H-ZSM-5 zeolite samples reduced at 200$^{o}$C for 1 hour | 36 |
| **Table 4.3** | Product selectivity of Mo/H-ZSM-5 and Pt/Mo/H-ZSM-5 zeolite catalysts taken at TOS of 245 minutes. | 42 |
| **Table 4.4** | Summarized TG and DTG results of coked Mo/H-ZSM-5 and Pt/Mo/H-ZSM-5 with various platinum loadings. | 43 |
| **Table 4.5** | Comparison results of the effect of noble metals on the MDA reaction and percentage product selectivities taken at 7% methane conversion after 245 minutes on-stream. | 45 |


## Chapter 5


| Table No. | | Page No. |
|---|---|---|
| **Table 5.1** | BET surface areas and pore volumes of the Sn doped Pt/Mo/H-ZSM-5 catalysts with different tin loadings. | 56 |
| **Table 5.2** | Acid sites distribution on Mo/H-ZSM-5, Pt/Mo/H-ZSM and Sn-doped Pt/Mo/H-ZSM-5 catalysts taken from ammonia TPD profiles. | 58 |
| **Table 5.3** | Summarized TGA and DTG results of coked Pt/Mo/H-ZSM-5 and Sn-Pt/Mo/H-ZSM-5 with various tin loadings. | 66 |

# Chapter 6


| Table No. | | Page No. |
|---|---|---|
| **Table 6.1** | Percentage metal dispersion and the amount of CO molecules adsorbed on the surface of platinum atoms in the tin modified 0.5Pt/2Mo/H-ZSM-5 zeolite catalysts. | 80 |
| **Table 6.2** | Product selectivity of tin modified Pt/Mo/H-ZSM-5 prepared using co-impregnation and sequential impregnation methods taken at a methane conversion of 7%. | 86 |


# Chapter 7


| Table No. | | Page No. |
|---|---|---|
| **Table 7.1** | TGA and DTG results of coked Mn/H-ZSM-5 zeolite catalysts after MDA reaction studied at different reaction temperatures. | 98 |
| **Table 7.2** | The effect of manganese loading on the surface area and pore volume of Mn/H-ZSM-5 catalyst prepared using $Mn(NO_3)_2$ manganese source. | 103 |
| **Table 7.3** | The effect of manganese loading on the product selectivity of Mn/H-ZSM-5 zeolite catalysts for MDA at 800 $^oC$ , taken at 6% methane conversion. | 110 |
| **Table 7.4** | TGA and DTG results of coked Mn/H-ZSM-5 zeolite catalysts with different manganese loadings after MDA reaction at 800 $^oC$ for 6 hours on-stream. | 111 |
| **Table 7.5** | The effect of tungsten loading on the product selectivity of Mn/H-ZSM-5 zeolite catalysts for MDA reaction at 800 $^oC$ taken after 245 minutes on stream. | 114 |
| **Figure 7.6** | TGA and DTG results of coked tungsten modified 2Mn/H-ZSM-5 zeolite catalysts with different tungsten loadings after MDA reaction at 800 $^oC$ for 6 hours on-stream. | 116 |
| **Figure 7.7** | Comparison results of the effect of noble metals on the MDA reaction and product selectivity taken at 4% methane conversion after 245 minutes on-stream. | 118 |
| **Figure 7.8** | TGA and DTG results of coked tungsten modified 2Mn/H-ZSM-5 zeolite catalysts with different tungsten loadings after the MDA reaction at 800 $^oC$ for 6 hours on-stream. | 120 |

# List of Abbreviations

| Abbreviations | Definitions |
|---|---|
| *a.u* | Arbitrary Units |
| *AHM* | Ammonium Heptamolybdate |
| *APT* | Ammonium Paratungstate |
| *BE* | Binding Energy |
| *BET* | Brunauer–Emmett–Teller |
| *BP* | British Petroleum |
| *BTX* | Benzene Toluene Xylenes |
| *DHCP* | Dihydrogen Hexachloroplatinate |
| *DTG* | Derivative Thermogravimetry |
| *EPR* | Electron Spin Resonance spectroscopy |
| *EXAFS* | Extended X-Ray Absorption Fine Structure |
| *FCC* | Fluid Catalytic Cracking |
| *FID* | Flame Ionization Detector |
| *FTIR* | Fourier Transform Infrared spectroscopy |
| *GC* | Gas Chromatography |
| *HRTEM* | High-Resolution Transmission Electron Microscopy |
| *H-ZSM-5* | Hydrogen-Zeolite Socony Mobil-5 |
| *MDA* | Methane Dehydroaromatization |
| *MFI* | Mordenite Framework Inverted |
| *MTG* | Methanol-to-Gasoline |
| *NMR* | Nuclear Magnetic Resonance spectroscopy |
| *OCM* | Oxidative Coupling of Methane |
| *PGMs* | Platinum Group Metals |
| *SASOL* | South Africa Synthetic Oil Liquid |
| *TCD* | Thermal Conductivity Detector |
| *TGA* | Thermogravimetric Analysis |
| *TOS* | Time-on-Stream |
| *TPABr* | Tetrapropylammonium Bromide |

| | |
|---|---|
| *TPD* | Temperature Programmed Desorption |
| *TPO* | Temperature Programmed Oxidation |
| *TPR* | Temperature Programmed Reduction |
| *TPSR* | Temperature Programmed Surface Reactions |
| *UOP* | Universal Oil Products |
| *UV vis.* | Ultraviolet Visible spectroscopy |
| *wt.%* | Weight percent |
| *XPS* | X-ray Photoelectron Spectroscopy |
| *XRD* | X-ray Diffraction |

# Chapter 1

# Introduction

## 1.1. Background

The rapid growth in the human population (which stood at 1.6 billion at the beginning of the 20th century has now increased to 6 billion) and economic growth in the 21st century has been phenomenal, and this has led to an increase in energy demand. The National Petroleum Council in the USA reported the energy demand will grow by 50% by 2030 [1, 2]. This suggests that for the next few decades oil, gas and coal will remain the primary energy sources. The use of oil and coal has some disadvantages associated with them. The increase in the oil price has made it difficult for developing countries to maintain their energy supply. There has been a depletion of coal reserves and the release of greenhouse gases to the atmosphere has an impact on the environment. These issues have raised concerns from other sectors. Ecologists have suggested that the consumption of fossil fuels and production patterns cause environmental destruction [3, 4]. Climate change which is mainly attributed to greenhouse gases has raised concerns by the public [5]. Geologists point out that we will soon reach or may surpass the peak of oil production in the next two decades. Hence, there is an increasing demand to find cleaner and abundant sources of energy and for the development of processes with less impact on the environment.

The predictions on the use of methane or natural gas in the petroleum industry relies on the price of crude oil compared to that of natural gas, with the latter being the cheaper feedstock to make valuable hydrocarbons and/or aromatic compounds. The reason relates to the low heteroatom content and high hydrogen content present in natural gas [6]. The importance of methane for the production of hydrocarbons in the petrochemical industry is linked to the production of synthesis gas via methane reforming, methanol synthesis and the methanol to gasoline (MTG) process [7, 8]. Comprehensive developments are needed to find economical processes and alternative

resources that can be used to produce gasoline, diesel and other important chemicals that will be of use in other chemical industries. The catalytic conversion of alkanes into desired chemical compounds is one promising process that can be of good use to enhance the economic state of the petroleum industry, especially in South Africa.

The demand for highly marketable products from refineries has grown and this has put pressure on the effective utilization of fossil fuel sources and low valued hydrocarbons. The abundance and lower cost of light alkanes have generated extraordinary interest in transforming them into useful compounds that may be beneficial to other industries. The conversion of light alkanes ($C_2$-$C_4$) into aromatic compounds mainly benzene, toluene and xylenes (BTX) is one of the important industrial processes that have attracted much attention due to the industrial application of BTX compounds [9]. These light hydrocarbons are produced by processes such as Fischer-Tropsch synthesis, from oil refineries and are found in natural gas. The BTX are regarded as highly useful compounds in the petroleum and chemical industries. In the petroleum industry aromatic compounds are used as additives for gasoline for the enhancement of octane levels. These aromatics can also be used as raw materials in other chemical industries for synthesizing other chemicals. In the polymer industry they are used as monomers (i.e. xylenes) in polyester engineering plastics, and they are also intermediates for detergents, pharmaceuticals, agricultural products and explosives manufacture [10].

Different catalytic processes have been utilized in producing the aromatic compounds, mainly benzene, toluene and xylenes (BTX) from different feed stocks. The catalytic reforming of naphtha was regarded as an effective process for producing petroleum-derived aromatics. However, it was considered not economical due to its inability to convert light hydrocarbons [10]. Mobil developed a process called M2-Forming in which light alkanes were converted into BTX over an unmodified H-ZSM-5 zeolite catalyst. Unfortunately, the unmodified H-ZSM-5 suffers fast deactivation and possesses substantial cracking activity that leads to a high selectivity for C1 and C2 products. However, the product selectivity to longer hydrocarbon chain compounds and coke resistant catalyst can be achieved by adding promoters which are transition metals (i.e. Cr, Cu, Fe, Mn, Mo, Ni, Os, Pt, V, W, Zn and Ga). These metals were added in the form of extra-framework species to facilitate the catalyst dehydrogenation function [11, 12]. The improved activity and selectivity due to the addition of extra-framework species has made

possible commercial application of the processes, i.e. the Cyclar and Aroforming processes [13].

## 1.2. An Overview on Utilization of Methane

Methane gas is the major component of natural gas, coal bed gas and methane hydrates and constitutes a large carbon reserve on earth. It is also available in large quantities (180 trillion $m^3$) as an undesirable by-product from certain natural and man-made processes. Its abundance has led to much interest for use in the production of hydrocarbon compounds which are useful in the production of fuels. There are a number of factors that have led many petroleum industries to focus on the use of methane or natural gas as alternative sources of hydrocarbons for fuel production. Natural gas is effective as an energy source because it burns cleaner and produces few pollutants. Its heat of combustion is larger compared to the $CO_2$ formed. When natural gas is used as feedstock $CO_2$ emissions are reduced by 45% relative to coal [6].

Natural gas is mostly distributed in remote areas relative to where it is processed into valuable products. So, transportation poses as a major challenge. The gas needs to be either liquefied or converted into other hydrocarbons, which are easy to transport. Liquefaction and construction of pipelines carry high cost and this has discouraged many companies from using methane as a feedstock for the production of fuel [14, 15]. In South Africa, SASOL has built a pipeline which transports natural gas from Mozambique to its Sasolburg plant for methane reforming for the production of synthesis gas.

Methane can be used as the feedstock for production of valuable hydrocarbons which are commonly produced by processing crude oil and coal. Methane can be transformed into hydrocarbons through both indirect and direct routes. The indirect conversion route is based on the reforming of methane into synthesis gas (CO and $H_2$). This can occur through steam or $CO_2$ reforming and catalytic partial oxidation of methane [16]. The catalytic partial oxidation of methane involves the oxidation of methane into methanol and dimethyl ether (DME) which are further transformed into gasoline (i.e. methanol to gasoline (MTG)) [17-19]. Currently, only the indirect conversion routes are used commercially for the Fischer-Tropsch synthesis.

The direct conversion route of converting methane into hydrocarbons is more thermodynamically favoured with the aid of oxidants. This has led to the discovery of catalytic oxidative coupling of methane (OCM process), whereby methane is converted into ethylene in the presence of oxidants [20, 21]. Based on thermodynamic studies, the OCM process is preferred over direct conversion of methane under non-oxidative conditions. In 1980 a study on OCM was conducted and the results showed no catalyst could reach a $C_{2+}$ yield higher than 25% and selectivity to $C_{2+}$ higher than 80% [22]. The use of oxidants as activators has led to a high yield of $CO_2$ and poor selectivity towards desired products. A conclusion based on the results was that no industrial application of the OCM process could be developed and the research interest on this topic gradually weakened.

Based on the results of the OCM process which is thermodynamically favoured but with limited selectivity, researchers started focusing on the alternative direct conversion of methane under non-oxidative conditions. Conversion of methane to aromatic hydrocarbons under non-oxidative conditions can be of commercial value to the petroleum industry due to high usage of aromatic compounds. The aromatic compounds are used as additives to fuels because of their high octane number and they constitute a significant part of the gasoline pool (about 30%) [23]. In this reaction benzene and hydrogen are produced with the latter having a potential use in fuel cells. This reaction might also be of benefit for use in the search for renewable energy and cleaner fuels. Methane (fossil fuel source) can be used as a practical source for hydrogen production due to its great abundance and its high H/C atomic ratio [16]. Therefore direct conversion of methane under non-oxidative conditions may be an efficient way of utilizing methane containing reserves for the improvement of living conditions for a growing population.

The direct aromatization of methane under non-oxidative conditions still remains in its early research stages. The transformation of a $C_1$ molecule into aromatics is obviously much more complex than aromatization of $C_3$–$C_4$ alkanes, not mentioning $C_{6+}$ hydrocarbons. Methane is the most stable among the alkanes. The structure of a $CH_4$ molecule, with its four C–H covalent bonds of high bond energies ($D(CH_3–H) \approx D(H–H) = 435$ kJ/mol), zero dipole moment, no multiple bonds or functional groups and no asymmetry, is responsible for the extremely low reactivity of $CH_4$ [22]. Thermodynamically, methane is unstable only above 530 $^oC$, becoming more unstable than benzene above 1030 $^oC$ [24].

$$6CH_4 \rightarrow C_6H_6 + 9H_2$$

The conversion of methane to benzene has a rather high enthalpy value of 523 kJ/mol. The methane thermodynamic equilibrium conversion at atmospheric pressure is low at moderate reaction temperatures (about 5% at 600 $^oC$, 11.4% at 700 $^oC$ and 16.2% at 750 $^oC$) [25]. The direct aromatization of methane to benzene (like the $CH_4$ transformation to ethylene or oxygen-containing compounds) requires an initial activation of the $CH_4$ molecule. The activation of a C–H bond in alkanes, and particularly in the most stable $CH_4$, under mild conditions is necessary for the selective synthesis of derivatives, and is one of the most intriguing and challenging problems in contemporary hydrocarbon chemistry and catalysis [22].

## 1.3. Aims and Objectives of the Study

The conversion of methane to aromatic hydrocarbons under non-oxidative condition is one reaction that will be of benefit to the petroleum industry. In this reaction benzene and hydrogen are produced with the latter being of potential use in fuel cells. Molybdenum and tungsten in their carbide form are regarded as the most active metals for methane dehydroaromatization (MDA) reaction under non-oxidative conditions. The thermal properties of both metals supported on H-ZSM-5 were studied and W/H-ZSM-5 zeolite catalyst was found to be a good catalyst for methane activation at reactions temperatures above 750 $^oC$. The properties of Mo, W and Mn catalysts in their carbide forms are similar to the properties of platinum. However, these catalysts suffer deactivation due to coke formation on the active sites of the catalyst during the MDA reaction. Hence our aim for the study was to investigate the non-oxidative conversion of methane into aromatic compounds over Mo/H-ZSM-5 and Mn/H-ZSM-5 zeolite catalysts. A comparative study on the effect of noble metals (Pt, Ru and Pd) as promoters to reduce the rate of deactivation caused by carbonaceous deposits formed on the active sites was also investigated. Characterization techniques such as BET surface area and pore volume analysis, Temperature Programmed Reduction/Desorption (TPR and TPD), CO Pulse Chemisorption, CO adsorption Fourier Transform infrared (FT-IR) spectroscopy, X-ray Photoelectron Spectroscopy (XPS) and X-ray powder diffraction (XRD) were also used to study the changes in catalytic properties and their influence on the catalytic

activity/behaviour. The total amount of carbonaceous deposits was quantified using thermogravimmetric analysis (TGA).

## 1.4. Thesis Outline

A literature review based on the MDA under non-oxidative conditions over metal-modified zeolite catalysts is presented in Chapter 2. This chapter focused on understanding the nature of the active sites, reaction mechanism of methane aromatization and catalyst deactivation caused by carbonaceous deposits.

The effect of platinum and other noble metals on the MDA reaction over a Mo/H-ZSM-5 zeolite catalyst at 700 $^{o}$C was investigated and presented in Chapter 4. The platinum-molybdenum interaction studied using CO adsorption under FT-IR spectroscopy was also discussed.

In Chapter 5 and 6 we focused on the effect of tin on the aromatization activity and coke deposition rate of platinum modified Mo/H-ZSM-5 zeolite catalysts. The effect of catalyst preparation methods was also investigated with the aid of CO adsorption techniques.

In Chapter 7 we present the results obtained from the study of the MDA reaction over Mn/H-ZSM-5 zeolite catalysts executed at 800 $^{o}$C. The results show the effect of metal precursor, reaction temperature, and manganese loading. The use of tungsten as promoter was explored. The effects of noble metals on reducing the total amount of carbonaceous deposits formed during the MDA reaction were also discussed in this chapter. General conclusions of the study are presented in Chapter 8.

## 1.5. Reference List

[1] V. Balzani, N. Armaroli, Energy for a Sustainable World, Wiley, 2010.

[2] G.A. Olah, A. Goeppert, G.K.S. Prakash, Beyond Oil and Gas: The Methanol Economy,

Wiley, 2009.

[3] H. Giradet, M. Mendonça, W.F. Council, A Renewable World: Energy, Ecology, Equality : a Report for the World Future Council, Green, 2009.

[4] G. Boyle, O. University, Renewable energy: power for a sustainable future, Oxford University Press in association with the Open University, 1996.

[5] A. Rojey, Energy and Climate: How to achieve a successful energy transition, Wiley, 2009.

[6] M. Golombok, W. Teunissen, *Industrial & Engineering Chemistry Research*, **42** (2003) 5003.

[7] J.A. Velasco, L. Lopez, M. Velásquez, M. Boutonnet, S. Cabrera, S. Järås, *Journal of Natural Gas Science and Engineering*, **2** (2010) 222.

[8] D.A. Wood, C. Nwaoha, B.F. Towler, *Journal of Natural Gas Science and Engineering*, **9** (2012) 196.

[9] N.S. Gnep, J.Y. Doyemet, M. Guisnet, *Studies in Surface Science and Catalysis*, **46** (1989) 153.

[10] W.J.H. Dehertog, G.F. Fromen, *Applied Catalysis A: General*, **189** (1999) 63.

[11] Y. Shu, M. Ichikawa, *Catalysis Today*, **71** (2001) 55.

[12] Y. Xu, L. Lin, *Applied Catalysis A: General*, **188** (1999) 53.

[13] P. Meriaudead, C. Naccache, *Catalysis Review-Science and Engineering*, **39** (1997) 5.

[14] T. Reddy Keshav, S. Basu, *Fuel Processing Technology*, **88** (2007) 493.

[15] I. Onwukwe Stanley, *Journal of Natural Gas Science and Engineering*, **1** (2009) 190.

[16] G. Ertl, H. Knözinger, J. Weitkamp, Environmental catalysis, Wiley-VCH, 1999.

[17] S.H. Taylor, J.S.J. Hargreaves, G.J. Hutchings, R.W. Joyner, *Applied Catalysis A: General*, **126** (1995) 287.

[18] Q. Liu, J. Rogut, B. Chen, J.L. Falconer, R.D. Noble, *Fuel*, **75** (1996) 1748.

[19] V.D. Sokolovskii, N.J. Coville, A. Parmaliana, I. Eskendirov, M. Makoa, *Catalysis Today*, **42** (1998) 191.

[20] L. Mleczko, M. Baerns, *Fuel Processing Technology*, **42** (1995) 217.

[21] M. Yamamura, H. Okado, N. Tsuzuki, T. Wakatsuki, K. Otsuka, *Applied Catalysis A: General*, **122** (1995) 135.

[22] K. Skutil, M. Taniewski, *Fuel Processing Technology*, **87** (2006) 511.

[23] T.J. Wallington, E.W. Kaiser, J.T. Farrell, *Chemical Society reviews*, **35** (2006) 335.

[24] C. Gueret, M. Daroux, F. Billaud, *Chemical Engineering Science*, **52** (1997) 815.

[25] Y. Zhang, D. Wang, J. Fei, *JOURNAL OF NATURAL GAS CHEMISTRY*, **12** (2003) 145.

# Chapter 2

# Literature Review

## 2.1. Background on the Production of Aromatic Hydrocarbons

The aromatization of alkanes was discovered by Csicsery in the early 1970s [1-3]. This reforming process used a dual-function catalyst having dehydrogenating and acid properties that catalyzes the dehydrocyclodimerization of light alkanes, into aromatics. The catalysts that were used were platinum-$Al_2O_3$ and chromia-$Al_2O_3$. The problem with these catalysts was their low selectivity towards aromatics and low conversions that were observed due to deactivation of the catalyst [4]. Great interest has since been shown in the development of high selectivity catalysts for the transformation of alkanes into more valuable organic compounds. For example, Mobil introduced high silica-based zeolites, viz. ZSM-5, to enhance the selectivity of the catalysts. This zeolite type has been used in a number of different commercial reactions, such as conversion of methanol and ethanol to gasoline and aromatics [5], alkylation of benzene [6], isomerization of xylenes [7], etc. The H-ZSM-5 zeolite was also found to be the most suitable catalyst for aromatization of alkanes due to the acidic character and shape selective effects due to the molecular sieving properties associated with its well-defined crystal pores [8].

Processes such as M-2 Forming, Cyclar and Aroforming have been used for the transformation of alkanes into more useful aromatic compounds, mainly BTX. M-2 Forming is the Mobil technology used for the conversion of light alkanes ($C_2$-$C_6$) into BTX over a H-ZSM-5 zeolite catalyst. Unfortunately, the unmodified H-ZSM-5 suffers fast deactivation and possesses substantial cracking activity that leads to a large selectivity for $C_1$ and $C_2$ products. However, the problem was overcome by adding activating agents which are transition metals such as Cr, Cu, Fe, Ga, Mn, Mo, Ni, Os, Pt, V, W and Zn. These metals were added in the form of extra-framework species to facilitate the dehydrogenation function in the bi-functional catalysts [9, 10]. Gallium, platinum and zinc additives appeared to be more active and selective

towards BTX. However, gallium and zinc were found to be more selective towards BTX over platinum [11]. Platinum has a high activity for the dehydrogenation of paraffins. Loading platinum increases considerably the conversion of alkanes into aromatics. However, the aromatization reaction is accompanied by the production of the less reactive intermediates, methane and ethane, through hydrogenolysis, hydrogenation, and dealkylation reactions [12]. The improved activity and selectivity due to the addition of extra-framework species has made possible commercial application of the other processes mentioned above i.e. Cyclar and Aroforming.

## 2.2. Dehydroaromatization of Methane

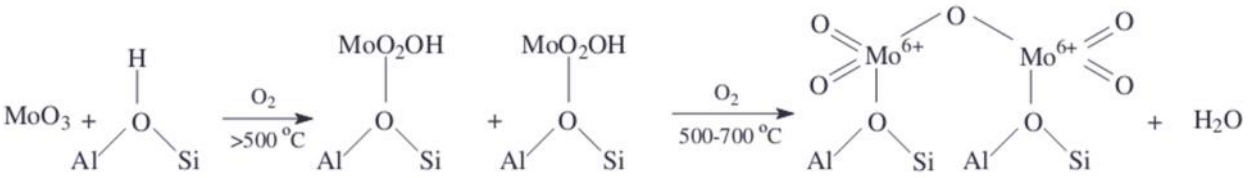
With long chain alkanes being more reactive and useful for production of aromatics and lead to the development of profitable processes; however, with the abundance of natural gas much interest was driven to use methane as the source for BTX. Wang et al [13] discovered that methane can be converted into benzene and other aromatic products under non-oxidative conditions over metal modified H-ZSM-5 zeolite catalysts at reaction temperatures above 700 $^{o}$C. The catalytic activity was greatly improved by addition of molybdenum (Mo) or zinc (Zn) without any detrimental effect on the benzene selectivity. Different transition metal ions supported on H-ZSM-5 were investigated and their activities towards methane conversion followed the trend Cr<V<Fe<W<Mo [14]. The use of molybdenum supported catalysts attracted much interest. These catalysts gave high activity and good benzene selectivity. High methane conversions were obtained for the acidified tungsten modified H-ZSM-5 zeolite catalyst [15-17]. It was found that W/H-ZSM-5 is a good catalyst for methane activation at reaction temperatures above 750 $^{o}$C because of its thermal properties. Tungsten based catalyst offer better resistance to sublimation that usually occurs for molybdenum based catalysts above 750 $^{o}$C. Ledoux et al. [18] studied the properties of Mo and W in their carbide forms and compared them with the properties of platinum. Based on their results they concluded that the catalytic properties of W/H-ZSM5 catalysts should be similar to that of a Mo/H-ZSM5 catalyst in their ability to activate $CH_4$. Hence, tungsten and molybdenum are regarded as the most promising catalytic components for dehydroaromatization of methane (MDA).

Further studies showed transition metal ions, strong acid sites, zeolite channel structures and small pore dimensions are vital for good catalytic activity and high benzene selectivity [19, 20]. ZSM-5, ZSM-8 and ZSM-11 zeolites were regarded as the best supports for molybdenum based catalysts for the MDA reaction because of their pore sizes and two dimensional channel structures [21-23]. Their catalytic activity for the MDA reaction was 5-10 times higher than that of catalysts supported on MCM-41 or SAPO 34. When using MOR, X and Y zeolite types low methane conversions were obtained with the formation of $C_2$ hydrocarbons and CO [9]. It was noted that the MDA reaction over Mo supported on MOR, USY and FSM-16 led to high selectivity towards carbonaceous deposits (>80%). Most authors agree that the structure of the ZSM-5 zeolite with two intersecting types; straight ($d$ = 5.3 X 5.6 Å) and zig-zag ($d$ = 5.1 X 5.6 Å) channels without large cavities favour the formation of small aromatic rings and prevents the accumulation for polyaromatic compounds leading to the formation of carbon deposits. Mo/MCM-22 catalysts were compared with Mo/H-ZSM-5 catalysts and it was found that Mo/MCM-22 gave better catalytic activity with a benzene selectivity of about 80%, as well as good resistance to carbonaceous deposits [24-26]. This proved that the presence of large cavities does not necessarily worsen the catalysts activity and catalyst lifetime during the MDA reaction is increased. The improved catalytic activity of the Mo/MCM-22 catalyst was ascribed to large cavities allowing better dispersion of molybdenum species and a rapid diffusion of aromatic compounds which led to the decrease in the polycondensation of aromatic compounds.

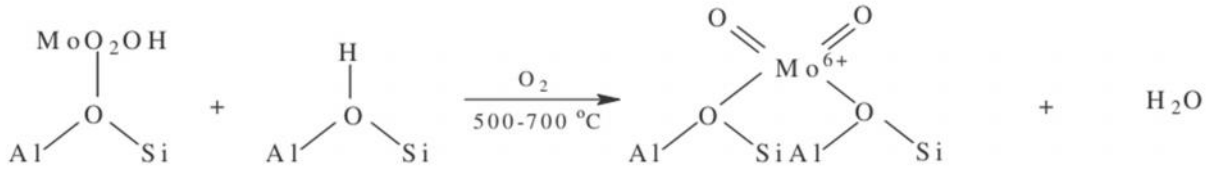
## 2.3. Formation and Nature of Active Sites

Since the aromatization of C2 and C3 alkanes proceed easily at lower reaction temperatures (ca. 300-500 $^{o}$C) over H-ZSM-5, Zn/H-ZSM-5 and Ga/H-ZSM-5 through a bi-functional mechanism, a similar bi-functional description of Mo/H-ZSM-5 catalysts is possible. This suggests that methane dehydrogenates and dimerizes on molybdenum species [27]. Based on the discovery of MDA over Mo/H-ZSM-5 [13] several researchers believed that $MoO_3$ crystallites were the active sites for methane activation. It was later discovered that molybdenum species and the Brønsted acid site of H-ZSM-5 zeolite are the active components of the catalyst [21]. It was shown by FT-IR spectroscopy that after impregnation with ammonium heptamolybdate (AHM) or ammonium paramolydate (APM) solutions that were dried overnight, molybdenum remained in its precursor form. During calcination at 400-500 $^{o}$C molybdenum oxide is formed in the Mo/H-ZSM-5 zeolite catalyst [20]. Borry et al. [28] studied the diffusion of $MoO_3$ species and their interaction

with the Brønsted acid sites. At 500 $^{o}$C low amounts of molybdenum oxide species were detected, as $MoO_3$ crystallites were finely dispersed on the external surface of the H-ZSM-5 before they migrated as $(MoO_x)_n$ oligomers into the zeolite channels via gas phase or surface diffusion. The $MoO_x$ species inside the zeolite channels react with $H^+$ atoms associated with Brønsted acid sites to form $[MoO_2(OH)]^+$ species, which can condense with one another to form $[Mo_2O_5]^{2+}$ dimers and $H_2O$ (Scheme 2.1). Using diffuse reflectance UV and Raman spectroscopy revealed that the molybdenum species anchored on the Brønsted acid sites exist in two different configurations, ($Mo_2O_7$) dimer and as a $MoO_4$ tetrahedral monomer [29]. The $[MoO_2(OH)]^+$ species can also react with zeolite OH groups to form $[MoO_2]^{2+}$ monomer. The monomer anchors on two bridging acid sites as illustrated in Scheme 2.2.




**Scheme 2.1:** Formation of a coordinated $[Mo_2O_5]^{2+}$ dimer on the Brønsted acid sites.




**Scheme 2.2:** Formation of the $[MoO_2]^{2+}$ cation bridging two Brønsted acid sites.

When the calcination temperature is increased to 700 $^{o}$C the extra-framework Al atoms will react with the molybdenum precursor to form aluminium molybdate $Al_2(MoO_4)_3$ [30, 31]. Jiang et al. [32] used Raman spectroscopy to identify that the molybdenum species have a octahedral geometry. Their findings were further confirmed by Zaikovskii et al. [33] who found molybdenum species in both octahedral and square pyramidal geometries using EPR. The anchoring sites and modes of Mo species are strictly dependent on the Si/Al ratio of the H-ZSM-5 zeolite. The dimeric species (Scheme 2.1) are more likely to form on the H-ZSM-5 zeolite

with high Si/Al ratio whereas the monomeric species form at low Si/Al ratio. The dimeric species are precursors for methane activation sites in Mo/H-ZSM-5 zeolite catalyst.

## 2.4. Induction Period of MDA Reaction

Molybdenum carbide species are the key component of molybdenum modified zeolite catalysts for methane activation in the MDA reaction. Ma et al [34] and Jiang et al. [32] studied the initial stage of methane aromatization and they found that the molybdenum oxide is transformed into molybdenum carbide, which they referred to as the induction period. With the use of temperature programmed surface reaction (TPSR) techniques using methane it was clearly demonstrated that there is a molybdenum phase transformation for the molybdenum modified catalysts during the early stage of the MDA reaction. After TPSR analysis the colour of the catalyst changed from blue-white to grayish-black indicating the transformation of molybdenum oxide species into molybdenum carbide species [10]. During the induction period methane partially reduces the $Mo^{6+}$ species on the external surface of the catalyst and some carbonaceous deposits react with partially reduced Mo species to form $Mo_2C$ species [32]. Only $H_2$, $CO_2$, CO and $H_2O$ were formed during the initial stage of the MDA reaction. Solymosi et al. [35-38] investigated the interaction of methane with supported and unsupported various molybdenum species (i.e. Mo, $MoO_2$, $MoO_3$, $Mo_2C$ and $MoC_{1-x}$) that might be present during the methane aromatization at 700 $^oC$. The results presented in their papers showed the formation of ethane, ethylene and benzene using the supported catalysts while the unsupported $Mo_2C$ catalyst showed low activity. The post-reaction catalyst analysis using X-ray photoelectron spectroscopy (XPS) revealed the presence of molybdenum carbide, which is formed when methane reduced $Mo^{6+}$ species into lower oxidation states [35, 39, 40]. However, a combination of XPS and EPR studies [6-9] of spent Mo/H-ZSM-5 zeolite catalysts showed that a small percentage of Mo remained in the higher oxidation state ($Mo^{5+}$) even after being exposed to methane for a long time. The presence of molybdenum carbide was clearly identified in the Mo/H-ZSM-5 and Mo/H-MCM-22 catalysts using other characterization techniques (EXAFS [41, 42], EPR [43-46], and HRTEM [33, 47]). In general, it was concluded that the presence of molybdenum carbide may be responsible for the activation of methane into a methyl radical.

TPSR profiles showed two reduction steps which indicated that the transformation of molybdenum oxide to molybdenum carbide occurred in two reduction stages before the formation of hydrocarbons [32, 34].

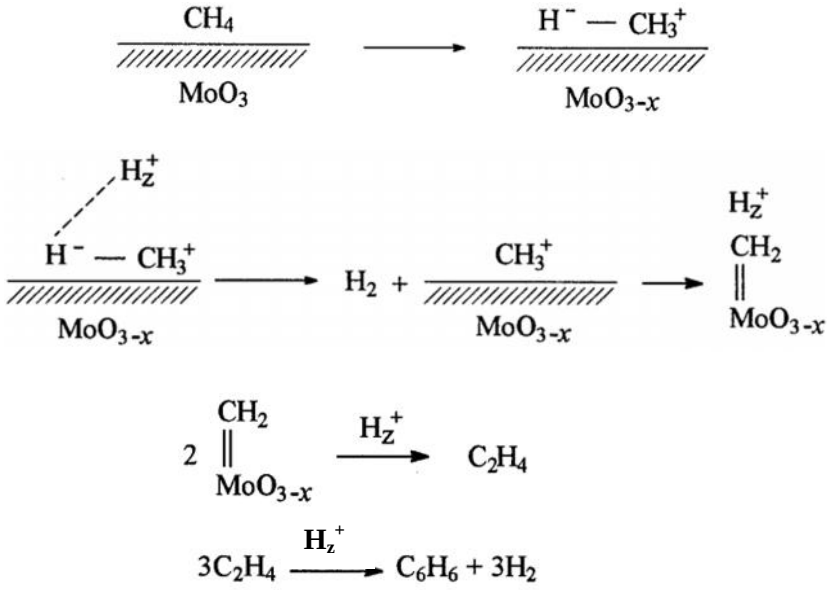
$$4MoO_3 + CH_4 \rightarrow 4MoO_2 + CO_2 + 2H_2O$$

$$2MoO_2 + 2CH_4 \rightarrow Mo_2C + 3H_2O + CO + H_2$$

The first stage involves the reduction of $MoO_3$ into $MoO_2$ by activated methane molecules. The activated methane retains its carbon in a form of methyl radical and releases the hydrogen. Both $CO_2$ and $H_2O$ are formed during the first stage [48, 49]. The second stage is said to be a rapid stage of the induction period. This stage is characterized by the formation of $H_2O$, CO and $H_2$ and is accompanied by a sharp increase of methane consumption. In this stage the activated methane releases both carbon and hydrogen. Once the catalyst bed is oxygen deficient the carbonaceous deposits interact with Mo species to form $Mo_2C$. The TPSR data showed that the formation of ethylene and benzene occurred after the induction period. However, Men et al. [50] in their studies detected the formation of benzene during the induction period and ascribed it to the reduction of $Mo^{6+}$ species which are considered to be slightly active methane aromatization species.

## 2.5. Reaction Mechanisms of Methane Aromatization

Based on the mechanism of the aromatization of short chain alkanes which is driven by a good balance between the dehydrogenating and acidic properties of the catalyst, Xu et al. [51] proposed a mechanism for methane aromatization over Mo/H-ZSM-5 catalysts (Scheme 2.3). They proposed that methane is adsorbed onto the surface of $MoO_3$ and one C-H bond in the $CH_4$ molecule is polarized through its interaction with $MoO_{3-x}$ species in the zeolite channel. The polarized $CH_4$ molecule will migrate onto the Brønsted acid site interface and form a cyclic intermediate with a proton and this will further lead to the formation of molybdenum carbene intermediates. Subsequently the carbene like intermediates will dimerize to produce ethylene and the ethylene will then aromatize on the Brønsted acid sites and the sites containing molybdenum species to produce benzene.




**Scheme 2.3:** Reaction mechanism of the MDA reaction proposed by Xu et al. [51].

Chen et al. [43] proposed another mechanism for methane aromatization. They suggested methane oligomerization is facilitated by molybdenum species in the zeolite channels and the Brønsted acid sites of H-ZSM-5. According to their mechanism methane is adsorbed on the MoOx species and dehydrogenated to $CH_3$ radicals. Two $CH_3$ radicals then couple with each other to form ethylene which then migrates onto the Brønsted acid site interface and aromatizes into benzene.

$$CH_4 \xrightarrow{MoO_x} CH_3^{\cdot} + H\cdot$$

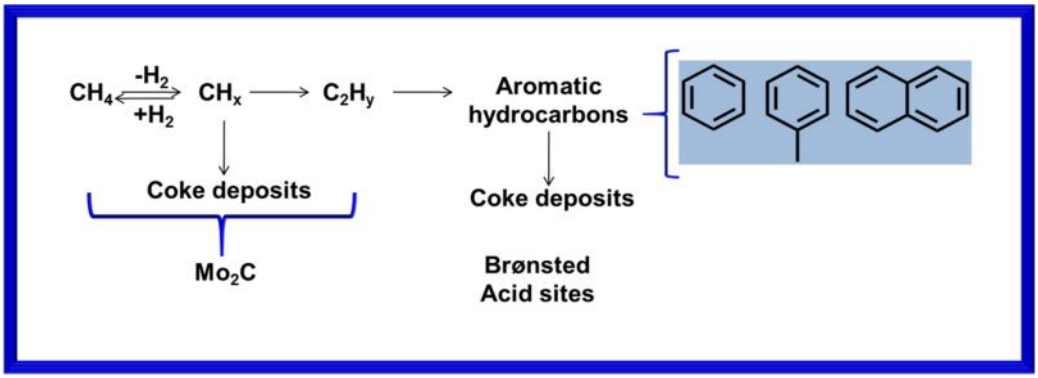
$$2CH_3^{\cdot} \xrightarrow{MoO_x} C_2H_4 + H_2$$

$$3C_2H_4 \xrightarrow{H^+} C_6H_6 + 3H_2$$

**Scheme 2.4:** Reaction mechanism of the MDA reaction proposed by Chen et al. [43].

The induction period studies brought clarity around the discourse about the active sites for methane aromatization. The Lunsford group [39] analyzed the catalyst after exposure to a methane gas mixture at 700 $^{o}$C. Using XPS they discovered the presence of $Mo_2C$ species in the Mo/H-ZSM-5 catalyst. From the work done by Solymosi's group [52, 53] it was concluded that

$Mo_2C$ species are the active sites for the activation of methane. The activation of methane is the cleavage of a C-H bond in the methane molecule that occurs on $Mo_2C$ and/or $Mo_xO_yC_z$ species. However, the $Mo_2C$ species are less active for further decomposition of the $CH_3$ and $CH_2$ species produced. The coupling of $CH_3$ and $CH_2$ radicals into ethylene has also been investigated and studies of the reaction of $CH_3$, $CH_2$ and $C_2H_5$ on $Mo_2C$/Mo(100) revealed that the formation of ethylene occurred on the $Mo_2C$ surface [27]. Ethylene which is regarded as the intermediate for benzene formation will migrate onto the Brønsted acid sites and it then undergoes oligomerization and cyclization reactions catalyzed by acid sites of the zeolite leading to the formation of benzene, toluene and naphthalene (Scheme 2.5). At high reaction temperatures, intermediates decompose into different carbonaceous species leading to the formation of an inactive carbon (i.e. coke) on the active sites [54].




**Scheme 2.5:** Reaction mechanism of the MDA reaction proposed by Ichikawa [55].

The three proposed mechanisms demonstrate that the transition metal carbides or metal oxides play a crucial role in methane activation and that the methane aromatization is also dependent on the acidic character of the H-ZSM-5 zeolite. However, based on the characterization of Mo/H-ZSM-5 zeolite catalyst before and after reaction it can be concluded that molybdenum carbide species are active to methane aromatization. This suggests that the mechanisms presented by Xu et al. [51] and Chen et al. [43] are out-dated as they propose that methane activation occurs on molybdenum oxide species as oppose to molybdenum carbide species.

## 2.6. The Role of Brønsted Acid Sites

It is generally accepted that the aromatization of alkane intermediates occurs on the Brønsted acid sites. However, zeolites possess both Lewis and Brønsted acid sites and it is understood that both acid sites facilitate the process of aromatization. In the proposed mechanisms, the $C_2$

intermediates are transformed to benzene on the Brønsted acid sites. MDA reactions were also investigated on $Mo/SiO_2$ catalysts with no Brønsted acid sites, and interestingly formation of aromatic compounds was noticed. It was suggested that Lewis acid sites facilitated the aromatization of $C_2$ intermediates. However, Liu et al. [56] and Su et al. [57] concluded that the formation of aromatic compounds is promoted by Brønsted acid sites and not by the Lewis acid sites.

A study on the effect of $SiO_2/Al_2O_3$ ratio on the catalytic activity and aromatic formation rate was performed in order to verify that Brønsted acid sites do form active component of the catalyst. The rate of benzene formation on Mo/H-ZSM-5 was found to be substantially dependent on the $SiO_2/Al_2O_3$ ratio. Ichikawa et al. [41] found maximum benzene yields and good catalytic activity with a 3%Mo/H-ZSM-5 catalyst with a $SiO_2/Al_2O_3$ ratio of about 40. The quantitative acid analysis by pyridine adsorption revealed that the concentration of Brønsted acid sites was at its optimum for the H-ZSM-5 with a $SiO_2/Al_2O_3$ ratio of 40. Bao and Lin [58, 59] found the catalytic activity of Mo/H-ZSM-5 catalysts with high Si/Al ratio was poor. The catalytic activity of Mo/H-ZSM-5 catalysts has been linked to the concentration of Brønsted acid sites of H-ZSM-5 present before and after calcination. Su et al. [57] pointed out that the Brønsted acid sites are the driving force for migration of $MoO_x$ species into the zeolite channel during calcination. On catalysts with a high Si/Al ratio (i.e. 125, the number of Brønsted acid sites per unit cell is less than 0.76) the degree of $MoO_x$ species to migrate into the zeolite channels will be drastically reduced. The location of $MoO_x$ species is thus important for the catalytic activity. Molybdenum species may be located on the external surface and in the zeolite channels. Iglesia and co-workers [60] demonstrated that the molybdenum species located on the external surface of the zeolite are less active and less stable in the MDA reaction over Mo/H-ZSM-5 catalysts when prepared by mechanical mixing.

Tessonnier et al. [61] studied the role of Brønsted acid sites in the MDA reaction over Mo/H-ZSM-5 catalysts. They demonstrated that the Si/Al ratio of H-ZSM-5 plays a role in the dispersion of molybdenum species in the zeolite channels. Acid sites act as anchoring sites for molybdenum inside the zeolite channels. Hence, $NH_3$-TPD studies showed a decrease in the concentration of Brønsted acid sites after loading molybdenum onto the zeolite. Molybdenum species replace the zeolitic proton in a 1:1 stoichiometry ratio and then form $(Mo_2O_5)^{2+}$ structures [28] as shown in Scheme 2.1. The Brønsted acid sites are also anchoring sites for carbonaceous deposits formed during the the MDA reaction. Relatively small concentrations of

Brønsted acid sites are required for the MDA reaction, while excessive amounts of free Brønsted acid sites cause a severe formation of carbonaceous deposits leading to catalyst deactivation [62-64].

## 2.7. Catalyst Deactivation

Most industries encounter a major problem from catalyst deactivation as a result of coke formation. The rate of deactivation seems to depend on the rate of formation of intermediates and products. However, the rate of deactivation can vary from one catalytic system to another. It has also been reported that only one atom of carbon out of 200 000 activated by the catalyst is transformed into coke during reforming, whereas in the cracking of heavy petroleum cuts there can even be more than one atom of carbon out of twenty form coke [65]. Some of the reasons that lead to deactivation are the following: (i) sites coverage, i.e. poisoning of the active sites by heavy carbonaceous products [66-68], (ii) pore blockage, i.e. deposition of carbonaceous compounds in cavities (this causes the pore to be inaccessible and therefore hinders the diffusion of reactants to the active sites in the pore) [69, 70] and (iii) structure alterations; this is caused by the change in the number and/or strength of the active sites [61].

### 2.7.1. Formation of Coke

Coke formation occurs through progressive dehydrogenation, condensation, polymerisation and cyclization of hydrocarbon species on the surface of the catalyst and most of the direct precursors are olefins and aromatics [71, 72]. These precursors are formed on the metallic active sites and they migrate to the support and get irreversibly deposited through condensation and polymerisation reactions forming a polyaromatic/graphite type of coke [73, 74]. An example of the coke components are: poly-aromatics that are mostly in linear conjunction forms, such as naphthalene, anthracene and tetracene. Coke formation is a process which is favoured by high temperatures and low pressures, but the chemical reactions producing coke can be diverse. Therefore the nature and origins of different types of coke should be taken into consideration. In the aromatization of an alkane, carbonaceous deposits form via bi-functional reactions with both the transition metal species and acid sites involved. The dehydrogenating character of the transition metal and the condensation-polymerisation capacity of the acid sites [26] are the active sites for the formation of carbonaceous deposits [75].

In methane aromatization, coke deposition has an effect on the catalysts activity and selectivity of the molybdenum modified catalysts. It was found that the selectivity towards coke was between 20 and 40% and with increase in time and reaction temperature the total amount of coke increased gradually. The amount of coke is also dependent on the concentration of molybdenum in the zeolite. Ma et al. [45, 76] found that the formation rate of coke at low molybdenum loadings (between 0 and 2 wt.%) increased linearly with increase in Mo loading of Mo/MCM-22 and remained constant for catalysts with high molybdenum loadings (i.e. 2-20%).

Weckhuysen et al. [77] studied the nature of carbonaceous deposits on Mo/HZSM-5 catalysts after the MDA reaction at 700 $^{o}$C for 13 hours. Three types of carbon species were identified by XPS. From their results they identified the presence of carbide carbon which is associated with $Mo_2C$ mainly located in the zeolite channels (C1 BE of 282.7 eV). Two other peaks of carbon were noted. A BE of C1 283.2 eV is associated with a pre-graphite carbon or hydrogen poor sp-type carbon, and carbon with graphite structure was assigned to a peak at BE of C1 284.6 eV. The pre-graphite carbonaceous deposits are located on the external surface of the zeolite whereas the graphite carbonaceous deposits are formed in the zeolite channels. During the MDA reaction at 700 $^{o}$C the hydrogen poor sp-type carbon anchors on the active sites and with increase in reaction time this carbon covers both the zeolite surface and the $Mo_2C$ phase. This type of carbon is responsible for deactivation of Mo/H-ZSM-5 catalysts during the MDA reaction. Jiang et al. [32] used $^{13}$C solid state NMR spectroscopy to distinguish the carbonaceous deposits. They concluded that there were two kinds of carbonaceous deposits; one associated with Brønsted acid sites and the other was associated with molybdenum carbide or partially reduced Mo species.

Several authors used temperature programmed techniques to characterize the nature of carbonaceous deposits on Mo/H-ZSM-5 and Mo/MCM-22 catalysts [58, 76, 78]. The two types of carbonaceous deposits were characterized by low oxidation temperatures (503 and 470 $^{o}$C) and high oxidation temperatures (543, 557 and 592 $^{o}$C) distinguished by TPO [34, 56, 79]. The TPO data is in agreement with the results obtained by the investigation of carbonaceous deposits by TGA. The TPO profile of Mo/H-ZSM-5 revealed three oxidation peaks at different temperatures (459, 511 and 558 $^{o}$C) which were assigned to three types of carbonaceous deposits; (i) carbon associated with Mo sites on the external surface of the zeolite, (ii) carbon associated with Mo sites in the zeolite channels and (iii) polyaromatic carbon associated with Brønsted acid sites [34, 56]. It is worth noting that it is difficult to distinguish the oxidation peaks of the two carbons associated with molybdenum species. Thus in many studies where TPO

has been used, only two oxidation peaks were obtained. Liu et al. [56] noticed that the amount of carbonaceous deposits associated with molybdenum species, almost remained constant while that associated with Brønsted acid sites decreased for catalysts calcined at higher temperature. This was ascribed to the decrease in the concentration of Brønsted acid sites at high calcination temperature. They concluded that Brønsted acid sites can provide active sites not only for the formation of desired products (i.e. aromatic products), but also for coke deposition, which usually lead to deactivation of Mo/H-ZSM-5 catalysts during the MDA reaction.

## 2.8. Summary

Dehydroaromatization of methane over H-ZSM-5 under non-oxidative conditions can be seen as a pathway which bridges the fossil fuel energy era with the new developments for hydrogen use in fuel cells. Hydrogen is a product of methane conversion, while other basic chemicals such as benzene can also be produced from the reaction. Therefore the development of MDA is a potentially important process for hydrogen production, together with formation of aromatics. However, the MDA reaction suffers from several shortcomings that have negative effects on its possible commercialization. The process is thermodynamically limited and the catalyst suffers rapid deactivation.

The physiochemical properties of the parent zeolite have a significant effect on the catalytic activity and product selectivity. It is very necessary to consider the zeolite type and the concentration of Brønsted acid sites of the zeolite before performing the MDA reaction. Zeolites (H-ZSM-5) with pore size close to the diameter of the benzene molecule provide good catalytic activity and high benzene selectivity. However, MCM-22 was found to be good in reducing the total amount of carbonaceous deposits because of the absence of diffusion limitations. The location of Mo species is determined by the concentration of Brønsted acid sites and $SiO_2/Al_2O_3$ ratios. The acid sites play a role for the Mo species to migrate into the zeolite channels and Mo species will also anchor on the Brønsted acid sites. Brønsted acid sites participate in the Mo stabilization process in the zeolite channels. Addition of molybdenum alters the textural and acid properties of the parent zeolite. The change in these properties depends extensively on the concentration of molybdenum and on the location of Mo species in the zeolite. Subsequently this may also influence the formation of carbonaceous deposits during the MDA reaction.

In the initial stage of the MDA reaction the $MoO_3$ is transformed into $Mo_2C$ species. It has been generally accepted that $Mo_2C$ species are the active sites for methane activation. Methane is converted into benzene via a bi-functional mechanism. Firstly, methane is activated on molybdenum carbide or oxy-carbide to form $C_2$ intermediates (ethane and ethylene) which subsequently migrate onto the Brønsted acid sites and then converted into aromatic compounds. The aromatization process is accompanied by the formation of carbonaceous deposits which contribute in the deactivation of the Mo/H-ZSM-5 catalyst. The nature of carbonaceous deposits has been identified as being due to carbonic carbon associated with $Mo_2C$, graphitic carbon and the hydrogen poor sp-type carbon. It was established that the hydrogen sp-type carbon forms on the Brønsted acid sites and is responsible for catalyst deactivation.

## 2.9. Reference List

[1] S.M. Csicsery, *Journal of Catalysis*, **17** (1970) 207.

[2] S.M. Csicsery, *Journal of Catalysis*, **17** (1970) 216.

[3] S.M. Csicsery, *Journal of Catalysis*, **17** (1970) 315.

[4] S.M. Campbell, D.M. Bibby, J.M. Coddington, R.F. Howe, *Journal of Catalysis*, **161** (1996) 350.

[5] X. Chen, S. Huang, D. Cao, W. Wang, *Fluid Phase Equilibria*, **260** (2007) 146.

[6] T.-C. Tsai, I. Wang, C.-K. Huang, S.-D. Liu, *Applied Catalysis A: General*, **321** (2007) 125.

[7] X. Wang, H. Carabineiro, F. Lemos, M.A.N.D.A. Lemos, F. Ramôa Ribeiro, *Journal of Molecular Catalysis A: Chemical*, **216** (2004) 131.

[8] Y. Xu, L. Lin, *Applied Catalysis A: General*, **188** (1999) 53.

[9] Y. Shu, M. Ichikawa, *Catalysis Today*, **71** (2001) 55.

[10] Y. Xu, X. Bao, L. Lin, *Journal of Catalysis*, **216** (2003) 386.

[11] M.G. Sanchez, *PhD Thesis*, *Eindhoven University of Technology, Netherlands*, (2003).

[12] P. Meriaudead, C. Naccache, *Catalysis Reveiw-Science and Engineering*, **39** (1997) 5.

[13] L. Wang, L. Tao, M. Xie, G. Xu, J. Huang, Y. Xu, *Catalysis Letters*, **21** (1993) 35.

[14] B.M. Weckhuysen, D. Wang, M.P. Rosynek, J.H. Lunsford, *Journal of Catalysis*, **175** (1998) 347.

[15] Z.-T. Xiong, H.-B. Zhang, G.-D. Lin, J.-L. Zeng, *Catalysis Letters*, **74** (2001) 233.

[16] Z.-T. Xiong, L.-L. Chen, H.-B. Zhang, J.-L. Zeng, G.-D. Lin, *Catalysis Letters*, **74** (2001) 227.

[17] J.L. Zeng, Z.T. Xiong, H.B. Zhang, G.D. Lin, K.R. Tsai, *Catalysis Letters*, **53** (1998) 119.

[18] M.J. Ledoux, P.H. Cuong, J. Guille, H. Dunlop, *Journal of Catalysis*, **134** (1992) 383.

[19] Y. Xu, S. Liu, X. Guo, L. Wang, M. Xie, *Catalysis Letters*, **30** (1994) 135.

[20] Y. Xu, Y. Shu, S. Liu, J. Huang, X. Guo, *Catalysis Letters*, **35** (1995) 233.

[21] C.-L. Zhang, S. Li, Y. Yuan, W.-X. Zhang, T.-H. Wu, L.-W. Lin, *Catalysis Letters*, **56** (1998) 207.

[22] G.A. Jablonski, L.B. Sand, J.A. Gard, *Zeolites*, **6** (1986) 396.

[23] M.A. Camblor, A. Corma, J. Pérez-Pariente, *Zeolites*, **13** (1993) 82.

[24] Y. Shu, R. Ohnishi, M. Ichikawa, *Applied Catalysis A: General*, **252** (2003) 315.

[25] V.T.T. Ha, L.V. Tiep, P. Meriaudeau, C. Naccache, *Journal of Molecular Catalysis A: Chemical*, **181** (2002) 283.

[26] Y. Shu, D. Ma, L. Xu, Y. Xu, X. Bao, *Catalysis Letters*, **70** (2000) 67.

[27] F. Solymosi, L. Bugyi, A. Oszkó, I. Horváth, *Journal of Catalysis*, **185** (1999) 160.

[28] R.W. Borry, Y.H. Kim, A. Huffsmith, J.A. Reimer, E. Iglesia, *Journal of Physical Chemistry B*, **103** (1999) 5787.

[29] W. Li, G.D. Meitzner, R.W. Borry Iii, E. Iglesia, *Journal of Catalysis*, **191** (2000) 373.

[30] G. Mestl, H. Knözinger, Vibrational Spectroscopy, in: Handbook of Heterogeneous Catalysis, Wiley-VCH Verlag GmbH & Co. KGaA, 2008.

[31] L. Mosqueira, S.a. Gómez, G.a. Fuentes, *Journal of Physics: Condensed Matter*, **16** (2004) S2319.

[32] H. Jiang, L. Wang, W. Cui, Y. Xu, *Catalysis Letters*, **57** (1999) 95.

[33] V.I. Zaikovskii, A.V. Vosmerikov, V.F. Anufrienko, L.L. Korobitsyna, E.G. Kodenev, G.V. Echevskii, N.T. Vasenin, S.P. Zhuravkov, E.V. Matus, Z.R. Ismagilov, V.N. Parmon, *Kinetics and Catalysis*, **47** (2006) 389.

[34] D. Ma, Y. Shu, M. Cheng, Y. Xu, X. Bao, *Journal of Catalysis*, **194** (2000) 105.

[35] F. Solymosi, J. Cserényi, A. Szöke, T. Bánsági, A. Oszkó, *Journal of Catalysis*, **165** (1997) 150.

[36] F. Solymosi, A. Erdöhelyi, A. Szöke, *Catalysis Letters*, **32** (1995) 43.

[37] F. Solymosi, A. Szöke, J. Cserényi, *Catalysis Letters*, **39** (1996) 157.

[38] A. Szöke, F. Solymosi, *Applied Catalysis A: General*, **142** (1996) 361.

[39] D. Wang, J.H. Lunsford, M.P. Rosynek, *Journal of Catalysis*, **169** (1997) 347.

[40] S. Qi, B. Yang, *Catalysis Today*, **98** (2004) 639.

[41] S. Liu, L. Wang, R. Ohnishi, M. Ichikawa, *Journal of Catalysis*, **181** (1999) 175.

[42] S. Liu, L. Wang, R. Ohnishi, M. Lchikawa, *Kinetics and Catalysis*, **41** (2000) 132.

[43] L.Y. Chen, L.W. Lin, Z.S. Xu, X.S. Li, T. Zhang, *Journal of Catalysis*, **157** (1995) 190.

[44] H. Liu, X. Bao, Y. Xu, *Journal of Catalysis*, **239** (2006) 441.

[45] D. Ma, Y. Shu, X. Bao, Y. Xu, *Journal of Catalysis*, **189** (2000) 314.

[46] N. Vasenin, V. Anufrienko, I. Ismagilov, T. Larina, E. Paukshtis, E. Matus, L. Tsikoza, M. Kerzhentsev, Z. Ismagilov, *Topics in Catalysis*, **32** (2005) 61.

[47] E.V. Matus, I.Z. Ismagilov, O.B. Sukhova, V.I. Zaikovskii, L.T. Tsikoza, Z.R. Ismagilov, J.A. Moulijn, *Industrial & Engineering Chemistry Research*, **46** (2006) 4063.

[48] J.H. Lunsford, *Catalysis Today*, **63** (2000) 165.

[49] S. Masiero, N. Marcilio, O. Perez-Lopez, *Catalysis Letters*, **131** (2009) 194.

[50] L. Men, L. Zhang, Y. Xie, Z. Liu, J. Bai, G. Sha, J. Xie, *Chemical Communications*, **0** (2001) 1750.

[51] Y. Shu, Y. Xu, S.-T. Wong, L. Wang, X. Guo, *Journal of Catalysis*, **170** (1997) 11.

[52] F. Solymosi, A. Szo˝ke, *Applied Catalysis A: General*, **166** (1998) 225.

[53] F. Solymosi, A. Szőke, *Studies in Surface Science and Catalysis*, **119** (1998) 355.

[54] A.M. Rigby, G.J. Kramer, R.A. van Santen, *Journal of Catalysis*, **170** (1997) 1.

[55] R. Ohnishi, S. Liu, Q. Dong, L. Wang, M. Ichikawa, *Journal of Catalysis*, **182** (1999) 92.

[56] H. Liu, W. Shen, X. Bao, Y. Xu, *Applied Catalysis A: General*, **295** (2005) 79.

[57] L. Su, Y. Xu, X. Bao, *Journal of Natural Gas Chemistry*, **11** (2002) 18.

[58] Y. Lu, D. Ma, Z. Xu, Z. Tian, X. Bao, L. Lin, *Chemical Communications*, **0** (2001) 2048.

[59] Y. Lu, Z. Xu, Z. Tian, T. Zhang, L. Lin, *Catalysis Letters*, **62** (1999) 215.

[60] W. Ding, G.D. Meitzner, E. Iglesia, *Journal of Catalysis*, **206** (2002) 14.

[61] J.-P. Tessonnier, B. Louis, S. Rigolet, M.J. Ledoux, C. Pham-Huu, *Applied Catalysis A: General*, **336** (2008) 79.

[62] J. Shu, A. Adnot, B.P.A. Grandjean, *Industrial & Engineering Chemistry Research*, **38** (1999) 3860.

[63] P.L. Tan, Y.L. Leung, S.Y. Lai, C.T. Au, *Applied Catalysis A: General*, **228** (2002) 115.

[64] Y. Shu, D. Ma, X. Bao, Y. Xu, *Catalysis Letters*, **66** (2000) 161.

[65] D.L. Trimm, *Catalysis Today*, **49** (1999) 3.

[66] J.H. Bitter, K. Seshan, J.A. Lercher, *Journal of Catalysis*, **183** (1999) 336.

[67] M. Guisnet, P. Magnoux, *Applied Catalysis A: General*, **212** (2001) 83.

[68] A.T. Aguayo, A.E.S.d. Campo, A.G. Gayubo, A. Tarrío, J. Bilbao, *Journal of Chemical Technology & Biotechnology*, **74** (1999) 315.

[69] S. van Donk, J.H. Bitter, K.P. de Jong, *Applied Catalysis A: General*, **212** (2001) 97.

[70] L.D.T. Câmara, K. Rajagopal, D.A.G. Aranda, *Studies in Surface Science and Catalysis*, **139** (2001) 61.

[71] S.K. Sahoo, P.V.C. Rao, D. Rajeshwer, K.R. Krishnamurthy, I.D. Singh, *Applied Catalysis A: General*, **244** (2003) 311.

[72] S. He, C. Sun, X. Yang, B. Wang, X. Dai, Z. Bai, *Chemical Engineering Journal*, **163** (2010) 389.

[73] H.G. Karge, *Studies in Surface Science and Catalysis*, **58** (1991) 531.

[74] R. Mann, *Catalysis Today*, **37** (1997) 331.

[75] K.-Y. Lee, M.-Y. Kang, S.-K. Ihm, *Journal of Physics and Chemistry of Solids*, **73** (2012) 1542.

[76] D. Ma, D. Wang, L. Su, Y. Shu, Y. Xu, X. Bao, *Journal of Catalysis*, **208** (2002) 260.

[77] B. Weckhuysen, M. Rosynek, J. Lunsford, *Catalysis Letters*, **52** (1998) 31.

[78] H. Liu, L. Su, H. Wang, W. Shen, X. Bao, Y. Xu, *Applied Catalysis A: General*, **236** (2002) 263.

[79] H. Liu, T. Li, B. Tian, Y. Xu, *Applied Catalysis A: General*, **213** (2001) 103.

# Chapter 3

# Experimental

## 3.1. Material Used

Fumed silica Aerosil 200 (Degussa), aluminium hydroxide (Fluka), Sodium hydroxide (Saarchem), tetrapropylammonium bromide (TPABr) (Fluka), ammonium heptamolybdate (Saarchem), tin chloride (Aldrich), dihydrogen hexachloroplatinate (Impala Platinum mine), manganese nitrate (Aldrich), ammonium paratungstate (Aldrich), 90% methane balance argon mixture (Afrox).

## 3.2. Synthesis of H-ZSM-5 Zeolite Catalyst

The hydrogen form ZSM-5 zeolite catalysts with $SiO_2/Al_2O_3$ ratio of 70 were synthesized by a hydrothermal treatment method at 150 $^oC$ [1, 2]. The MFI structure and percentage XDR crystallinity of the H-ZSM-5 zeolite was confirmed by powder-XRD. A sodium aluminate solution was prepared by mixing 17.9 g of NaOH with 2.98 g of $Al(OH)_3$ in 75 mL of distilled water. The mixture is then heated and stirred to obtain a clear solution. The template solution was prepared by dissolving 29.7 g of tetrapropylammonium bromide (TPABr) in 75 mL of distilled water. A slurry solution of fumed silica was prepared by mixing 80.4 g of Aerosil 200 with 650 mL distilled water. A blender was used to stir the mixture until a smooth jellylike form was consistently obtained. The sodium aluminate and template mixtures were then added to the silica slurry under vigorous stirring and the mixture was transferred to an autoclave equipped with a 1000 mL Teflon vessel. The contents were allowed to crystallize at a specific temperature, for 72 hours, under stirring conditions. After the hydrothermal treatment, the autoclave contents were filtered and washed with deionized water until the filtrate was bromide and hydroxide free. This was detected by using a silver nitrate solution. The resulting product was then dried at 120 $^oC$ for 16 hours and calcined at 630 $^oC$ for 3.5 hours to remove the

template. The resulting product is Na-ZSM-5. To obtain the $NH_4$-ZSM-5 form of the zeolite, the calcined Na form of the zeolite was treated with a 1M $NH_4Cl$ solution at room temperature under stirring conditions for 1 hour. The contents were filtered and washed to remove the chloride ions. The sample was further calcined at 530 $^oC$ for 3 hours to obtain the acidic form of the zeolite i.e. H-ZSM-5.

## 3.3. Catalysts Characterization

### *3.3.1. Nitrogen Adsorption (BET) Analysis*

BET surface areas and pore volumes were determined using an ASAP-2000 Tristar Micromeritics 3300 series instrument. About 0.20 g of a sample was degassed at 400 $^oC$ for 4 hours prior to surface measurements. After the degassing process the samples were then loaded on the analysis station for determination of the isotherms at -195 $^oC$.

### *3.3.2. Ammonia Temperature Programmed Desorption ($NH_3$-TPD)*

The $NH_3$-TPD experiments were performed in a U-shaped quartz tubular reactor charged with 0.2 g sample. The sample was degassed with helium gas flowing at 40 mL/min with the temperature increasing to 500 $^oC$ at a rate of 10 $^oC$/min. The sample was held at 500 $^oC$ for 30 min and then cooled to 100 $^oC$ in helium. A mixture of ammonia and helium (4% $NH_3$, balance He) was passed over the sample for 1 hour at 100 $^oC$ for the adsorption of ammonia on the surface of the catalyst. Desorption of ammonia was carried out in helium at a flow rate of 40 mL/min while heating the sample from 100 to 700 $^oC$ at a 10 $^oC$/min heating rate. The $NH_3$-TPD profiles were obtained by measuring the amount of ammonia desorbed relative to the temperature, using a mass spectrometer.

### 3.3.3. Hydrogen Temperature Programmed Reduction ($H_2$-TPR)

Experiments were carried out in a Micromeritics Autochem 2910 instrument. Samples of 0.15 g were loaded in a U-shaped quartz tubular reactor and heated under an argon gas atmosphere at a rate of 10 °C/min to 500 °C for 30 minutes, then cooled to 50 $^{o}$C under argon. When performing the TPR analysis the sample was exposed to a gas mixture of hydrogen and argon (5% $H_2$, balance Ar) at a flow rate of 50 mL/min and heated to 900 °C at a 10 °C/min heating rate. The change in the amount of hydrogen flowing in both the reference and reactor was monitored by TCD.

### 3.3.4. Carbon Monoxide Adsorption: Fourier Transform Infrared (FTIR) Spectroscopy

The IR spectra were recorded using a Perkin-Elmer 100 spectrometer with a maximum resolution of 4 $cm^{-1}$. Self-supporting discs of 16 mm in diameter, weighing about 40 mg were prepared from a powder sample by applying 3 tons using a presser. The discs were then suspended in a quartz disc holder and mounted in a IR cell connected to a vacuum line. Prior to adsorption measurements the discs were heated to 400 $^{o}$C in nitrogen for 1 hour and evacuated to a pressure of approximately 3 x $10^{-3}$ mbar for 1 hour. The IR CO adsorption measurements were performed at various CO pressures (range of 1 and 50 Torr) at beam temperature of ca. 25 $^{o}$C. The IR spectra were captured after 15 minutes intervals.

### 3.3.5. Pulse Carbon Monoxide Chemisorption

Carbon monoxide chemisorption experiments were carried out using a Micromeritics Autochem 2910 instrument. All catalysts were reduced at 200 $^{o}$C in a hydrogen mixture (5% $H_2$, balance Ar) for 1 hour and cooled to room temperature in helium. The pulsing experiments were carried out using a 404 µL sample loop filled with a mixture of carbon monoxide and helium (5% CO, balance He) being injected to the sample which was held at 50 $^{o}$C in helium. The percentage metal dispersion was calculated from the CO uptake assuming a CO/Pt stoichiometry of 1. The

stoichiometry ratio was taken from the CO adsorption FT-IR spectra which showed only a linear interaction between CO and platinum.

### *3.3.6. X-ray Photoelectron Spectroscopy (XPS) Analysis*

XPS spectra were captured with a PHI 5000 Versaprobe Scanning ESCA Microprobe spectrometer equipped with a monochromatic Al X-ray beam (100 µm, 12.5W, 15 kV). The sample were sputtered with Ar ion gun (2 kV,2 µA, 1x1 raster) at a sputter rate of 17 nm/min. The binding energies are referenced to the C(1s) binding energy of adventitious carbon contamination taken to be 284.7 eV.

### *3.3.7. Powder X-Ray Diffraction (XRD)*

Powder X-ray diffraction data were collected using a Brucker AXS D8 diffractometer equipped with a primary beam Gobel mirror, a radial Soller slit, a VAntec-1 detector and using Cu-Kα radiation (40 kV, 40 mA). Data were collected in the 2θ range 5 to $90^{o}$ in $0.021^{o}$ steps, using a scan speed resulting in an equivalent counting time of 14.7 s per step.

### *3.3.8. Thermogravimetric Analysis (TGA) Measurements*

TGA measurements of coked catalysts were performed in a TGA-4000 (Perkin Elmer) analyzer using Pyris software. These experiments were performed under air atmosphere to quantify the amount of coke deposited on the catalyst during the MDA reaction. About 10 mg of the catalyst was placed on the sample holder and the air flow rate was adjusted to 20 mL/min. The sample was heated from 35 $^{o}$C to 900 $^{o}$C at a heating rate of 10 $^{o}$C/min.

## 3.4. Catalytic Evaluation of the MDA Reaction

The direct conversion of methane was carried out in a fixed bed quartz tubular reactor at atmospheric pressure. A 0.50 g catalyst sample was loaded in a reactor and pretreated at 700 °C for 1 hour under a flow of nitrogen. A gas mixture of methane and argon (90% $CH_4$, balance Ar) was then introduced at a flow rate of 13.5 mL/min. The effluents were analyzed using an online gas chromatography (GC) equipped with a Porapak Q and Carboxen-1000 columns and coupled to a FID and TCD, respectively using. The GC traces were monitored by a computer equipped with Clarity software.

### *3.4.1. Calculations*

$$Methane\ Conversion\ (\%) = \left\{1 - \frac{CH_{4(in)} \times Ar_{(out)}}{CH_{4(out)} \times Ar_{(out)}}\right\} X\ 100\%$$

$$Selectivity\ (\%)_{Pi} = \frac{\%P_i}{Methane\ Conversion\ (\%)}\ X\ 100\%$$

$$Coke\ Selectivity\ (\%) = \left\{100 - \sum Selectivity_{Pi}\right\}$$

## 3.5. Reference List

[1] C.P. Nicolaides, *Applied Catalysis A*, **185** (1999) 211.

[2] NP Sincadu, PhD thesis, University of the Witwatersrand, 2003.

# Chapter 4

# Dehydroaromatization of Methane over Noble Metal loaded Mo/H-ZSM-5 Zeolite Catalysts

## 4.1. Introduction

Since the discovery of methane aromatization using molybdenum modified H-ZSM-5 zeolite catalysts at 700 $^{o}$C by Wang [1] many papers on the catalytic activity, reaction mechanism and catalyst characterization have been published [2-8]. Solymosi et al. [9, 10] investigated the interaction of methane with various supported and unsupported molybdenum species (i.e. Mo, $MoO_2$, $MoO_3$, $Mo_2C$ and $MoC_{1-x}$) that might be present during the methane aromatization at 700 $^{o}$C. The results presented in their papers showed the formation of ethane, ethylene and benzene on the supported catalysts. The post reaction analysis using XPS revealed the presence of molybdenum carbides and unreduced $Mo^{4+}$ and $Mo^{5+}$ species formed during the catalytic reaction. They also suggested that $Mo_2C$ is the active surface species in the Mo-containing catalysts. The Jiang group [11] studied the formation of molybdenum carbide during the aromatization of methane, which they referred to as the induction period. The Lunsford group [12-16] carried out some work using XPS to characterize Mo/H-ZSM-5 catalysts during the methane dehydroaromatization (MDA) reaction. Their results indicated a gradual reduction of $Mo^{6+}$ species to lower oxidation state molybdenum species occurring with reaction time leading to the formation of molybdenum carbide species. The formation of the molybdenum carbide species within the channels and pores of the zeolites is considered as the induction period. Ha et al. [17] and Tan et al. [18] have drawn some conclusions and proposed that the formation of molybdenum carbide or oxycarbide from reduction of MoOx with methane is responsible for the activation and conversion of methane into $C_2$ intermediates, which are then transformed into aromatic compounds, mainly benzene. Based on the induction period reaction studies, they proposed that coke-modified $Mo_2C$ surface species are the active sites responsible for the formation of ethylene

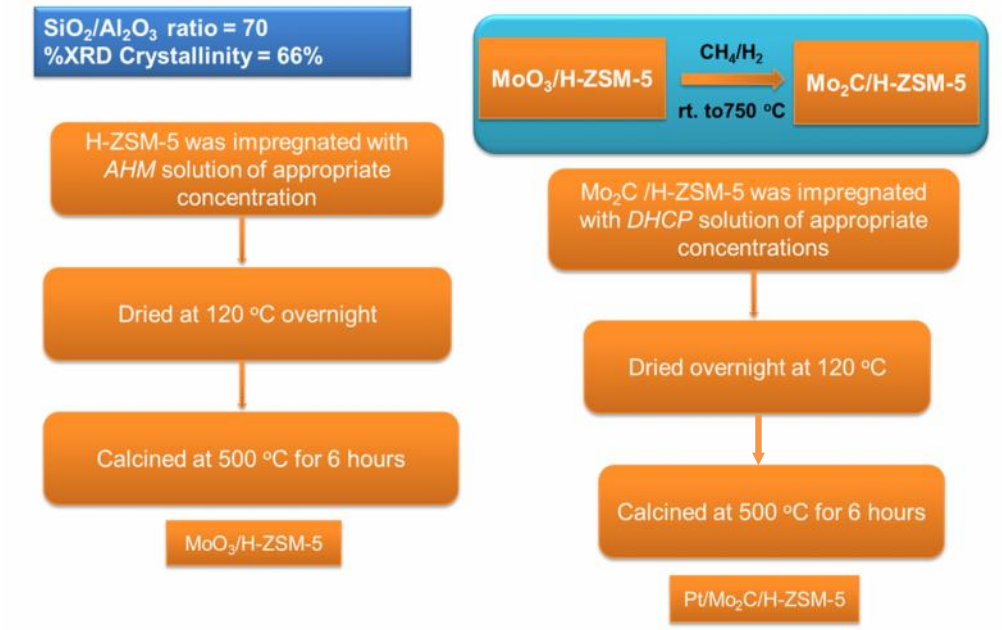
rather than the clean $Mo_2C$ surface. Ma et al. [19] concluded that the activation of methane is the crucial step in the MDA reaction. Regarding catalytic activity, there are drawbacks associated with carbonaceous deposits forming on the catalyst active sites leading to a shortened catalyst life cycle and rapid catalyst deactivation. Addition of a second metal to Mo/H-ZSM-5 could have a positive effect on the activity, selectivity and catalyst deactivation rate [3]. For instance, addition of cobalt or iron to a Mo/H-ZSM-5 zeolite catalyst effectively enhanced the catalytic stability in the presence of $CO_2$ [20-22]. Metals such as Cu [11], Zr and W [2] improved the catalytic activity and selectivity to aromatics. Shu et al. [23] studied the effect of ruthenium on the catalyst characteristics of Mo/H-ZSM-5. Their results showed that addition of ruthenium decreased the concentration of Brønsted acid sites and increased the concentration of weak acid sites. On the other hand, the presence of ruthenium led to the generation of medium acid sites. However, all secondary metals added will have a positive effect on the catalytic activity and selectivity of Mo/H-ZSM-5. For example, the presence of lithium [24], phosphorus [24] or vanadium [2] to the Mo/H-ZSM-5 zeolite catalyst was found to produce a low catalytic activity and this was attributed to a decrease in concentration of Brønsted acid sites. The difference between the Ru and other metals is that ruthenium facilitates the hydrogenolysis of carbon and this led to reduction of coke deposits and improves the catalytic activity by reducing the amount of coke deposit generated during the reaction. The presence of noble metals also facilitates the formation of $\alpha$-$Mo_2C$ which is regarded to be more stable than $\beta$-$Mo_2C$ [7, 25].

The bimetallic noble metal containing catalyst systems have attracted much attention in catalysis. The noble and secondary metal interaction changes both the catalytic and chemisorptive properties of both the metals added to the catalyst. In this chapter we have focused on the effect of platinum on the catalytic properties of Mo/H-ZSM-5 zeolite catalyst at low molybdenum loadings (i.e. 2 wt%Mo). The ex-situ carburization of a Mo/H-ZSM-5 catalyst was performed at 750 $^{o}$C prior to addition of platinum. The Pt-Mo interaction was studied at low platinum loadings, from 0.5 to 2 wt.%, using infrared spectroscopy with CO as the probe molecule. Furthermore, the effect of platinum on the catalytic activity of methane aromatization was performed at 700 $^{o}$C for 7 hours and the influence of platinum on coke suppression during the reaction was analyzed by TGA. The effect of other noble metals (i.e. palladium and ruthenium) on the MDA over Mo/H-ZSM-5 was investigated for comparison purpose.

## 4.2. Experimental

### 4.2.1. Catalysts Preparation

The preparation of $MoO_3$/HZSM-5 catalysts involved the incipient wetness impregnation of H-ZSM-5 with an aqueous solution of ammonium heptamolybdate, $(NH_4)_6Mo_7O_{24}\cdot 4H_2O$. The samples were dried at 120 $^oC$ and then calcined at 500 $^oC$ for 6 hours. The carbided form of the Mo/H-ZSM-5 samples were prepared by heating $MoO_3$/H-ZSM-5 under a flow of $CH_4/H_2$ (in 10/90 ratio by flow rate) from room temperature to 750 $^oC$ at a 10 $^oC$/min heating rate and held at 750 $^oC$ for 1 hour. The samples were allowed to cool to room temperature under a flow of nitrogen. Platinum was loaded on the $Mo_2C$/H-ZSM-5 samples by the incipient wetness impregnation methods with solutions of dihydrogen hexachloroplatinate, $H_2PtCl_6$, of appropriate concentration to give 0.5 to 2 wt.% loadings. The samples were dried at 120 $^oC$ overnight and then calcined at 500 $^oC$ for 6 hours.




**Scheme 4.1:** Schematic representation of the catalyst preparation steps of platinum modified $Mo_2C$/H-ZSM-5 catalysts.

## 4.3. Results and Discussion

### *4.3.1. Characterization Results*

The influence of platinum on the surface area properties of Mo/H-ZSM-5 zeolite catalysts was investigated by nitrogen adsorption studies. The BET surface areas and pore volume results of platinum modified Mo/H-ZSM-5 zeolite catalyst are shown in Table 4.1.

**Table 4.1:** Nitrogen adsorption (BET) results of Pt loaded Mo/H-ZSM-5 zeolite catalysts.

| Catalysts | Surface Area ($m^2/g$) | Pore Volume ($cm^3/g$) |
|---|---|---|
| H-ZSM-5 | 392 | 0.261 |
| 2Mo/H-ZSM-5 | 385 | 0.248 |
| 0.5Pt/2Mo/H-ZSM-5 | 381 | 0.247 |
| 1Pt/2Mo/H-ZSM-5 | 380 | 0.246 |
| 2Pt/2Mo/H-ZSM-5 | 362 | 0.237 |
| 2Pt/H-ZMS-5 | 380 | 0.237 |

*Loading in wt.%.

The results show an insignificant decrease in BET surface area and pore volume with increase in platinum loading from 0 to 1 wt.%. A noticeable decrease in surface area from 380 to 360 $m^2/g$ is observed when increasing the platinum content to 2 wt.% loading. The decrease in surface area may be associated with the location of metal particles on/in the zeolite. These results suggest that the platinum species are too small to block the pores of the zeolites; consequently they have an insignificant effect on the surface area.

The effect of platinum on the acid site distribution was investigated using the ammonia desorption technique. The $NH_3$-TPD profiles of the parent H-ZSM-5, 2Mo/H-ZSM-5 and platinum impregnated 2Mo/H-ZSM-5 zeolite catalysts are shown in Figure 4.1. The H-ZSM-5 profile exhibits two well defined peaks (at 183 $^oC$ and 438 $^oC$), designated as the low temperature (LT) peak and the high temperature (HT) peak, respectively. Wang et al. [26] and Hidalgo et al. [27]

suggested that if the ammonia desorption peak temperature is above 350 $^{o}$C, the peak represents desorption of ammonia from strong acid sites, while the peaks with desorption temperature below 350 $^{o}$C represent desorption of ammonia from weak acid sites. A shift to lower temperature and a decrease in the intensity of the HT peak at 438 $^{o}$C was observed after the H-ZSM-5 was impregnated with a molybdenum precursor solution followed by calcination at 500 $^{o}$C. This decrease is associated with the migration of molybdenum oxide species inside the zeolite channels. The Mo anchor on the acid sites leading to a decrease in the concentration of Brønsted acid sites. This decrease in the HT peak intensity may be attributed to the metal interaction with the bridging hydroxyl group acting as Brønsted acid sites. Addition of platinum also led to a decrease in the peak intensity and the desorption temperature of the HT peak, which shifted to lower temperature (< 400 $^{o}$C). There is a third desorption peak at ca. 260 $^{o}$C, which is associated with medium acid sites. When the platinum loading was increased an increase in the concentration of medium acid sites was observed. This suggests that as the metal content increases the generation of medium acid sites is more pronounced, while the concentration of weak acid sites insignificantly affected by increase in total metal loading.

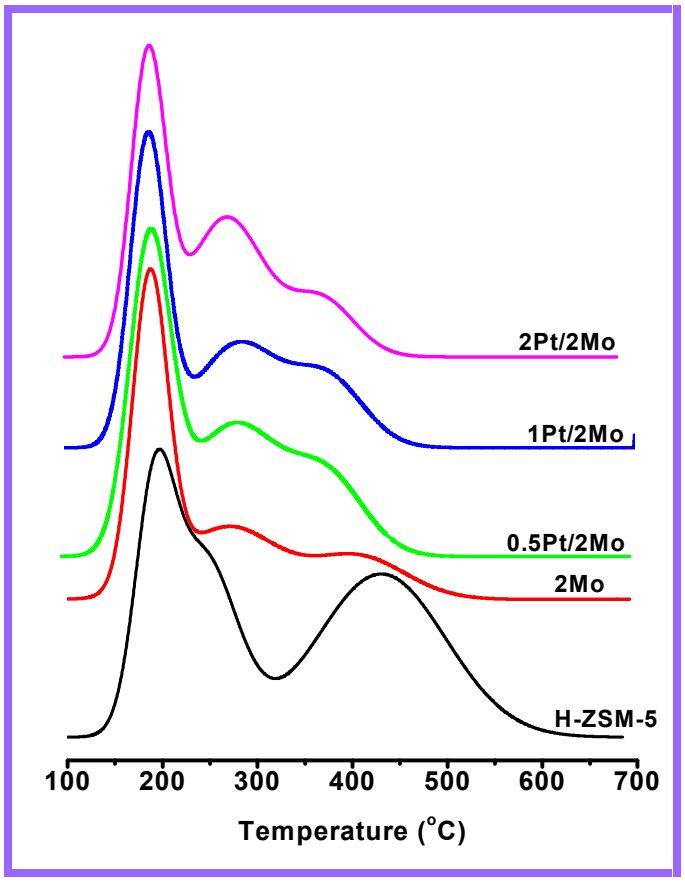



**Figure 4.1:** $NH_3$-TPD profiles of the parent H-ZSM-5, 2Mo/H-ZSM-5 and Pt/2Mo/H-ZSM-5 zeolite catalysts with various platinum loadings.

In order to obtain more information about the platinum species or oxidation states of the metals present in the catalysts, CO adsorption experiments were performed on both nitrogen-treated and reduced catalysts. The IR spectra were recorded at room temperature in 15 minute intervals of CO adsorption and the CO pressure was varied from 1 to 55 Torr. The results of CO adsorption of the 2Pt/H-ZSM-5, 0.5Pt/2Mo/H-ZSM-5, 1Pt/2Mo/H-ZSM-5 and 2Pt/2Mo/H-ZSM-5 zeolite catalysts are presented in Figure 4.2. The IR spectra of the Pt/H-ZSM-5 catalyst show a number of bands (2207, 2193, 2171, 2158, 2132, 2122, 2113, 2100 and 2078 $cm^{-1}$). The intensities of the two bands at 2206 and 2171 $cm^{-1}$ changed concurrently, which suggest they are associated with one platinum carbonyl complex. When CO pressure is increased these bands disappeared without generating any new bands. Chakarova et al. [28-30] observed similar results in the study of polycarbonyl species in a Pt/H-ZSM-5 zeolite catalyst. They observed similar bands at 2212 and 2176 $cm^{-1}$ and they attributed them to dicarbonyl complexes of $Pt^{3+}$ (i.e. a $Pt^{3+}(CO)_2$ complex) which decomposed without generating any $Pt^{3+}$ monocarbonyl complexes. This suggests that at high CO pressure the $Pt^{3+}$ which is considered to be one of the less stable oxidation states of platinum is reduced to lower oxidation states of platinum. The IR spectra also showed two major bands with high intensities at 2158 and 2078 $cm^{-1}$. The band at 2158 $cm^{-1}$ is due to the CO on $Pt^{2+}$ species forming a monocarbonyl complex [31]. This band was initially at 2161 $cm^{-1}$ at low CO pressures and as the CO pressure increased the band shifted to lower wavenumbers (i.e. below 2158 $cm^{-1}$). The band at 2078 $cm^{-1}$ is due to the adsorption of CO on metallic platinum species [32, 33]. The intensity of both bands increased with increase in CO pressure. The CO molecules adsorbed on small platinum particles have low energy stretching frequencies [33-35]. This led the authors to assign bands at 2113 and 2100 $cm^{-1}$ to CO adsorbed on $Pt^{2+}$ and $Pt^{0}$ species respectively, even though the band intensities were low. The band at 2100 $cm^{-1}$ has been previously assigned to CO adsorbed on small (i.e. 2-3.5 nm) platinum particles [36]. However, this band tends to disappear with an increase in CO pressure. The band at 2193 $cm^{-1}$ has been assigned to CO being adsorbed on $Pt^{3+}$ species forming a monocarbonyl complex [37]. The IR bands associated with CO adsorbed on $Pt^{2+}$ species shifted to lower wavenumbers. Other bands developed due to the presence of the molybdenum species. The band at 2158 $cm^{-1}$ observed during CO adsorption on Pt/H-ZSM-5 shifted to 2141 $cm^{-1}$ when CO was adsorbed on the molybdenum containing samples and a new band at 2162 $cm^{-1}$ was also observed. The band at 2162 $cm^{-1}$ is attributed to CO adsorbed on molybdenum species and it is more noticeable in a 1Pt/2Mo/H-ZSM-5 sample. According to several authors this band may be attributed to the adsorption of CO on $Mo^{4+}$ [38-40]. However, the adsorption of CO on platinum free Mo/H-ZSM-5 samples showed no band (in the 2160 $cm^{-1}$ region) of the CO adsorbed on the

molybdenum species (Figure 4.3). Studies of CO adsorbed on the 2Mo/H-ZSM-5 sample showed no bands of CO adsorbed on a molybdenum carbide surface. This was verified by increasing the concentration of molybdenum carbide from 2 to 15 wt.% loading; no significant change was observed in the CO adsorption part of the IR spectrum. However, some work has been reported on the adsorption of CO on molybdenum carbide on different supports, which were pre-carbided in-situ. Two bands at 2175 and 2050 $cm^{-1}$ were observed and the band at 2050 $cm^{-1}$ shifted depending on the support used in the study. The bands were attributed to two kinds of molybdenum species that may be present in the catalyst. Several researchers reported CO adsorption on $Mo^{4+}$ and $Mo^{2+}$ at 2175 and 2050 $cm^{-1}$ respectively. DeCanio and Storm [41] did some CO adsorption studies on $Mo_2C/Al_2O_3$ and observed these bands at 2178 and 2060 $cm^{-1}$. Rasko and Kiss [42] studied the CO adsorption on $Mo_2C/SiO_2$ and observed a band at 2079 $cm^{-1}$ and they ascribed this band to CO adsorption on $Mo^{2+}$.

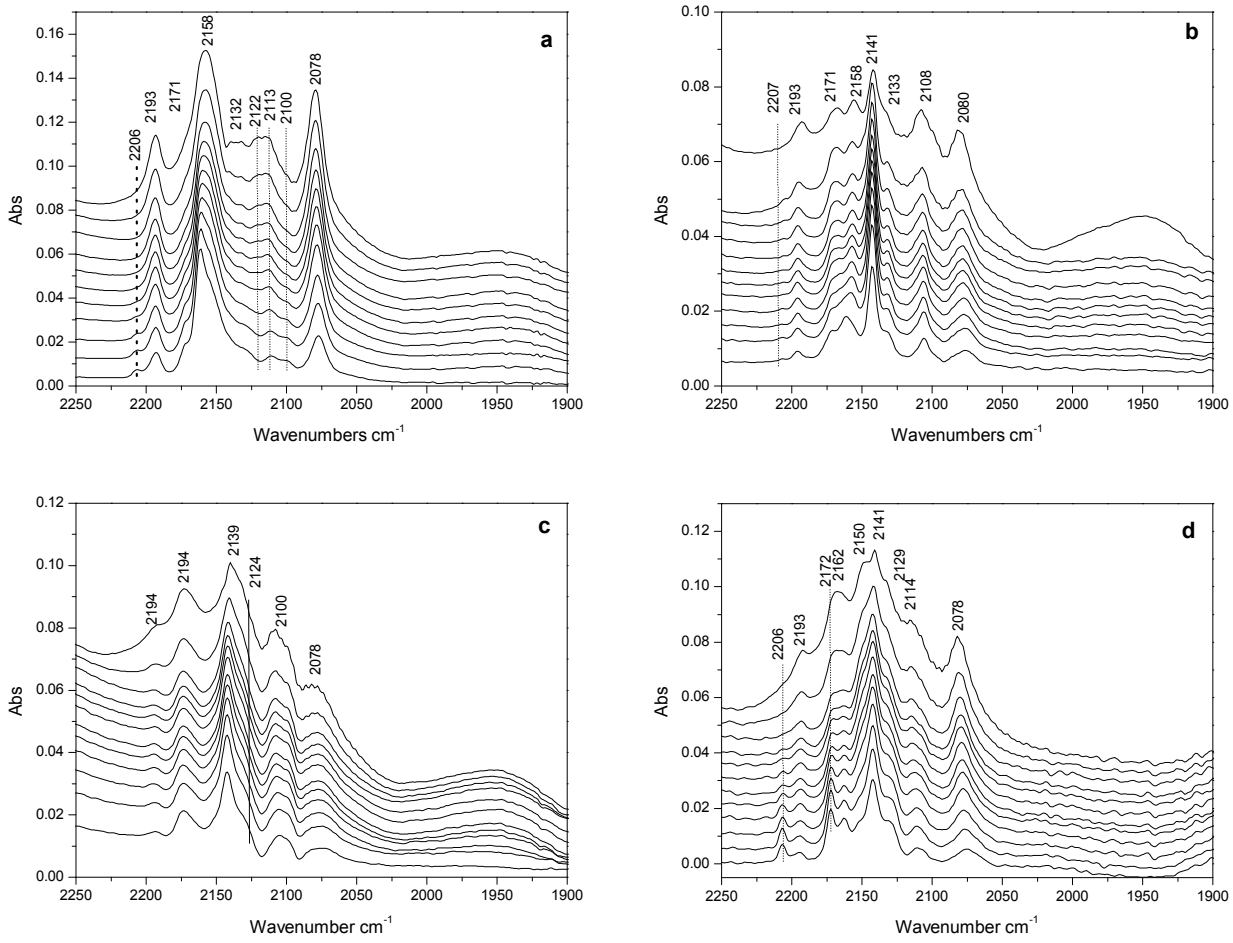



**Figure 4.2:** Adsorption of CO on platinum loaded samples at CO pressures between 1 and 50 Torr. a) 2Pt/H-ZSM-5, b) 0.5Pt/2Mo/H-ZSM-5, c) 1Pt/2Mo/H-ZSM-5 and d) 2Pt/2Mo/H-ZSM-5.

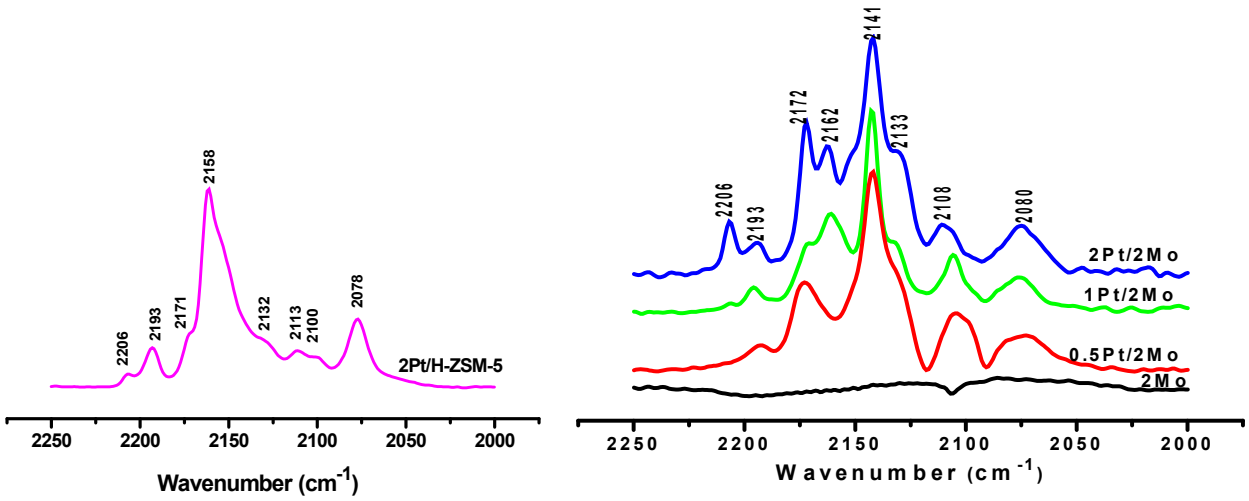



**Figure 4.3:** IR spectra of CO adsorption on 2Mo/H-ZSM-5 and Pt/Mo/H-ZSM-5 zeolite catalysts with various platinum loadings taken at 5 Torr CO pressure.

The influence of the platinum loading on the amount of CO adsorbed was further studied using a CO pulse chemisorption technique. The platinum loaded Mo/H-ZSM-5 catalysts were reduced at 200 $^{o}$C for 1 hour and the CO uptake results are presented in Table 4.2.

**Table 4.2:** CO Chemisorption on Pt/Mo/H-ZSM-5 zeolite samples reduced at 200$^{o}$C for 1 hour.

| Catalysts | CO uptake (µmol/g) | Dispersion (%) |
|---|---|---|
| 2Mo/H-ZSM-5 | - | - |
| 0.5Pt/2Mo/H-ZSM-5 | 1.45 | 0.86 |
| 1Pt/2Mo/H-ZSM-5 | 2.58 | 4.20 |
| 2Pt/2Mo/H-ZSM-5 | 3.99 | 7.78 |
| 2Pt/H-ZMS-5 | 6.18 | 24.1 |

The results show that large amounts (i.e. 6.18 µmol/g) of CO were adsorbed on the molybdenum free 2Pt/H-ZSM-5 catalyst and catalysts with molybdenum gave an increase in the amount of CO uptake with an increase in platinum loading from 1.45 to 3.99 µmol/g of CO (Table 4.2). Relatively low amounts of CO uptake were observed with catalysts containing both molybdenum and platinum when compared with the 2Pt/H-ZSM-5 catalyst. The amount of CO adsorbed is associated with the number of platinum species in the metallic state available to bond with CO molecules. The decrease in CO uptake may therefore suggest that during the reduction step molybdenum species migrate to the large platinum particles and form a mixed oxide surface layer

that is inactive to chemically adsorb CO [43]. It might also be due to the electronic effects contributed by molybdenum that weaken the CO-Pt interaction.

The FT-IR results of the CO adsorption of the samples after hydrogen treatment at 200 $^{o}$C are shown in Figure 4.4 below. Small amounts of CO were taken up by for Pt-Mo/H-ZSM-5 catalysts as shown by pulse CO chemisorption and the FT-IR results shown in Figure 4.4. The intensity of the CO adsorbed on the metallic platinum species increased with increase in platinum loading as shown by the broad bands at 2084 cm$^{-1}$. However, the spectrum of the 2Pt/H-ZSM-5 molybdenum free catalyst shows a clearly defined band at 2074 cm$^{-1}$ with high intensity. The intensity of the band is associated with the amount or concentration of CO adsorbed on the metallic platinum species. The shift in band position is due to the electronic interaction between platinum and molybdenum. The band at 2173 cm$^{-1}$ is ascribed to CO adsorbed on unreduced $Mo^{4+}$ species and the intensity of the band decreases with an increase in platinum loading.

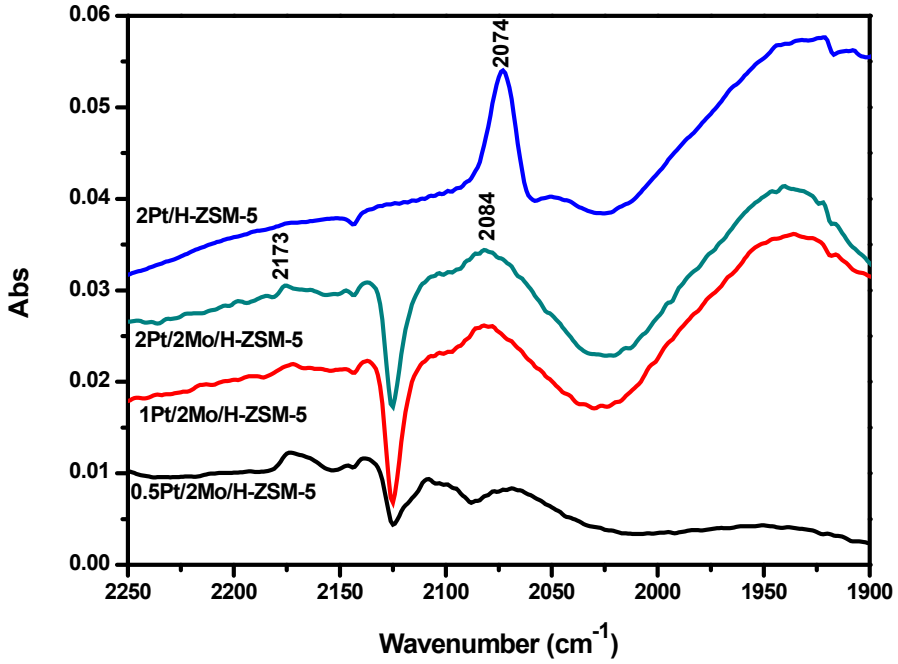



**Figure 4.4:** FT-IR spectra of the CO adsorption on the 2%$Mo_2C$ reduced at 200 $^{o}$C for 1 hour. a) 0.5Pt/2Mo/H-ZSM-5, b) 1Pt/2Mo/H-ZSM-5, c) 2Pt/2Mo/H-ZSM-5 and d) 2Pt/H-ZSM-5.

### 4.3.2. Catalytic Results

#### *4.3.2.1. Effect of Platinum Loading on the MDA Reaction*

The effect of platinum loading on the catalytic performance of 2%Mo/H-ZSM-5 zeolite catalysts on the MDA reaction was investigated. Reactions were performed at 700 $^{o}$C using a mixture of methane and argon (90% $CH_4$, balance Ar) flowing at 13.5 mL/min. Figure 4.5 shows the effect of platinum loading on the methane conversion after 245 minutes on-stream

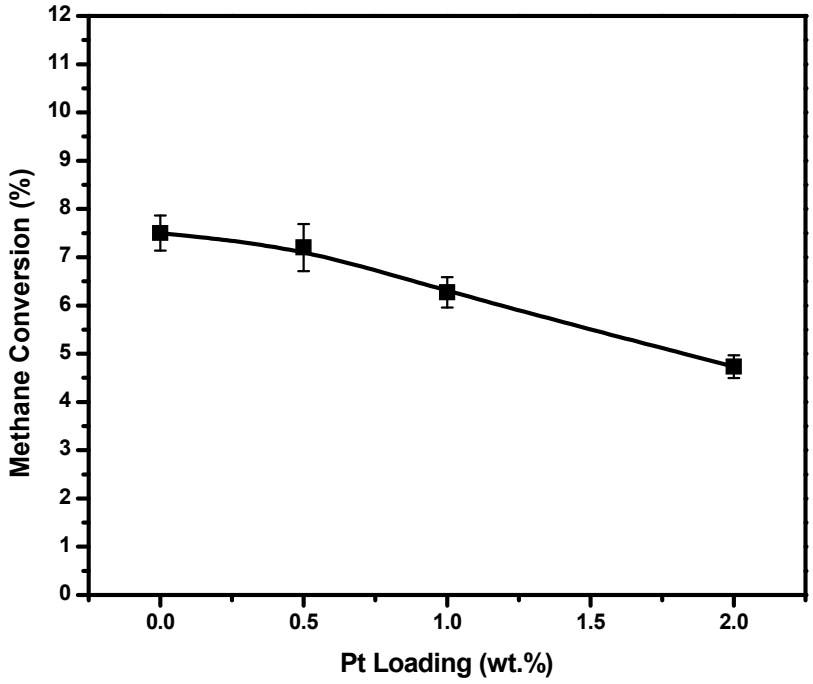



**Figure 4.5:** The effect of platinum loading on methane conversion at 700 $^{o}$C at steady state after a time-on-stream of 245 minutes.

The catalytic conversion of methane over the Mo/H-ZSM-5 catalyst was 7.5% and upon addition of 0.5 wt.% platinum the conversion of methane was recorded to be 7.2% (Figure 4.5). Further increase of the platinum loading led a linear decrease in methane conversion reaching a minimum of 4.7% for a 2 wt.% platinum containing catalyst. A decrease in methane conversion observed when the platinum loading was increased from 0.5 to 2 wt.% may be attributed to the hydrogenolysis activity of platinum, which is more pronounced with an increase in platinum loading. Platinum group metals are well known to promote hydrogenation of the reaction intermediates of lower carbon number into methane [44].

Figure 4.6 shows the results of the catalytic conversion of methane with time-on-stream (TOS). The influence of platinum loading on the catalyst stability of the Mo/H-ZSM-5 zeolite catalysts was studied at 700 $^{o}$C for 6 hours.

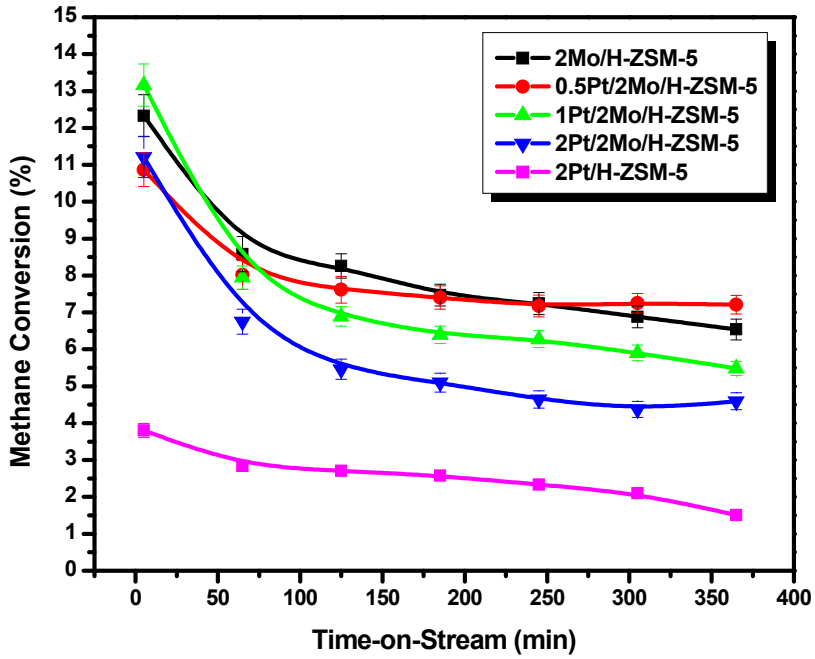



**Figure 4.6:** Effect of platinum loading on the catalytic conversion of methane versus time-on-stream taken a 700 $^{o}$C for 6 hours on-stream.

From the results it can be observed that the high initial conversions of methane were followed by a gradual decrease with increase in TOS that reached a steady state after 168 minutes on-stream. A decrease in methane conversion with increase in TOS was observed with the 2%Mo/H-ZSM-5 zeolite catalyst. This can be attributed to a rapid deactivation of the catalyst which is caused by coke accumulation on the catalyst during the reaction [45]. Coke anchors on the active sites rendering them inactive [46]. This prevents methane from accessing the active sites; hence the decrease in methane conversion with increase in TOS was observed. Addition of platinum enhanced the stability of the catalyst with the 0.5 wt.% platinum loaded catalyst showing good catalytic performance when compared with the higher platinum loaded catalysts. Methane conversions between 7 and 11% were observed for the 0.5 wt.% Pt loaded catalyst while the 1 and 2 wt.% platinum loaded catalysts showed conversions between 4 and 11%. Low methane conversions (i.e. between 4 and 2%) were observed for the 2Pt/H-ZSM-5 catalyst. This is

attributed to the absence of molybdenum species responsible for activating methane into reactive intermediates. In this work a decrease in methane conversion with increase in total metal content was observed (Figure 4.5). However, upon the addition of platinum an increase in the deactivation rate was observed in Figure 4.6 with increase in platinum loading. It has been reported that the presence of noble metals decreases the amount of carbonaceous deposits formed during the MDA reaction by hydrogenolysis of coke [44, 47].

Figure 4.7 shows the effect of platinum loading on the aromatic and coke selectivity of Mo/H-ZSM-5 and Pt/Mo/H-ZSM-5 catalysts with various platinum loadings. The aromatic selectivity of platinum loaded Mo/H-ZSM-5 catalysts is between 60 and 90%, with the 0.5wt.% platinum catalyst possessing a high aromatic selectivity. A gradual decrease in the aromatic selectivity with TOS was observed when the platinum loading was increased from 0.5 to 2 wt.%. This decrease can be attributed to a decrease in the concentration of Brønsted acid sites with increase in total metal loading as shown by the $NH_3$-TPD results in Figure 4.1. The decrease in the aromatic selectivity is compensated for by the increase in the coke selectivity with increase in TOS. This increase in coke selectivity can be attributed to the decrease in surface area and pore volume as the total metal loading was increased. The formation of benzene was significantly high (about 80%) for the catalysts with 0.5 wt.% platinum loading and remained stable with increase in TOS (Figure 4.8). From the results presented in Table 4.3, we observed a decrease in benzene selectivity with increase in platinum loading while the selectivity towards toluene and naphthalene increased. This can be attributed to an increase in the alkylation of benzene with increase in platinum concentration [48]. Hence, the addition of platinum to Mo/H-ZSM-5 favoured the formation of toluene and naphthalene.

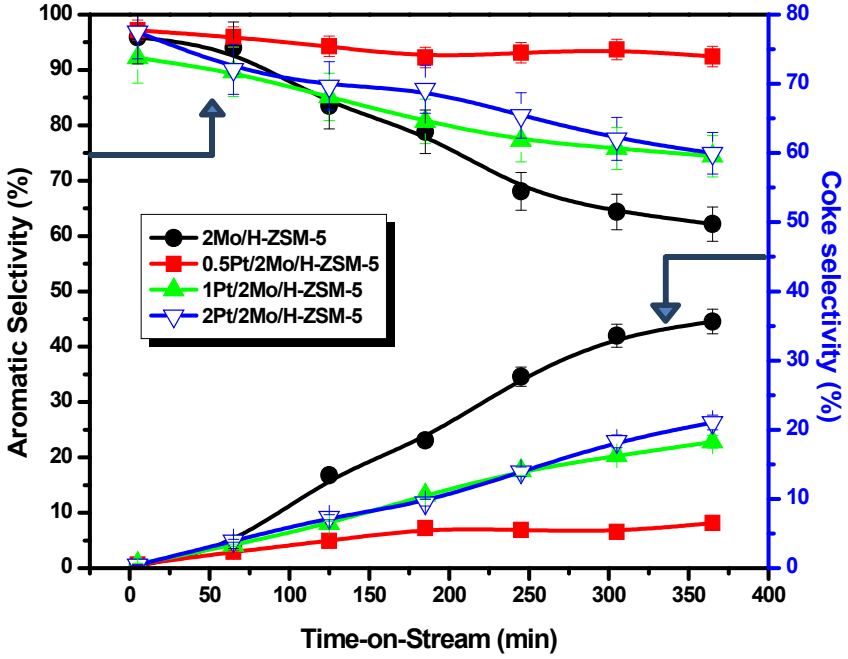



**Figure 4.7:** Aromatic and coke selectivities of Mo/H-ZSM-5 and Pt/H-ZSM-5 with various platinum loadings (i.e. between 0.5 and 2 wt.%) plotted against time-on-stream.

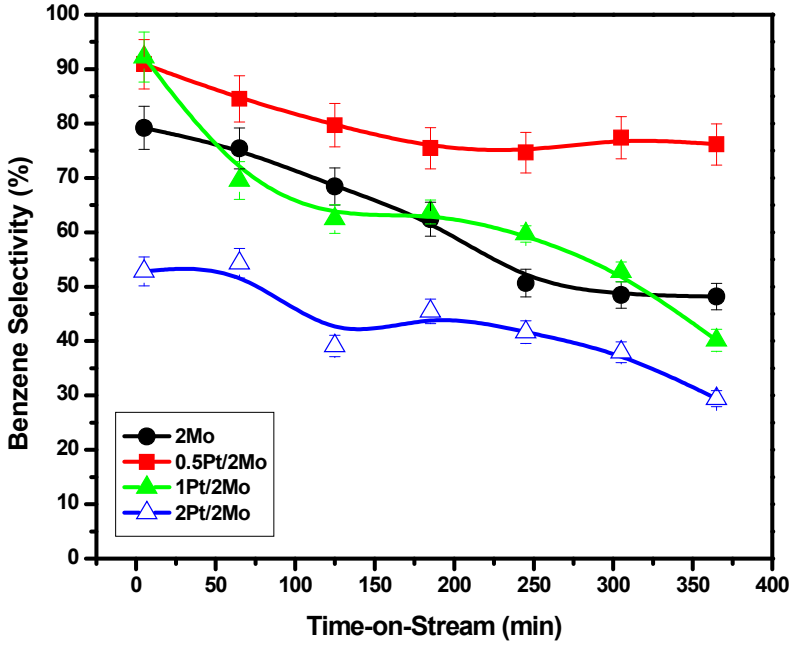



**Figure 4.8:** Benzene selectivity of Mo/H-ZSM-5 and Pt/Mo/H-ZSM-5 with various platinum loadings (i.e. between 0.5 and 2 wt.%) plotted against time-on-stream.

Results of the effect of platinum loading on the product selectivity to hydrocarbons over platinum loaded Mo/H-ZSM-5 zeolite catalyst are shown in Table 4.3. Catalysts were compared at similar conversions of methane taken after 245 minutes on stream.

**Table 4.3:** Product selectivity of Mo/H-ZSM-5 and Pt/Mo/H-ZSM-5 zeolite catalysts taken at TOS of 245 minutes.

| Pt Loading (wt.%) | Conversion (%) | Percentage Product Selectivity | | | | | |
|---|---|---|---|---|---|---|---|
| | | $C_{2's}$ | Benzene | Toluene | Naphthalene | Aromatics | Coke |
| 0 | 7.5 | 2.3 | 50.5 | 7.4 | 10.1 | 70.3 | 29.7 |
| 0.5 | 7.2 | 1.4 | 70.7 | 4.7 | 13.7 | 89.1 | 9.5 |
| 1.0 | 6.2 | 8.7 | 59.7 | 3.4 | 14.2 | 77.3 | 14.0 |
| 2.0 | 4.7 | 4.1 | 50.6 | 5.8 | 14.4 | 71.8 | 24.1 |

The results show that the product distribution is affected by the levels of platinum added onto the Mo/H-ZSM-5 catalyst. The effect of platinum is noticeable at a 0.5 wt.% platinum loading. Here the selectivity towards benzene increased from 50 to 70% and the total aromatic selectivity increased by 20% reaching a maximum of 89%. An increase in platinum loading led to a decrease in benzene selectivity, reaching a minimum of 52% for the 2 wt.% platinum loaded catalyst. The selectivity towards the heavy toluene and naphthalene was hardly affected by the increase in platinum loading. The selectivity towards toluene was between 4 and 6% and naphthalene increased from 10 to 14%. Furthermore, a noticeable effect of platinum loading on the coke selectivity was observed with the coke selectivity decreasing from 30% to 9.5% upon addition of 0.5 wt.% of platinum. However, an increase in platinum led to undesired results and the coke selectivity increased to 24%. These results were confirmed by TGA results presented in Figure 4.9 below.

The results of TGA and DTG measurements of the Mo/H-ZSM-5 and the platinum modified Mo/H-ZSM-5 zeolite catalysts with platinum loadings between 0.5 and 2 wt.% are shown in Figure 4.9(a) and Figure 4.9(b) respectively.

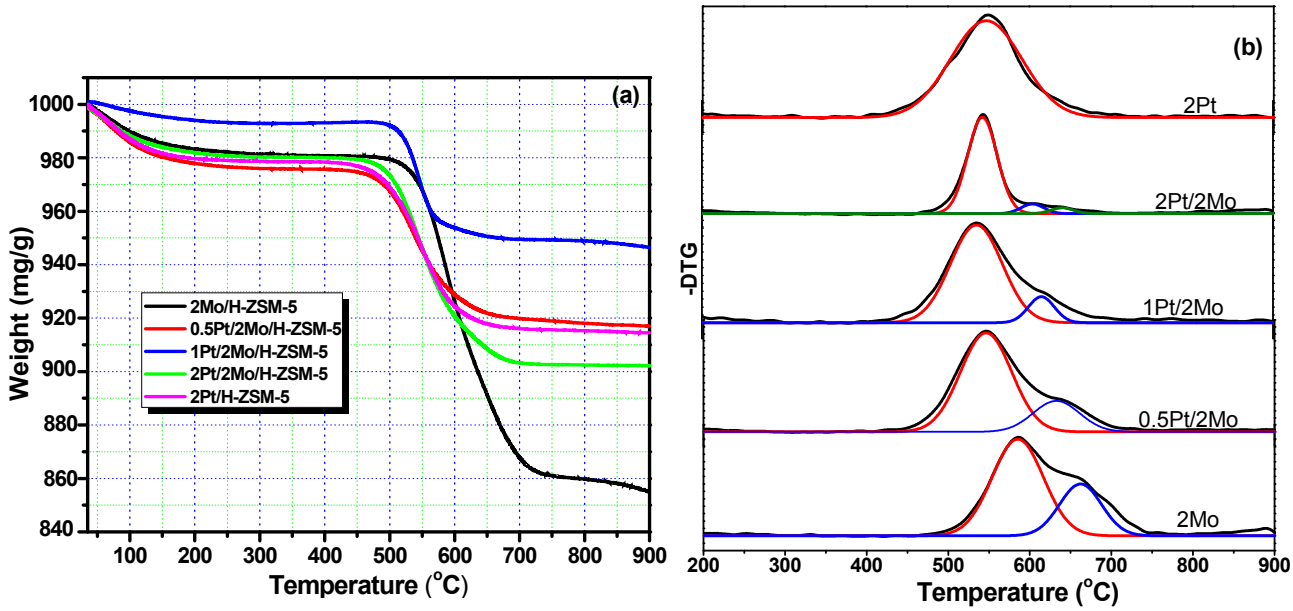



**Figure 4.9:** TGA (a) and DTG (b) profiles of coked Mo/H-ZSM-5, Pt/Mo/H-ZSM-5 and Pt/H-ZSM-5 zeolite catalysts after MDA reactions at 700 °C after 6 hours on-stream.

**Table 4.4:** TGA and DTG results of coked Mo/H-ZSM-5 and Pt/Mo/H-ZSM-5 with various platinum loadings.

| Catalyst | Amount of Coke (mg/g cat.) | Low Decomposition Temperature (°C) | High Decomposition Temperature (°C) |
|---|---|---|---|
| 2Mo/H-ZSM-5 | 121 | 583 | 660 |
| 0.5Pt/2Mo/H-ZSM-5 | 54 | 529 | 634 |
| 1Pt/2Mo/H-ZSM-5 | 45 | 538 | 622 |
| 2Pt/2Mo/H-ZSM-5 | 75 | 542 | 607 |
| 2Pt/H-ZSM-5 | 63 | 548 | - |

Catalyst deactivation by coke deposition on Mo/H-ZSM-5 during the MDA reaction remains a prevalent problem as this reaction is only feasible at high reaction temperatures. The most pronounced problems associated with coke are catalyst deactivation which is due to the formation

of coke on the active sites of the catalysts, blocking the reactants from accessing the reactive sites of the catalyst. In H-ZSM-5 coke is formed on the Brønsted acid sites. On the other hand, coke deposition can alter the geometry of the channels and pores of the zeolite, which can lead to a change in the product selectivity of the catalyst [49]. Heavy aromatic compounds formed in the channels will now be intermediates for the formation of polyaromatic coke. The sizes of polyaromatic intermediates prevents smaller molecular intermediates from diffusing through the coke modified channels of the zeolite [50-52]. The TGA and DTG results show the effect of platinum on the amount of coke deposited during the MDA reaction at 700 $^{o}$C after 6 hours. From the TGA profiles presented in Figure 4.9(a) and Table 4.4 it can be noted that over 120 mg/g.cat of coke was deposited on the Mo/H-ZSM-5 catalyst. Addition of platinum led to a decrease in the coke deposited on the Pt/Mo/H-ZSM-5 catalysts. For the 0.5 wt.% platinum catalyst, 54 mg/g.cat of coke was deposited and upon increasing the platinum loading to 1 and 2 wt.% 45 and 75 mg/g.cat of coke deposition was observed, respectively. These results show that addition of platinum reduces the amount of coke deposition by ca. 50% and this is in agreement with the product selectivity results presented in Table 4.3. The suppression of coke is attributed to the presence of platinum which aids in the hydrogenation capability in the MDA reaction [53]. The hydrogen produced during the reaction will be adsorbed onto the platinum species which then dissociates into hydrogen atoms. These hydrogen atoms will then migrate onto the coke interface and hydrogenate the polyaromatic hydrocarbon into lighter hydrocarbons. The DTG profiles show two well defined peaks which can be attributed to decomposition of two different types of coke/carbon formed during the MDA reaction. The first peak (at 583 $^{o}$C) is due to the oxidation of carbon that is associated with carbidic carbon of $Mo_2C$ while the second peak (at 660 $^{o}$C) is due to the oxidation of polyaromatic carbon formed on the Brønsted acid sites [14, 54, 55]. The presence of platinum catalyzes the oxidation of the carbonaceous deposit and this leads to a decrease of the oxidation temperature of both forms of coke (i.e. on molybdenum and Brønsted acid sites) as shown in Figure 4.9(b). This can be attributed to the decrease in the stability of coke formed during the MDA over the platinum modified catalysts caused by the hydrogenation of coke occurring simultaneously with the aromatization reaction [56]. Other reasons have been suggested for the decrease in oxidation temperature of the DTG peaks associate with carbon. For example, platinum is a good oxidation catalyst and could decrease the oxidation temperatures of coke/carbon observed on the platinum loaded Mo/H-ZSM-5 zeolite catalysts [57, 58]. Only a single oxidation peak at 548 $^{o}$C oxidation temperature was observed for 2Pt/H-ZSM-5. This was assigned to the oxidation of coke deposited on the Brønsted acid sites; the absence of the second peak is due to the absence of $Mo_2C$ in the catalyst.

### *4.3.2.2. Comparison Study of the Effect of Pt, Pd and Ru on the MDA reaction*

A comparison study was performed to investigate the influence of other noble metals on the MDA reaction over a Mo/ H-ZSM-5 zeolite catalyst. Palladium and ruthenium were chosen as addition metals of interest. These noble metal catalysts were prepared by impregnation of Mo/H-ZSM-5 with 0.5 wt.% of the noble metals which were calcined at 500 $^{o}$C for 6 hours. The MDA reaction was performed at 700 $^{o}$C for 6 hours. Prior to the reaction the catalysts were treated with nitrogen at 700 $^{o}$C for 1 hour and exposed to methane for 30 minutes.

Figure 4.10 shows the results for the methane conversion over Mo/H-ZSM-5, Pt/Mo/H-ZSM-5, Pd/Mo/H-ZSM-5 and Ru/Mo/H-ZSM-5 catalysts.

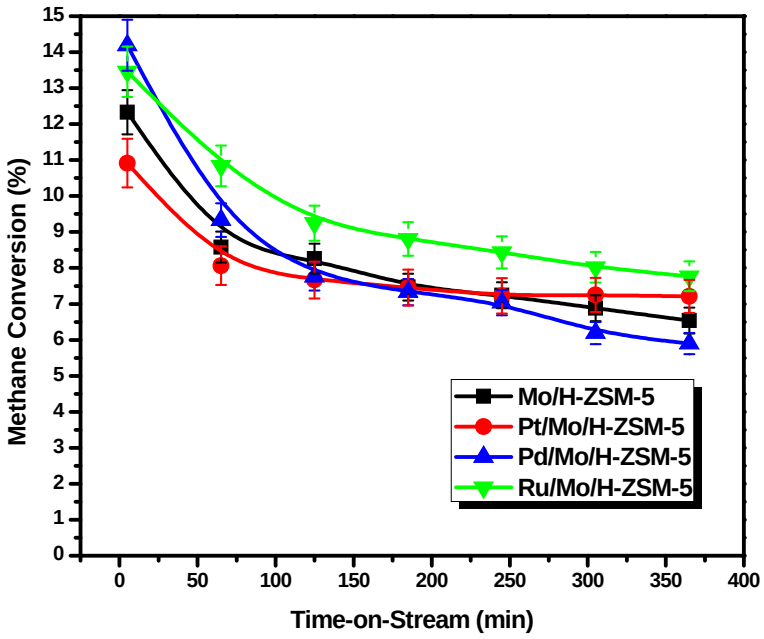



**Figure 4.10:** The catalytic conversion of methane as a function of time-on-stream over noble metal modified 2Mo/H-ZSM-5 zeolite catalysts with a of 0.5 wt.% loading of the noble metal.

The conversion of methane at low TOS (i.e. first two data points) is to be noted. After 5 and 65 minutes on-stream a high methane conversion for the ruthenium and palladium Mo/H-ZSM-5 catalysts was observed. Addition of palladium and platinum to the Mo/H-ZSM-5 catalyst had a

major effect on the catalytic activity of MDA over the un-promoted Mo/H-ZSM-5 catalysts. An improvement in the catalytic activity was observed upon addition of ruthenium to the Mo/H-ZSM-5 catalyst. Conversions of between 8 and 13% were observed, with 13% being recorded at the start of the TOS measurements. The profile shows a steady exponential decrease in methane conversion with time on-stream. This decrease can be attributed to catalytic deactivation which is associated with coke deposition as mentioned above. There are other factors that have to be taken into account when employing noble metals in catalysis. Noble metals are well known to have a high hydrogenolysis activity towards hydrocarbons. During the reaction methyl radicals are formed on the molybdenum carbide species and if there is enough hydrogen formed in the presence of a noble metal it is possible for the methyl radical to react with the hydrogen atoms to form methane. Hence, the decrease in methane conversion might not only be associated with catalyst deactivation caused by coke formation during the MDA reaction over noble metal modified Mo/H-ZSM-5 catalysts.

Results of the effect of noble metals on the product selectivity of the Mo/H-ZSM-5 zeolite catalyst for the MDA reaction at 700 $^{o}$C after 245 minutes on-steam are shown in Table 4.5. Catalysts were compared at 7% iso-conversion of methane taken after 245 minutes on-stream. From the results presented in Table 4.5 below it is clear that addition of a noble metal to the Mo/H-ZSM-5 catalyst has an influence on the product distribution. Addition of a noble metal led to high aromatic selectivity and a decrease in coke selectivity. The results demonstrate that the ruthenium loaded Mo/H-ZSM-5 catalyst is a good catalyst and yields high aromatic selectivity (i.e. 92%) and low selectivity to coke (i.e. 5.8%). For the Mo/H-ZSM-5 catalyst, the selectivity to benzene was 50% and upon addition of noble metals an increase in benzene was observed with the platinum loaded catalyst reaching an optimum of 70%. The palladium and ruthenium promoters gave 66 and 61% selectivities respectively. Ruthenium loaded Mo/H-ZSM-5 showed a higher selectivity to naphthalene (25%) compared with the naphthalene selectivity of platinum (14%) and palladium (16%) catalysts. The low naphthalene selectivities observed for platinum and palladium may be attributed to the ability of the two metals to catalyze hydrogenolysis of condensed aromatics in the presence of hydrogen [59, 60]. The presence of platinum and palladium decreased the formation of naphthalene which was compensated by the high selectivity to benzene.

**Table 4.5:** Comparison results of the effect of noble metals on the MDA reaction and percentage product selectivities taken at 7% methane conversion after 245 minutes on-stream.

| Catalyst | Conversion (%) | Percentage Product Selectivity | | | | | |
|---|---|---|---|---|---|---|---|
| | | $C_{2s}$ | Benzene | Toluene | Naphthalene | Aromatics | Coke |
| Mo | 7.5 | 2.3 | 50.5 | 7.4 | 10.1 | 70.3 | 29.7 |
| Pt/Mo | 7.2 | 1.4 | 70.7 | 4.7 | 13.7 | 89.1 | 9.5 |
| Pd/Mo | 7.0 | 1.1 | 65.6 | 9.0 | 15.5 | 90.1 | 8.8 |
| Ru/Mo | 8.5 | 1.8 | 60.8 | 6.5 | 25.1 | 92.4 | 5.8 |

The effect of noble metals on the total amount of coke deposited during the MDA reaction at 700 $^{o}$C was studied by thermal gravimetric measurements. The TGA and DTG results of the noble metal modified Mo/H-ZSM-5 zeolite catalysts are shown in Figure 4.11(a) and Figure 4.11(b) respectively.

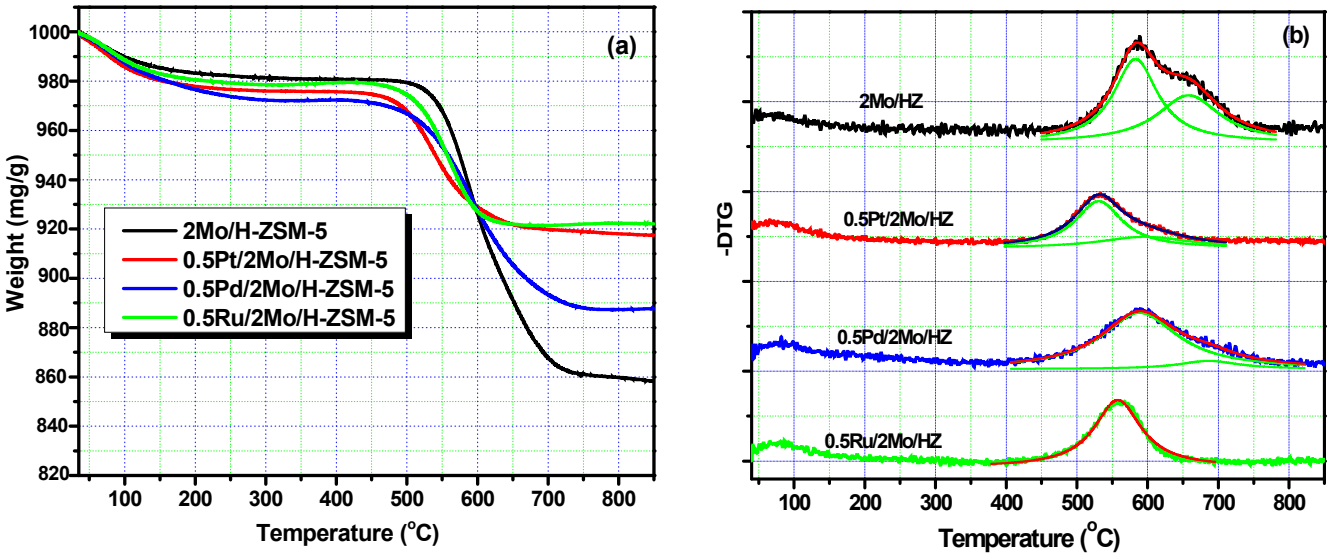



**Figure 4.11:** TGA (a) and DTG (b) profiles of coked Mo/H-ZSM-5, Pt/Mo/H-ZSM-5 Pd/Mo/H-ZSM-5 and Ru/Mo/H-ZSM-5 zeolite catalysts after MDA reactions for 6 hours at 700 $^{o}$C.

The amount of coke deposited on Mo/H-ZSM-5 catalyst was 121 mg/gcat. and upon addition of a noble metal a decrease in the amount of coke was observed. The platinum and ruthenium promoted catalysts gave 54 and 59 mg/gcat. coke deposit. From the TGA profile of the palladium promoted catalyst, 86 mg/g of coke deposit was observed. The decrease in the amount of coke deposited on the noble metal catalysts is associated with the hydrogenolysis of heavy aromatic compounds which contribute towards coke formation when they condense on the Brønsted acid sites. The DTG profile of Mo/H-ZSM-5 catalyst showed two peaks at 584 and 660 $^{o}$C oxidation temperatures associated with different types of coke. Upon addition of the noble metals a shift in the peak position was observed, with peaks shifting to lower oxidation temperatures. The decrease in coke stability is caused by the hydrogenation of coke that might be taking place during the MDA reaction. The hydrogen produced during the MDA can be used to hydrogenate the coke formed and this leads to a decrease in the carbon to hydrogen ratio. The decrease in area under the deconvoluted curves is associated with the amounts of coke deposited on the active sites. The intensity of the peak appearing at high temperature decreased upon addition of the noble metals and for the ruthenium catalyst the peak is not visible. This can be attributed to the decrease in the amount of coke formed on the Brønsted acid site in the presence of a noble metal.

## 4.4. Summary

The MDA reaction over platinum modified Mo/H-ZSM-5 zeolite at 700 $^{o}$C was successfully studied. The influence of platinum on the surface properties of molybdenum species was investigated by FT-IR CO adsorption and pulse chemisorption techniques. The FT-IR results showed the presence of various platinum cations which are less stable. However, these cations are expected to have little significance in the MDA reaction as this reaction is performed at a high reaction temperature. The lack of adsorption of CO on molybdenum carbide in the Pt/Mo/H-ZSM-5 zeolite catalysts is a mystery. In the FT-IR spectra no band corresponding with CO adsorbed on $Mo_2C$ was present. However, a band at 2162 $cm^{-1}$ was identified, which is associated with CO adsorbed on $Mo^{4+}$ species in the catalyst. The shift in band position from 2162 to 2174 $cm^{-1}$ is due to Mo-Pt interaction after the catalyst was reduced with hydrogen at 200 $^{o}$C.

The addition of platinum to the Mo/H-ZSM-5 zeolite catalyst enhanced the stability of the Mo/H-ZSM-5 catalyst during the MDA reaction. This is attributed to the coke deposits caused by the presence of platinum species. High aromatic selectivities (i.e. 90%) were observed when a 0.5 wt.% platinum loaded catalyst was used, with benzene being the most prominent product. The TGA results revealed that the presence of platinum in Mo/H-ZSM-5 led to a decrease in coke deposition by 50%.

The addition of noble metals to the Mo/H-ZSM-5 catalyst significantly affected the methane conversion but the catalytic stability was enhanced. The ruthenium promoted catalyst showed a higher methane conversion than found for the un-promoted and the Pt and Pd promoted catalysts. Only a small amount of deactivation was noted. The overall effect of a noble metal addition to the Mo/H-ZSM-5 catalyst was to modify the aromatic selectivity. The selectivity to aromatics was enhanced by 20% for the promoted catalysts, with an aromatic selectivity of 90% attained. Benzene selectivity of about 60% was observed for ruthenium and palladium promoted catalysts while the total aromatic selectivity was maintained at 90%. The presence of a noble metal favoured the formation of naphthalene with 14%, 16% and 25% observed for Pt, Pd and Ru promoted catalyst respectively. Low selectivities to coke were observed for the promoted Mo/H-ZSM-5 zeolite catalysts. This was confirmed by TGA results which showed a 50% reduction in the carbon deposit on the promoted Mo/H-ZSM-5 catalyst

## 4.5. Reference List

[1] L. Wang, L. Tao, M. Xie, G. Xu, J. Huang, Y. Xu, *Catalysis Letters*, **21** (1993) 35.

[2] L. Wang, Y. Xu, S.-T. Wong, W. Cui, X. Guo, *Applied Catalysis A: General*, **152** (1997) 173.

[3] Y. Xu, L. Lin, *Applied Catalysis A: General*, **188** (1999) 53.

[4] K. Honda, X. Chen, Z.G. Zhang, *Applied Catalysis A: General*, **351** (2008) 122.

[5] K. Honda, T. Yoshida, Z.-G. Zhang, *Catalysis Communications*, **4** (2003) 21.

[6] Z. Sobalík, Z. Tvarůžková, B. Wichterlová, V. Fíla, Š. Špatenka, *Applied Catalysis A: General*, **253** (2003) 271.

[7] Y. Xu, X. Bao, L. Lin, *Journal of Catalysis*, **216** (2003) 386.

[8] M.-S. Xie, X. Yang, W.-H. Chen, L.-X. Tao, X.-L. Wang, G.-F. Xu, L.-S. Wang, Y.-D. Xu, S.-T. Liu, X.-X. Guo, *Studies in Surface Science and Catalysis*, **105** (1997) 869.

[9] A. Szöke, F. Solymosi, *Applied Catalysis A: General*, **142** (1996) 361.

[10] F. Solymosi, J. Cserényi, A. Szöke, T. Bánsági, A. Oszkó, *Journal of Catalysis*, **165** (1997) 150.

[11] H. Jiang, L. Wang, W. Cui, Y. Xu, *Catalysis Letters*, **57** (1999) 95.

[12] D. Wang, J.H. Lunsford, M.P. Rosynek, *Topics in Catalysis*, **3** (1996) 289.

[13] D. Wang, J.H. Lunsford, M.P. Rosynek, *Journal of Catalysis*, **169** (1997) 347.

[14] B. Weckhuysen, M. Rosynek, J. Lunsford, *Catalysis Letters*, **52** (1998) 31.

[15] B.M. Weckhuysen, D. Wang, M.P. Rosynek, J.H. Lunsford, *Journal of Catalysis*, **175** (1998) 347.

[16] B.M. Weckhuysen, M.P. Rosynek, J.H. Lunsford, *Catalysis Letters*, **52** (1998) 31.

[17] V.T.T. Ha, L.V. Tiep, P. Meriaudeau, C. Naccache, *Journal of Molecular Catalysis A: Chemical*, **181** (2002) 283.

[18] P.L. Tan, K.W. Wong, C.T. Au, S.Y. Lai, *Applied Catalysis A: General*, **253** (2003) 305.

[19] D. Ma, Y. Shu, M. Cheng, Y. Xu, X. Bao, *Journal of Catalysis*, **194** (2000) 105.

[20] S. Liu, L. Wang, R. Ohnishi, M. Lchikawa, *Kinetics and Catalysis*, **41** (2000) 132.

[21] S. Masiero, N. Marcilio, O. Perez-Lopez, *Catalysis Letters*, **131** (2009) 194.

[22] R. Ohnishi, S. Liu, Q. Dong, L. Wang, M. Ichikawa, *Journal of Catalysis*, **182** (1999) 92.

[23] Y. Shu, Y. Xu, S.-T. Wong, L. Wang, X. Guo, *Journal of Catalysis*, **170** (1997) 11.

[24] L.Y. Chen, L.W. Lin, Z.S. Xu, X.S. Li, T. Zhang, *Journal of Catalysis*, **157** (1995) 190.

[25] L.C. Browning, P.H. Emmett, *Journal of the American Chemical Society*, **74** (1952) 4773.

[26] J. Liang, H. Li, S. Zhao, W. Guo, R. Wang, M. Ying, *Applied Catalysis*, **64** (1990) 31.

[27] C.V. Hidalgo, H. Itoh, T. Hattori, M. Niwa, Y. Murakami, *Journal of Catalysis*, **85** (1984) 362.

[28] K. Chakarova, M. Mihaylov, K. Hadjiivanov, *Microporous and Mesoporous Materials*, **81** (2005) 305.

[29] K. Chakarova, M. Mihaylov, K. Hadjiivanov, *Catalysis Communications*, **6** (2005) 466.

[30] K. Chakarova, K. Hadjiivanov, G. Atanasova, K. Tenchev, *Journal of Molecular Catalysis A: Chemical*, **264** (2007) 270.

[31] Y. Barshad, X. Zhou, E. Gulari, *Journal of Catalysis*, **94** (1985) 128.

[32] J. Ryczkowski, *Catalysis Today*, **68** (2001) 263.

[33] B.A. Riguetto, S. Damyanova, G. Gouliev, C.M.P. Marques, L. Petrov, J.M.C. Bueno, *The Journal of Physical Chemistry B*, **108** (2004) 5349.

[34] P. Hollins, *Surface Science Reports*, **16** (1992) 51.

[35] M.S. Tzou, B.K. Teo, W.M.H. Sachtler, *Journal of Catalysis*, **113** (1988) 220.

[36] P. Kubanek, H.W. Schmidt, B. Spliethoff, F. Schüth, *Microporous and Mesoporous Materials*, **77** (2005) 89.

[37] K. Chakarova, E. Ivanova, K. Hadjiivanov, D. Klissurski, H. Knozinger, *Physical Chemistry Chemical Physics*, **006** (2004) 3702.

[38] P.A. Aegerter, W.W.C. Quigley, G.J. Simpson, D.D. Ziegler, J.W. Logan, K.R. McCrea, S. Glazier, M.E. Bussell, *Journal of Catalysis*, **164** (1996) 109.

[39] W. Wu, Z. Wu, C. Liang, X. Chen, P. Ying, C. Li, *Journal of Physical Chemistry B*, **107** (2003) 7088.

[40] S. Yang, C. Li, J. Xu, Q. Xin, *Chemical Communications*, (1997) 1247.

[41] E.C. Decanio, D.A. Storm, *Journal of Catalysis*, **130** (1991) 653.

[42] J. Raskó, J. Kiss, *Applied Catalysis A: General*, **253** (2003) 427.

[43] E.C. Decanio, D.A. Storm, *Journal of Catalysis*, **132** (1991) 375.

[44] G. Leclercq, L. Leclercq, R. Maurel, *Journal of Catalysis*, **44** (1976) 68.

[45] H. Liu, T. Li, B. Tian, Y. Xu, *Applied Catalysis A: General*, **213** (2001) 103.

[46] J.-P. Tessonnier, B. Louis, S. Rigolet, M.J. Ledoux, C. Pham-Huu, *Applied Catalysis A: General*, **336** (2008) 79.

[47] S. Jongpatiwut, P. Sackamduang, T. Rirksomboon, S. Osuwan, D.E. Resasco, *Journal of Catalysis*, **218** (2003) 1.

[48] A. Corma, V. Martínez-Soria, E. Schnoeveld, *Journal of Catalysis*, **192** (2000) 163.

[49] S.M. Csicsery, *Zeolites*, **4** (1984) 202.

[50] L.D. Rollmann, D.E. Walsh, *Journal of Catalysis*, **56** (1979) 139.

[51] D.E. Walsh, L.D. Rollmann, *Journal of Catalysis*, **49** (1977) 369.

[52] D.E. Walsh, L.D. Rollmann, *Journal of Catalysis*, **56** (1979) 195.

[53] A.K. Aboul-Gheit, A.E. Awadallah, S.M. El-Kossy, A.-L.H. Mahmoud, *Journal of Natural Gas Chemistry*, **17** (2008) 337.

[54] V.R. Choudhary, S. Banerjee, D. Panjala, *Journal of Catalysis*, **205** (2002) 398.

[55] D. Ma, D. Wang, L. Su, Y. Shu, Y. Xu, X. Bao, *Journal of Catalysis*, **208** (2002) 260.

[56] T.Q. Hoang, X. Zhu, T. Danuthai, L.L. Lobban, D.E. Resasco, R.G. Mallinson, *Energy & Fuels*, **24** (2010) 3804.

[57] T.C. Basso, Z. Zhang, W.M.H. Sachtler, *Applied Catalysis A: General*, **79** (1991) 227.

[58] O. Bayraktar, E.L. Kugler, *Applied Catalysis A: General*, **233** (2002) 197.

[59] M.C. Alvarez-Galvan, R.M. Navarro, F. Rosa, Y. Briceño, F. Gordillo Alvarez, J.L.G. Fierro, *International Journal of Hydrogen Energy*, **33** (2008) 652.

[60] K.C. Mouli, V. Sundaramurthy, A.K. Dalai, Z. Ring, *Applied Catalysis A: General*, **321** (2007) 17.

# Chapter 5

# Dehydroaromatization of Methane over Sn Doped Pt/Mo/H-ZSM-5 Zeolite Catalysts

## 5.1. Introduction

Methane dehydroaromatization (MDA) to aromatic compounds over Mo/H-ZSM-5 catalysts under non-oxidative conditions has been widely studied [1-6]. The conditions best suited for this reaction are high temperatures, low pressures, and low hydrogen concentrations. The molybdenum supported on H-ZSM-5 zeolite catalyst is regarded as the most active catalyst for the MDA reaction near equilibrium conversion of methane can be achieved with high aromatic selectivity at 700 $^{o}$C [7] using this catalyst. Addition of platinum group metals (PGMs) to Mo/H-ZSM-5 enhanced the durability and catalyst resistance to coke deposition [8, 9]. When Pt-based catalysts are used, it is sometimes necessary to add hydrogen to the feed to reduce deactivation. However, in commercial applications, the use of high hydrogen to hydrocarbon feed ratios is highly undesirable because the equilibrium methane conversion decreases and the compression costs greatly increases [10]. On the other hand, the removal of hydrogen during the reaction favours the forward reaction (i.e. enhances the production levels of benzene or aromatic compounds) and leads to high amounts of coke deposition on the Mo/H-ZSM-5 zeolite catalyst [11]. Efforts to reduce the amount of coke deposited on the H-ZSM-5 catalyst in several reactions is still being studied and the use of platinum-based mono- and bimetallic catalysts has been explored in the naphtha reforming reaction. These catalysts show good resistance to catalyst deactivation and exhibit a high selectivity to aromatic compounds [12-14]. Several researchers [15-17] have studied the dehydrogenation of paraffins over platinum-based monometallic ($Pt/Al_2O_3$) and bimetallic ($Pt\text{-}Sn/Al_2O_3$) catalysts supported on $\gamma$-$Al_2O_3$. Their results show that the bimetallic $Pt\text{-}Sn/Al_2O_3$ supported catalysts gave better selectivity and the

rate of deactivation due to coke was reported to be low. The increase in selectivity in the dehydrogenation reactions and the reduction of coke formation is associated with the promotional effect of tin species. The effect of tin to platinum ratios in bimetallic Pt-Sn supported catalysts has been studied in depth. The electronic effects of tin due to electron transfer from platinum to tin changes the bond strength between platinum and the chemisorbed hydrocarbon [2, 15, 18]. The geometric effect of tin on platinum, described by Armend'ariz et al. [15], suggested that tin decreases the surface platinum-platinum particle interaction and led to an increase in the dispersion of platinum; this is attributed to tin particles acting as spacers that decrease the probability of sintering [2, 19, 20]. Ballarini et al. [1, 21] described the decreased poisoning of the acid sites of $Al_2O_3$ supports as due to tin coverage that inhibited carbon deposits from forming on the acid sites of an alumina supports.

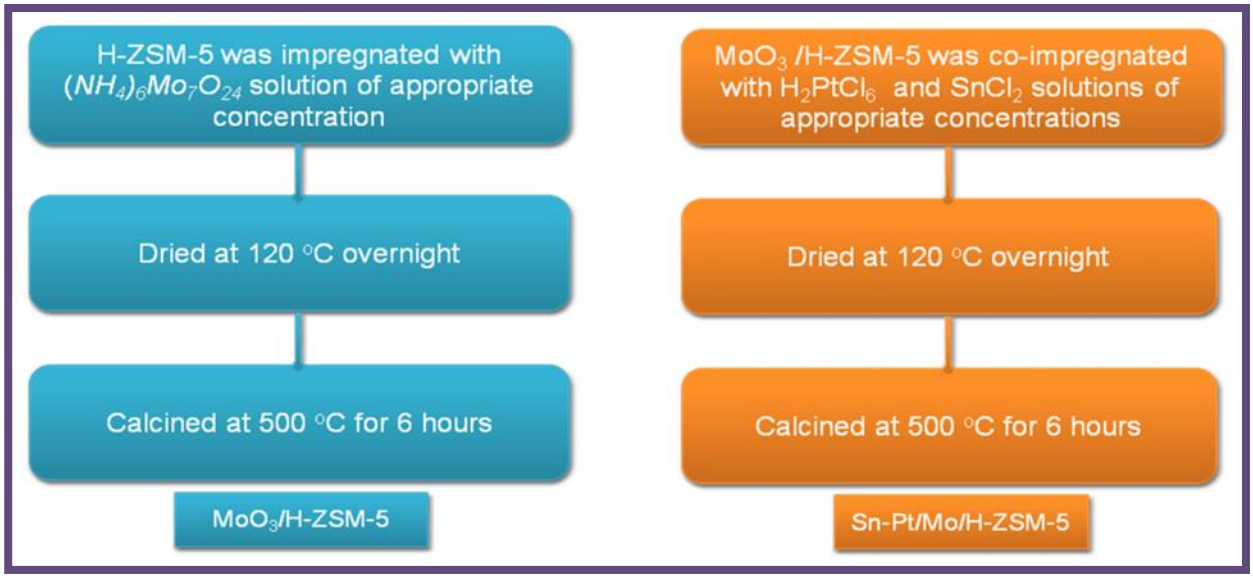
More work has been reported on the dehydrogenation of short and long chains hydrocarbons using Pt-Sn supported catalysts at reaction temperatures less that 550 $^oC$. However, to our knowledge little has been done on evaluating the effect of tin as a promoter on the catalytic activity and coke deposition of platinum modified Mo/H-ZSM-5 zeolite catalysts in the aromatization of methane at high reaction temperature (i.e. at 700 $^oC$). In this chapter, we investigate the effect of tin on the aromatization of methane over platinum modified Mo/H-ZSM-5 catalysts which were prepared by an incipient impregnation method. The methane aromatization reactions were studied at 700 $^oC$ for 6 hours. The effect of tin on the catalytic properties of the catalyst was studied using XRD, $H_2$-TPR, $NH_3$-TPD and BET surface area measurements. The ability of tin to reduce the coke content deposited on the catalysts during MDA reactions was investigated by TGA measurements.

## 5.2. Experimental

### 5.2.1. Catalyst Preparation

The preparation of $MoO_3$/H-ZSM-5 catalysts involved the incipient wetness impregnation of H-ZSM-5 with an aqueous solution of ammonium heptamolybdate, $(NH_4)_6Mo_7O_{24}\cdot 4H_2O$. The

sample was dried at 120 $^{o}$C for 16 hours and then calcined at 500 $^{o}$C for 6 hours. Platinum and tin were loaded on $MoO_3$/H-ZSM-5 samples by a co-impregnation method with solutions of dihydrogenhexachloroplatinate, $H_2PtCl_6$, and tin chloride, $SnCl_2$, of appropriate concentrations. The samples were dried at 120 $^{o}$C overnight and then calcined at 500 $^{o}$C for 6 hours (see Scheme 4.1).




**Scheme 5.1:** Schematic representation of the catalyst preparation steps of impregnation method.

## 5.3. Results and Discussion

### 5.3.1. Catalyst Characterization

Results presented in Table 5.1, show the effect of tin on the BET surface area and pore volume of a Pt/Mo/H-ZSM-5 zeolite catalyst. The incorporation of tin in the Pt/Mo/H-ZSM-5 catalyst does not greatly affect the BET surface areas and pore volumes. This shows the absence of a significant pore blockage effect on formation of Sn-Pt species. This is also shown by the XRD profiles of Sn doped Pt/Mo/H-ZSM-5 (Figure 5.1); the XRD patterns show the retention of the H-ZSM-5 structure with increase in total metal loading.

**Table 5.1:** BET surface areas and pore volumes of the Sn doped Pt/Mo/H-ZSM-5 catalysts with different tin loadings.

| Catalysts | BET Surface Area ($m^2/g$) | Pore Volume ($cm^3/g$) |
|---|---|---|
| 2Mo/H-ZSM-5 | 364 | 0.242 |
| 0.5Pt/2Mo/H-ZSM-5 | 357 | 0.213 |
| 0.05Sn-0.5Pt/2Mo/H-ZSM-5 | 346 | 0.208 |
| 0.1Sn-0.5Pt/2Mo/H-ZSM-5 | 346 | 0.208 |
| 0.2Sn-0.5Pt/2Mo/H-ZSM-5 | 344 | 0.213 |

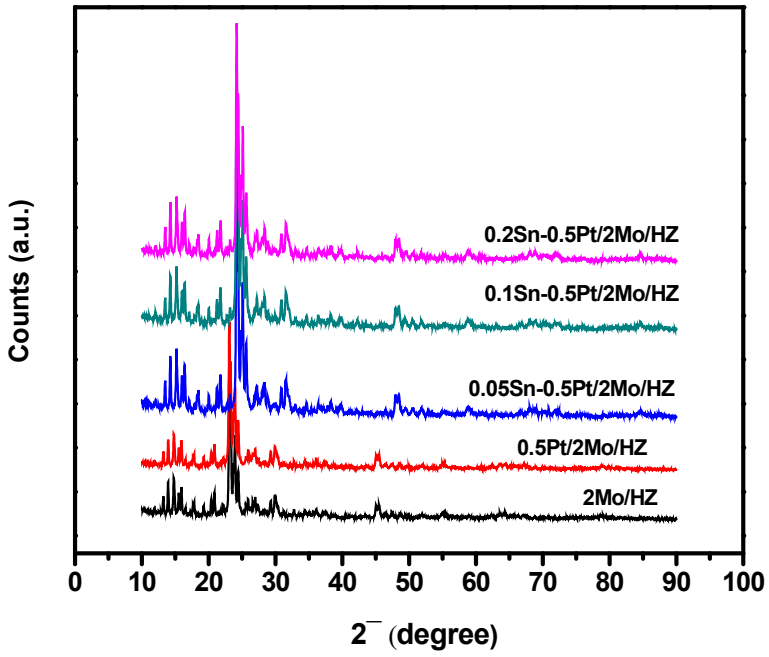



**Figure 5.1:** XRD profiles of Mo/H-ZSM-5 and Sn doped Pt/Mo/H-ZSM-5 catalysts.

In view of the bi-functional character of the Mo/H-ZSM-5 zeolite catalyst, due to the participation of the metal species and the Brønsted acid sites, it is of interest to study the effect of metal on the acidic properties of the H-ZSM-5 catalyst. The acid site properties were studied using ammonia temperature programmed desorption ($NH_3$-TPD). A typical ammonia-TPD profile of H-ZSM-5 shows two peaks centred at low temperature (i.e. about 200 $^oC$) and high temperature (i.e. above 400 $^oC$) as shown in Figure 5.2. The former desorption peak is assigned

to desorption of physisorbed ammonia or ammonia adsorbed on weak acid sites. The latter peak is due to desorption of ammonia from strong acid sites, known to possess Brønsted acid character. Figure 5.2 and Table 5.2 show the $NH_3$-TPD profiles and the amount of ammonia desorbed relative to the acid sites of the Sn doped Pt/Mo/H-ZSM-5 catalysts, respectively. The 2Mo/H-ZSM-5 TPD profile shows two peaks, one at 200 $^oC$ and the other above 400 $^oC$. The concentration of Brønsted acid sites decreased with increase in total metal loading. This is due to an exchange that might be taking place between the zeolitic proton and metal species during the calcination process. Addition of tin led to a decrease in the concentration of the Brønsted acid sites (i.e. from 204 to 140 µmol/g). However, an insignificant decrease was observed for the weak acid sites, (from 520 to 511 µmol/g). The decrease in concentration of Brønsted acid sites is due to the interaction of $Sn^{n+}$ species with the Brønsted acid sites. On the alumina supported catalysts tin poisoned the acidic sites [1], and the same effect was observed for the Brønsted acid sites and weak acid sites possessed by the catalyst under study. A significant change in the total acidity of the Sn-doped Pt/Mo/H-ZSM-5 catalysts was observed upon addition of tin, with total acidity decreasing from 729 to 651 µmol/g (Table 5.2).

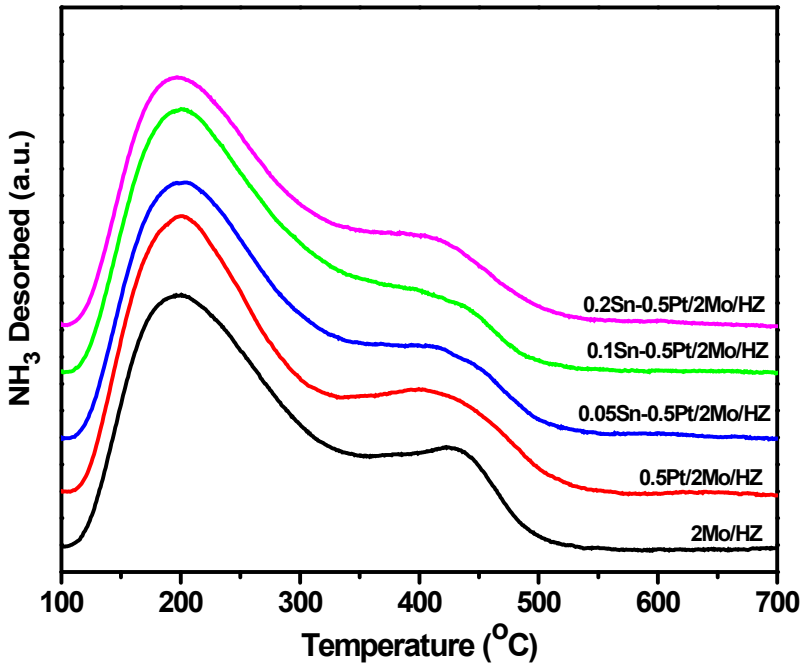



**Figure 5.2:** $NH_3$-TPD profiles of Mo/H-ZSM-5, Pt/Mo/H-ZSM-5 and Sn doped Pt/Mo/H-ZSM-5 zeolite catalysts.

**Table 5.2:** Acid site distribution on Mo/H-ZSM-5, Pt/Mo/H-ZSM and Sn-doped Pt/Mo/H-ZSM-5 catalysts taken from ammonia TPD profiles**.**

| Catalyst | $NH_3$ desorbed at Low Temperature (µmol/g) | $NH_3$ desorbed at High Temperature (µmol/g) | Total Acidity (µmol/g) |
|---|---|---|---|
| 2Mo/H-ZSM-5 | 520 | 234 | 754 |
| 0.5Pt/2Mo/H-ZSM-5 | 525 | 204 | 729 |
| 0.05Sn-0.5Pt/2Mo/H-ZSM-5 | 518 | 171 | 689 |
| 0.1Sn-0.5Pt/2Mo/H-ZSM-5 | 515 | 152 | 667 |
| 0.1Sn-0.5Pt/2Mo/H-ZSM-5 | 511 | 140 | 651 |

Figure 5.3 shows the TPR profiles of 5Sn/H-ZSM-5 and 0.5Pt/5Sn/H-ZSM-5 zeolite catalysts.

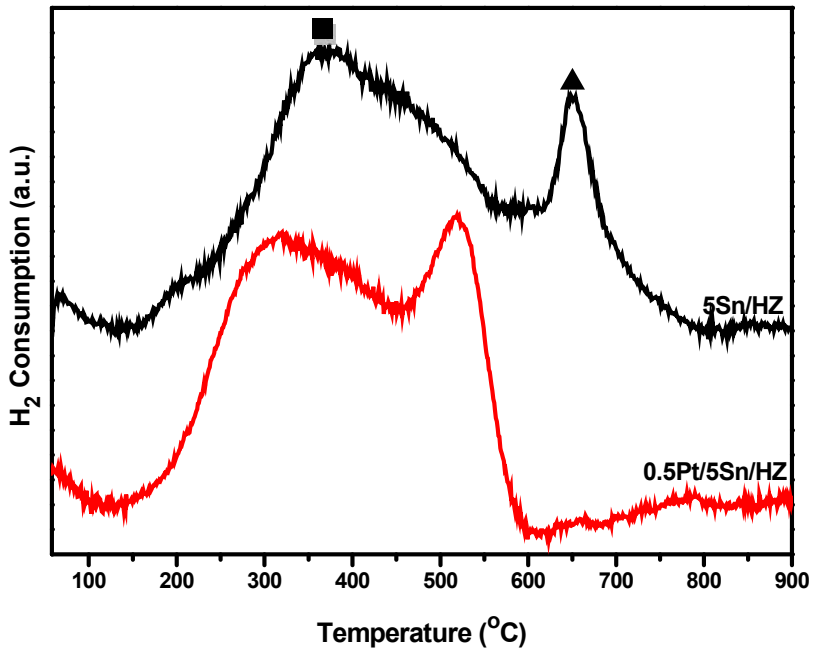



**Figure 5.3:** Hydrogen TPR profiles of 5Sn/H-ZSM-5 and 0.5Pt/5Sn/H-ZSM-5 zeolite catalysts.

The TPR profile of the 5Sn/H-ZSM-5 showed two well defined reduction peaks; one with a maximum temperature at 366 $^{o}$C (square) and the other peak at about 648 $^{o}$C (triangle). The former reduction temperature is attributed to the reduction of $SnO_2$ species to SnO species, while the latter may be attributed to the reduction of SnO species to metallic Sn species. Addition of

0.5 wt.% Pt led to an increase in reducibility of the tin oxide species. A decrease in reduction temperature of both reduction steps was observed upon addition of platinum. The reduction temperature of $SnO_2$ species to SnO species shifted to a lower reduction temperature (319 $^oC$) and the reduction temperature of the SnO species to metallic Sn species shifted from 648 to 518 $^oC$.

Temperature programmed (hydrogen) reduction (TPR) profiles for Mo/H-ZSM-5 and Pt/Mo/H-ZSM-5 zeolite catalysts are presented in Figure 5.4**.**

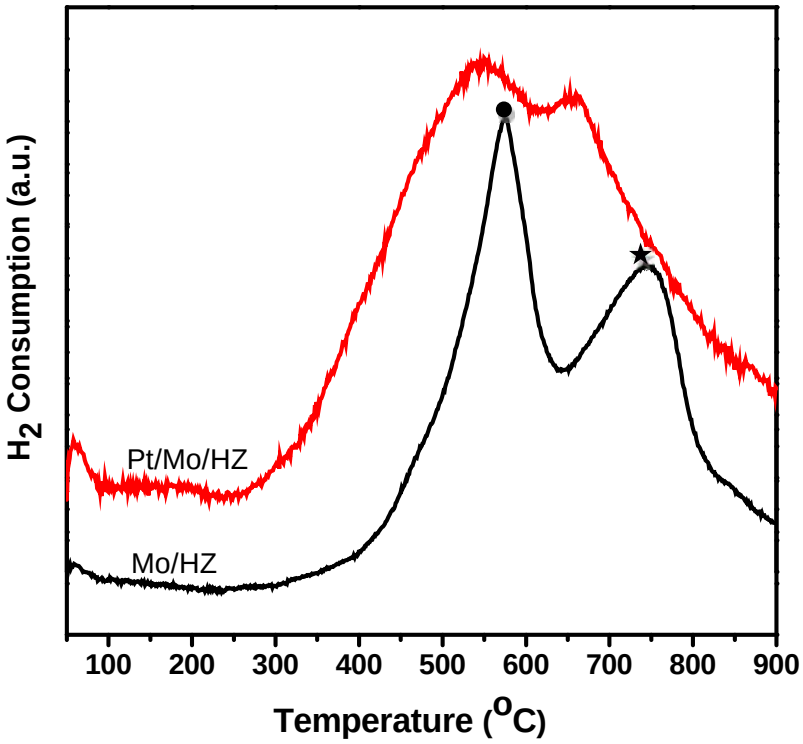



**Figure 5.4:** Hydrogen TPR profiles of Mo/H-ZSM-5 and Pt/Mo/H-ZSM-5 zeolite catalysts.

The profile of the Mo/H-ZSM-5 catalyst shows two distinct reduction peaks. The first peak at 573 $^oC$ (dot) is attributed to the reduction of $MoO_3$ to MoO and second peak at 745 $^oC$ (star) is attributed to the reduction of MoO to metallic Mo [2, 22-24]. Upon addition of platinum onto the Mo/H-ZSM-5 catalyst, a decrease in the reduction temperature of molybdenum was observed with the first peak shifting from 570 to 550 $^oC$ and second peak shifting from 780 to 660 $^oC$. The

shift in the reduction temperature of molybdenum oxide can be associated with the presence of platinum species in the catalyst, i.e. the presence of platinum enhanced the reducibility of the molybdenum oxides. This happens through a hydrogen spill-over mechanism [25]. In the hydrogen spill-over mechanism the hydrogen molecules are firstly adsorbed onto platinum active sites, $H_2$ then dissociates into hydrogen atoms, and these H atoms then migrate onto the molybdenum oxide interface and help in reducing the molybdenum oxides into metallic molybdenum at lower reduction temperatures [26].

The influence of tin on the reducibility of molybdenum in the Pt/Mo/H-ZSM-5 zeolite catalyst is presented in Figure 5.5.

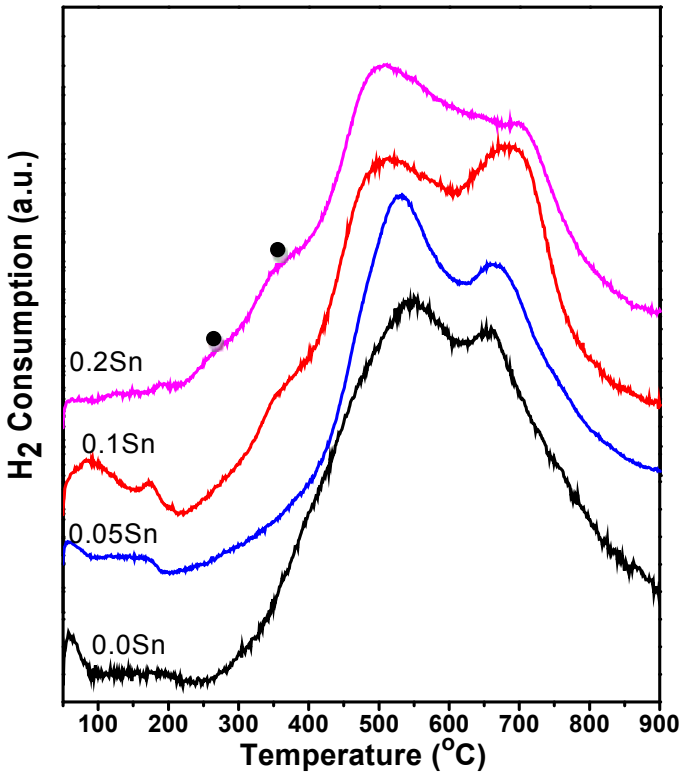



**Figure 5.5:** Hydrogen TPR profiles for the Sn-containing Pt/Mo/H-ZSM-5 zeolites catalysts with tin loadings between 0 and 0.2 wt.%.

Co-impregnated Sn-Pt/Mo/H-ZSM-5 catalysts with various tin loadings raging from 0 to 0.2 wt.% were investigated. The results show that an increase in tin loading led to a decrease in the reduction temperature of $MoO_3$ to MoO (i.e. peak shifted from 570 to 495 $^oC$). However, an

opposite effect was observed on the reduction temperature of MoO to Mo metallic; an increase in tin loading led to an increase in reduction temperature of MoO to Mo. The increase in the reducibility of molybdenum oxide is mainly dependent on the number of platinum species available on the catalyst that can facilitate the hydrogen spillover mechanism. In the presence of tin there is an opportunity for Sn/Pt bimetallic species to be formed [21, 27]. Increasing the tin loading will increase the amount of platinum incorporated into Sn/Pt bimetallic species. Hence a decrease in the reducibility of MoO was observed which led to an increase in reduction temperature of MoO to Mo. The profiles of the tin containing catalysts possess shoulder peaks (dot) at temperatures below 450 $^{o}$C which may be attributed to the reduction process of $SnO_2$ to SnO and SnO to Sn metallic respectively as shown in Figure 5.3. The reduction peak at low temperature i.e. 178 $^{o}$C is attributed to the reduction of platinum oxide [28].

### 5.3.2. Catalytic Results of MDA Reaction

In this section we explore the effect of tin loading on the aromatization of methane over a Pt/Mo/H-ZSM-5 zeolite catalyst at 700 $^{o}$C, using tin loadings between 0 and 0.2 wt.%. The results of the effect of tin on the catalytic conversion of methane into aromatics are shown in Figure 5.6. After use, the catalysts changed from white to black indicating that there was some carbon deposition on the catalysts. The activities of the all catalysts decreased with time-on-stream (TOS). This might be due to deactivation taking place that was caused by coke formed on the active sites of H-ZSM-5. A rapid decrease in catalytic performance between TOS of 15 and 65 minutes is related to the induction period, which is associated with the adsorption of methane onto the zeolite and conversion of molybdenum oxide into molybdenum carbide [29]. The catalytic conversion of methane was improved upon addition of platinum onto the Mo/H-ZSM-5 zeolite catalyst. However, addition of tin led to a decrease in methane catalytic performance of the Pt/Mo/H-ZSM-5 zeolite catalyst. An 8% conversion of methane over a tin free Pt/Mo/H-ZSM-5 catalyst was observed and in the presence of tin a methane conversion between 7.2 and 4.3% was observed with 4.3% assigned to the catalyst with high tin loading (i.e. 0.2 wt.%).

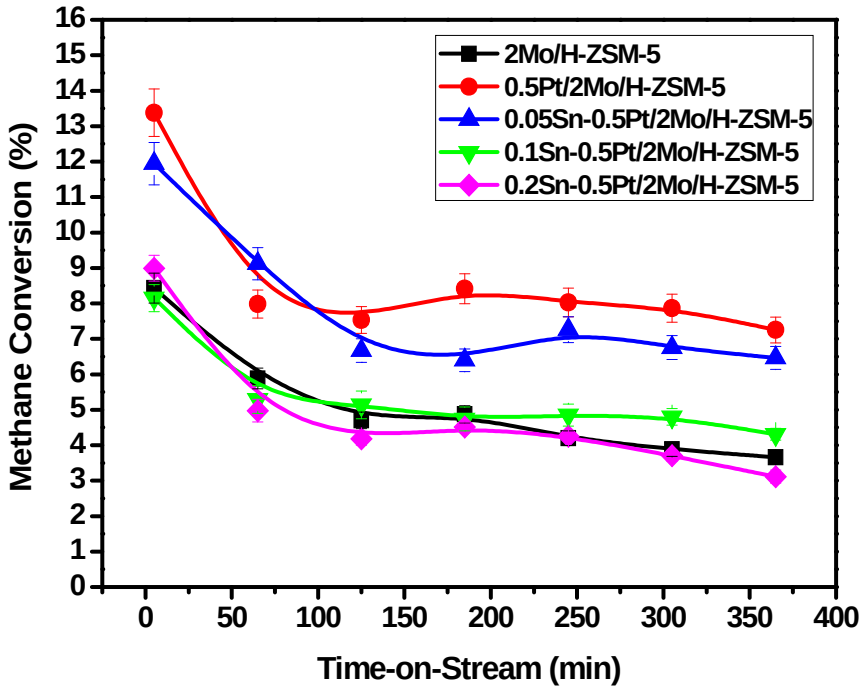



**Figure 5.6:** The catalytic conversion of methane over Sn doped Pt/Mo/H-ZSM-5 catalysts with Sn loadings between 0.05 and 0.2 wt.% loadings.

In contrast to the methane conversion results, the aromatic selectivity (Figure 5.7) showed positive results. High aromatic selectivities were observed with 0.05 and 0.1 wt.% tin containing Pt/Mo/H-ZSM-5 catalysts. Aromatic selectivities between 96 and 84% were observed with a catalyst containing 0.05 wt.% Sn and the 0.1 wt.% Sn catalyst showed aromatic selectivity between 88 and 73%. The aromatic selectivity decreased with increase in TOS due to catalyst deactivation. The high aromatic selectivity is attributed to the dehydrogenation character of the catalyst that is introduced by the presence of tin in Pt/Mo/H-ZSM-5 catalysts [30, 31]. However, increasingly the 0.2 wt.% tin loading gave an aromatic selectivity below 70%. The decrease in the aromatic selectivity with increase in tin loading might be due to formation of a Pt-Sn alloy species which is formed during MDA at 700 $^{o}$C.

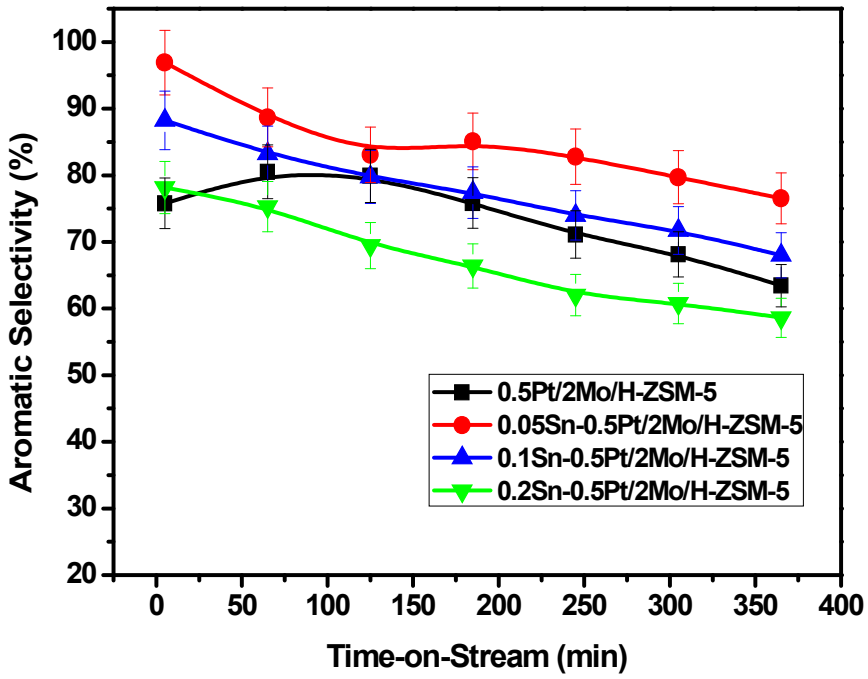



**Figure 5.7:** The percentage aromatic selectivity as a function of time-on-stream of tin doped Pt/Mo/H-ZSM-5 catalysts.

The influence of tin on the product distribution is shown in Figure 5.8. The product selectivities of the catalysts with various tin loadings, at similar methane conversions of 7% were compared. It can be seen that addition of 0.05 wt.% Sn decreased the selectivity of coke and increased the aromatic selectivity. A further increase in tin loading favoured the formation of coke over the aromatic compounds; hence a decrease in aromatic selectivity with increase in tin loadings was seen. Low $C_2$ selectivities were observed for the catalyst with a 0.05 wt.% Sn loading. An increase in tin loadings led to an increase in $C_2$ selectivity. This can be attributed to the decrease in Brønsted acid sites concentration with increase in metal loading. According to the methane aromatization mechanism, the $C_2$ species have to migrate onto the Brønsted acid site interface before oligomerization and cyclization will occur. A noticeable decrease in concentration of Brønsted acid sites will decrease the conversion of $C_2$ species into aromatic compounds [32]. The selectivity to benzene increased with increasing tin loading reaching a maximum of 58% with a 0.1wt.% Sn loaded catalyst.

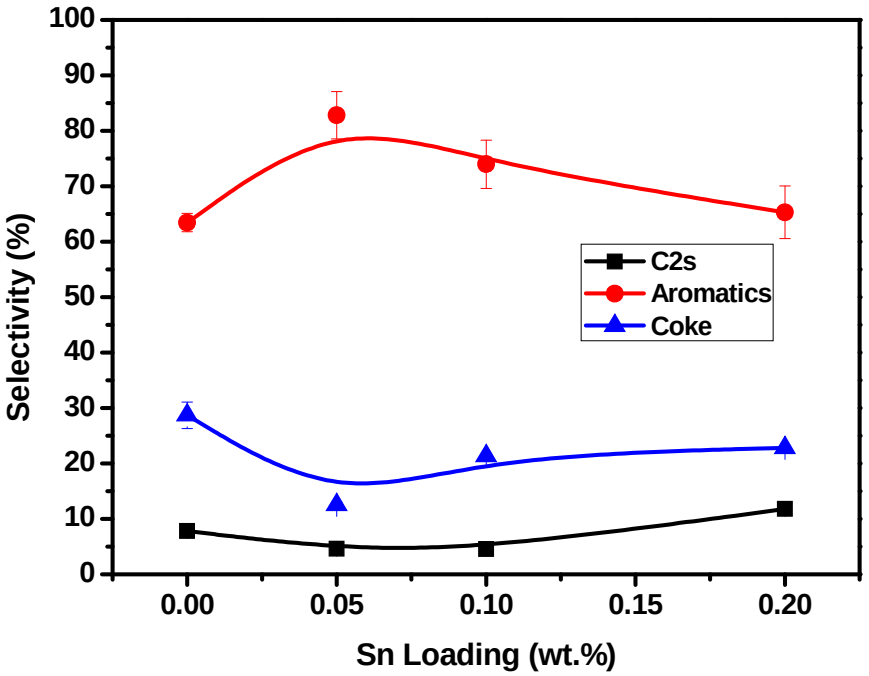



**Figure 5.8:** The effect of tin loading on the $C_2$ species, aromatics and coke selectivity during methane aromatization at 700 $^{o}$C. Catalysts were compared at methane conversions of approximately 7%.

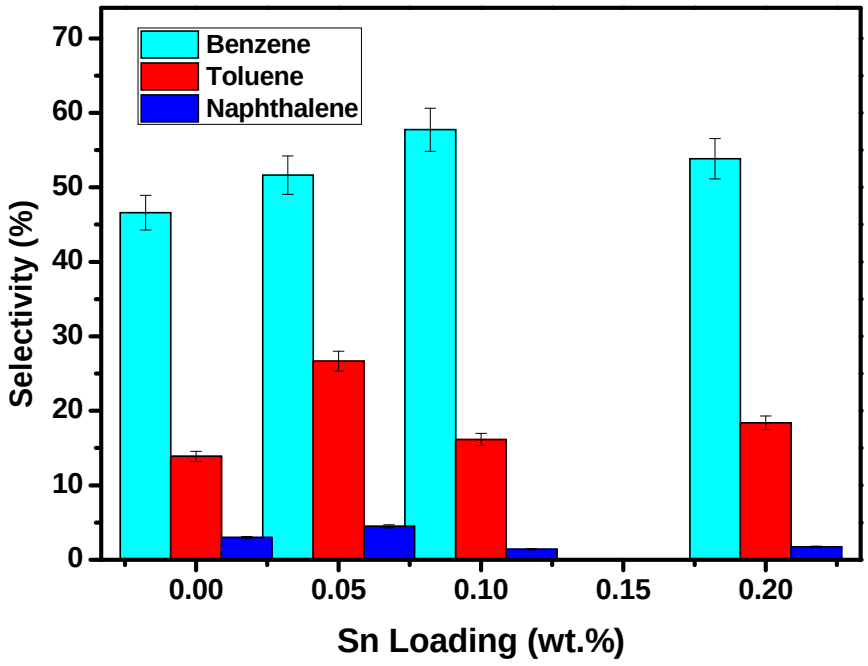



**Figure 5.9:** The effect of tin loading on the aromatic product distribution of MDA at 700 $^{o}$C taken at a methane conversion of 7%.

Figure 5.9 shows the results of the effect of tin loading on the aromatic product distribution of MDA at 700 $^{o}$C at a methane conversion of 7%. The selectivity to benzene increased with tin loading, reaching an optimum of 57 % over the 0.1 wt.% tin loaded catalyst. Selectivity to toluene and naphthalene were observed to be below 30% and 10% respectively with the 0.5wt.% tin loaded catalysts being the best catalyst. The formation of aromatic products is mainly influenced by the tin loading. The distribution plots show that for tin loadings between 0.05 and 0.1 wt.% a high selectivity to benzene and toluene is observed. The decrease in the percentage selectivity of aromatic products can be attributed to the decrease in Brønsted acid sites with increase in the total metal loading [33] as shown by the $NH_3$-TPD results.

The promotion effect of tin was further corroborated by TGA measurements of the spent catalysts that had been exposed to methane at 700 $^{o}$C for 7 hours. The TGA and DTG profiles are shown in Figure 5.10(a) and Figure 5.10(b) respectively.

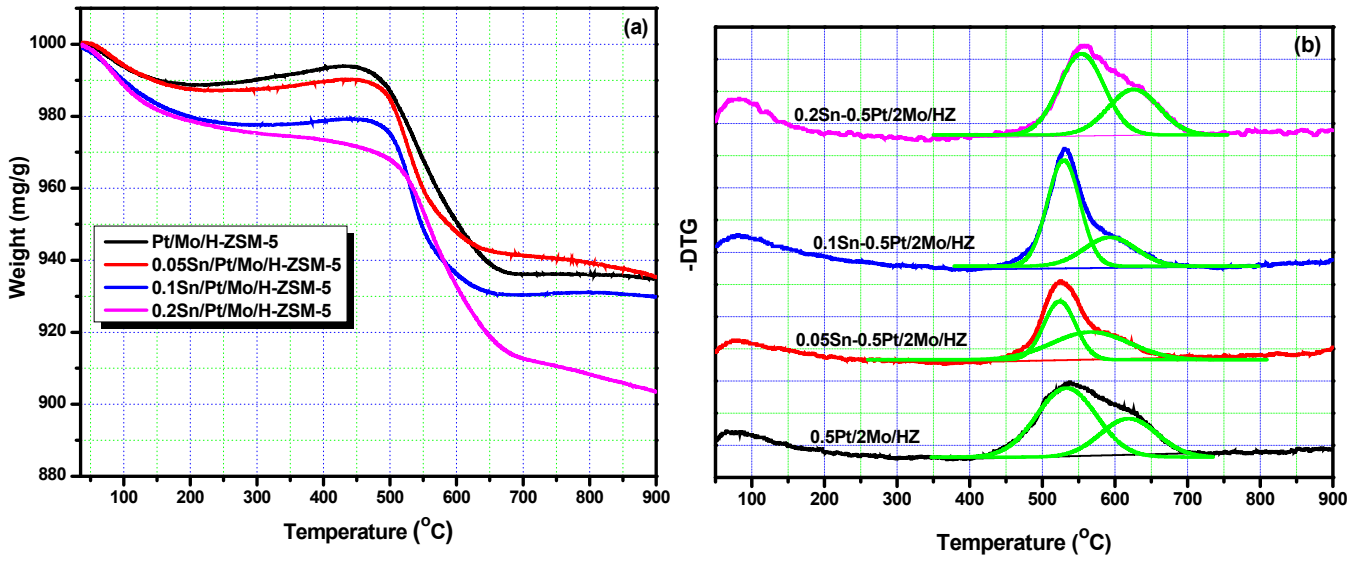



**Figure 5.10:** TGA (a) and DTG (b) profiles of coked Pt/Mo/H-ZSM-5 and Sn-containing Pt/Mo/H-ZSM-5 zeolite catalysts after MDA at 700 $^{o}$C.

From the TGA profiles, it is clear that the presence of tin decreases the amount of coke deposit formed during the MDA reaction. The amount of coke formed on the Pt/Mo/H-ZSM-5 was 56.9 mg per gram of catalyst (Table 5.3). The Sn-doped Pt/Mo/H-ZSM-5 catalyst gave 46.7 and 48.5

mg of coke per gram of catalyst for the 0.05 and 0.1 wt.% tin loaded catalysts, respectively. This translates to a 16% of reduction of coke deposits with catalysts containing low tin loadings. A typical DTG profile of spent Pt/Mo/H-ZSM-5 has two peaks, both at temperatures above 500 $^{o}$C. The two peaks indicate two types of coke formed on the Mo/H-ZSM-5 catalyst. Xu et al. [34] and Weckhuysen et al. [35] used XPS to characterize the coked catalyst. From their XPS results they reported three different types of coke formed during the MDA reaction over Mo/H-ZSM-5, which they referred to as carbidic carbon in molybdenum carbide, molybdenum-associated coke and aromatic-type coke on acid sites.

**Table 5.3:** Summarized TGA and DTG results of coked Pt/Mo/H-ZSM-5 and Sn-Pt/Mo/H-ZSM-5 with various tin loadings.

| Sn Loading (wt.%) | Amount of Coke (mg/g cat.) | Low Decomposition Temperature ($^{o}$C) | High Decomposition Temperature ($^{o}$C) |
|---|---|---|---|
| 0 | 56.9 | 535 | 628 |
| 0.05 | 46.7 | 530 | 611 |
| 0.1 | 48.5 | 530 | 613 |
| 0.2 | 58.4 | 558 | 632 |

For the Pt/Mo/H-ZSM-5 catalysts the TGA data listed in Figure 5.9b and Table 5.3 reveals two peaks. The first peak at 535 $^{o}$C, is due to the oxidation of carbon that is associated with molybdenum and the carbidic carbon in the molybdenum carbide and the second peak at 628 $^{o}$C is due to the oxidation of aromatic carbon formed on Brønsted acid sites [7, 29, 33, 36, 37]. The areas under the peaks show the relative ratio of the amounts of coke deposits on each active site (i.e. Brønsted acid sites or molybdenum carbides). This implies that the amount of coke deposited on molybdenum carbides is a small fraction of the total content of coke formed during MDA. The oxidation temperature of coke on the Brønsted acid site remained in the 530 $^{o}$C region but a decrease in oxidation temperature of coke deposit associated with molybdenum was observed with catalysts containing 0.05 and 0.1 wt.% tin loadings. This might be due to the decrease in the stability of coke formed on the molybdenum carbide. However, with the 0.2 wt.% tin loaded catalyst, there was an increase in the oxidation temperature of coke associated

with molybdenum. This might be due to the decrease in the rate of the hydrogen spill over reaction observed from TPR results.

Nagai et al.[37] proposed a mechanism in which aromatic compounds are formed over a carburized Mo/Al-FSM-16 catalyst. The schematic representation of the mechanism is shown in Figure 5.11.

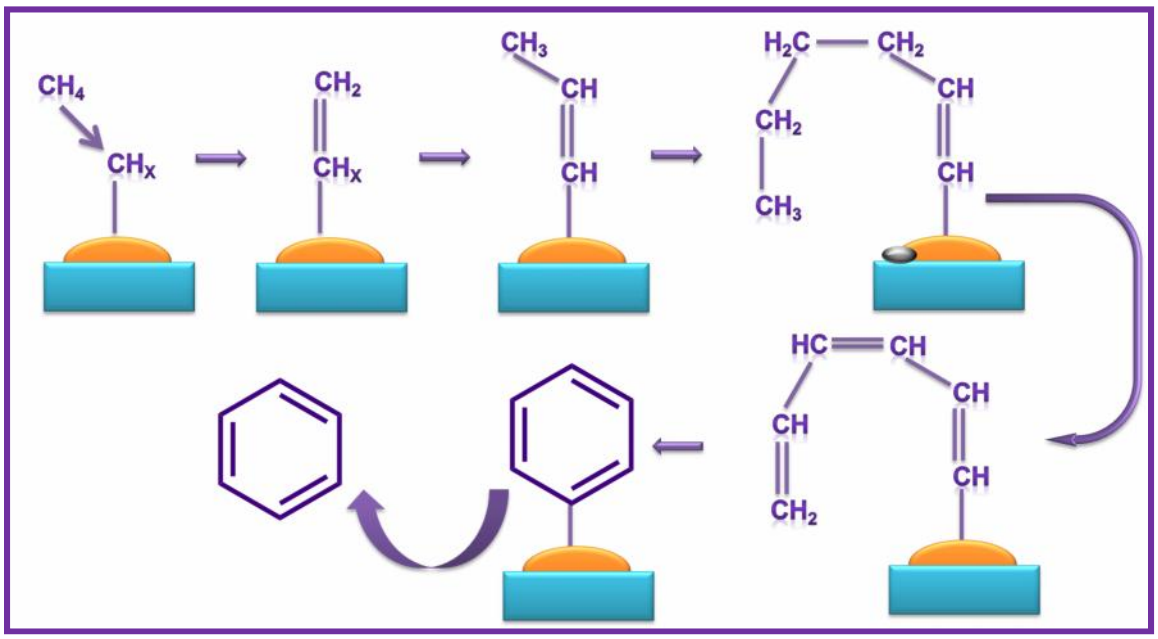



**Figure 5.11:** Schematic representation of the dehydroaromatization of methane with tin adding the dehydrogenation character to the reaction [37].

Their mechanism suggests that for the aromatic compounds to form there should be some chain growth taking place on the molybdenum carbide sites. In the mechanism, methane is first adsorbed on $Mo_2C$ to form $CH_x$ ($CH_2$ and $CH_3$) species by abstracting a hydrogen atom with release of $H_2$. The $CH_x$ species can subsequently react to form adsorbed $C_4H_8$. The growing carbon chain then converts into a ring to form benzene. Adsorbed $C_3H_8$ (or $C_2H_4$) species were also formed through the dehydrogenation of $C_2$ and $C_3$ alkyl species. The presence of tin in Pt/Mo/H-ZSM-5 zeolite catalyst enhances the dehydrogenation of adsorbed alkanes to alkenes by decreasing the cracking activity. This will favour cyclization reactions and formation of aromatic compounds from short chain hydrocarbons.

## 5.4. Summary

Dehydroaromatization of methane was studied over Sn-Pt/Mo/HZSM-5 catalysts and compared to Pt/Mo/H-ZSM-5 at 700 $^{o}$C. Catalysts containing tin showed low activity towards dehydroaromatization of methane. However, the formation of aromatic compounds was favoured. Deactivation due to coke formation is still dominant, but a reduction in the amounts of coke deposit was observed with 0.05 and 0.1 wt.% tin containing catalysts and the selectivity reached 12%. TGA measurements demonstrated a reduction in coke deposits by 16%. Upon addition of tin, a decrease in the reducibility of molybdenum oxide to metallic molybdenum was observed.

## 5.5. Reference List

[1] L.Y. Chen, L.W. Lin, Z.S. Xu, X.S. Li, T. Zhang, *Journal of Catalysis*, **157** (1995) 190.

[2] P.L. Tan, Y.L. Leung, S.Y. Lai, C.T. Au, *Applied Catalysis A: General*, **228** (2002) 115.

[3] F. Solymosi, J. Cserényi, A. Szöke, T. Bánsági, A. Oszkó, *Journal of Catalysis*, **165** (1997) 150.

[4] D. Ma, Y. Shu, X. Bao, Y. Xu, *Journal of Catalysis*, **189** (2000) 314.

[5] W. Liu, Y. Xu, *Journal of Catalysis*, **185** (1999) 386.

[6] D. Wang, D.G. Ivey, *Materials Science and Engineering: B*, **41** (1996) 289.

[7] L. Wang, L. Tao, M. Xie, G. Xu, J. Huang, Y. Xu, *Catalysis Letters*, **21** (1993) 35.

[8] A. Hassan, A. Sayari, *Applied Catalysis A: General*, **297** (2006) 159.

[9] P.D. Sily, F.B. Noronha, F.B. Passos, *Journal of Natural Gas Chemistry*, **15** (2006) 82.

[10] S.M. Stagg, C.A. Querini, W.E. Alvarez, D.E. Resasco, *Journal of Catalysis*, **168** (1997) 75.

[11] S. Liu, L. Wang, Q. Dong, R. Ohnishi, M. Ichikawa, *Studies in Surface Science and Catalysis*, **119** (1998) 241.

[12] C. Audo, J.F. Lambert, M. Che, B. Didillon, *Catalysis Today*, **65** (2001) 157.

[13] J. Beltramini, D.L. Trimm, *Applied Catalysis*, **31** (1987) 113.

[14] S. Pisduangdaw, J. Panpranot, C. Methastidsook, C. Chaisuk, K. Faungnawakij, P. Praserthdam, O. Mekasuwandumrong, *Applied Catalysis A: General*, **370** (2009) 1.

[15] H. Armendáriz, A. Guzmán, J.A. Toledo, M.E. Llanos, A. Vázquez, G. Aguilar-Ríos, *Applied Catalysis A: General*, **211** (2001) 69.

[16] L. Rodríguez, D. Romero, D. Rodríguez, J. Sánchez, F. Domínguez, G. Arteaga, *Applied Catalysis A: General*, **373** (2010) 66.

[17] G. Padmavathi, K.K. Chaudhuri, D. Rajeshwer, G. Sreenivasa Rao, K.R. Krishnamurthy, P.C. Trivedi, K.K. Hathi, N. Subramanyam, *Chemical Engineering Science*, **60** (2005) 4119.

[18] F.B. Passos, D.A.G. Aranda, M. Schmal, *Journal of Catalysis*, **178** (1998) 478.

[19] B. R, *Journal of Catalysis*, **71** (1981) 348.

[20] R. Bacaud, P. Bussiere, F. Figueras, J.P. Mathieu, *Studies in Surface Science and Catalysis*, (1976) 509.

[21] A.D. Ballarini, C.G. Ricci, S.R. de Miguel, O.A. Scelza, *Catalysis Today*, **133–135** (2008) 28.

[22] M.W. Ngobeni, A.F. Carley, M.S. Scurrell, C.P. Nicolaides, *Journal of Molecular Catalysis A: Chemical*, **305** (2009) 40.

[23] H. Jiang, L. Wang, W. Cui, Y. Xu, *Catalysis Letters*, **57** (1999) 95.

[24] B. Liu, Y. Yang, A. Sayari, *Applied Catalysis A: General*, **214** (2001) 95.

[25] J. Wang, W. Li, C. Yu, Y. Chen, Y. Zhang, *Reaction Kinetics and Catalysis Letters*, **62** (1997) 217.

[26] L. Chen, A.C. Cooper, G.P. Pez, H. Cheng, *Journal of Physical Chemistry C*, **112** (2008) 1755.

[27] R. Srinivasan, R.J. De Angelis, B.H. Davis, *Journal of Catalysis*, **106** (1987) 449.

[28] J.C. Serrano-Ruiz, A. Sepúlveda-Escribano, F. Rodríguez-Reinoso, *Journal of Catalysis*, **246** (2007) 158.

[29] D. Ma, Y. Shu, M. Cheng, Y. Xu, X. Bao, *Journal of Catalysis*, **194** (2000) 105.

[30] B.H. Davis, G.A. Westfall, J. Watkins, J. Pezzanite Jr, *Journal of Catalysis*, **42** (1976) 247.

[31] S. Scire, R. Maggiore, S. Galvagno, C. Crisafulli, L. Solarino, *Reaction Kinetics and Catalysis Letters*, **40** (1989) 349.

[32] J. Shu, A. Adnot, B.P.A. Grandjean, *Industrial & Engineering Chemistry Research*, **38** (1999) 3860.

[33] V.R. Choudhary, S. Banerjee, D. Panjala, *Journal of Catalysis*, **205** (2002) 398.

[34] Y. Xu, X. Bao, L. Lin, *Journal of Catalysis*, **216** (2003) 386.

[35] B. Weckhuysen, M. Rosynek, J. Lunsford, *Catalysis Letters*, **52** (1998) 31.

[36] Y. Shu, R. Ohnishi, M. Ichikawa, *Journal of Catalysis*, **206** (2002) 134.

[37] M. Nagai, T. Nishibayashi, S. Omi, *Applied Catalysis A: General*, **253** (2003) 101.

# Chapter 6

# Dehydroaromatization of Methane over Sn-Pt Modified Mo/H-ZSM-5 Zeolite Catalysts: Effect of Preparation Method

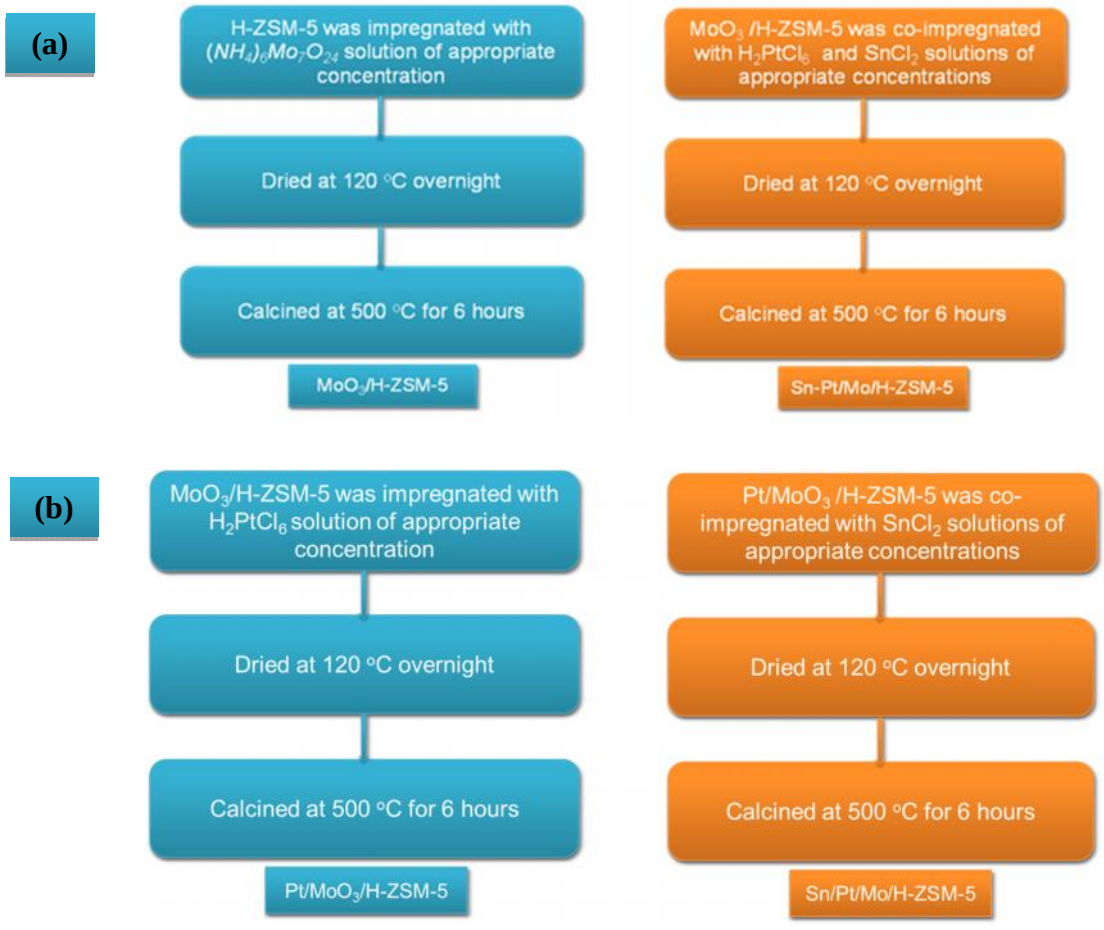
## 6.1. Introduction

In the previous chapter we observed that the presence of tin in the Pt/Mo/H-ZSM-5 zeolite catalyst had a significant influence on the catalytic behavior in the MDA reaction. The interaction between tin and platinum has attracted much attention and aided in understanding the role of tin during the catalytic reactions. From the results presented in the previous chapter we found that at low tin loadings the methane conversion decreased, while an improvement in the aromatic selectivity was observed. Catalysts that contained a high tin loading showed low coke resistance when compared with the 0.05wt.% tin loaded catalyst. This led us to investigate the influence of tin on the accessibility of platinum surface atoms by the reactants during the MDA reaction over tin modified Pt/Mo/H-ZSM-5 catalysts. Different methods were employed to prepare catalysts. The main focus of this chapter relates to the characterization of catalysts using CO probe molecules to assess the influence of tin on the accessibility of platinum to the reactants. The surface character of the tin-platinum modified Mo/H-ZSM-5 zeolite catalysts was studied using FT-IR CO adsorption spectroscopy and a CO pulse chemisorption technique. These adsorption techniques were used as indirect methods to investigate the influence of the catalyst preparation methods on the catalytic behaviour of the tin-platinum modified Mo/H-ZSM-5 zeolite catalysts prepared by sequential impregnation and co-impregnation methods.

## 6.2. Experimental

### 6.2.1. Catalysts Preparation

The preparation of $MoO_3$/H-ZSM-5 catalysts involved the incipient wetness impregnation of H-ZSM-5 with an aqueous solution of ammonium heptamolybdate, $(NH_4)_6Mo_7O_{24}•4H_2O$. The sample was dried at 120 $^oC$ for 16 hours and then calcined at 500 $^oC$ for 6 hours. Platinum and tin were loaded on $MoO_3$/H-ZSM-5 using a co-impregnation and sequential impregnation methods. Solutions of dihydrogenhexachloroplatinate, $H_2PtCl_6$, and tin chloride, $SnCl_2$, of appropriate concentrations, were used to achieve 0.5 wt.% and 0.2 wt.% loadings of platinum and tin, respectively. The samples were dried at 120 $^oC$ overnight and then calcined at 500 $^oC$ for 6 hours.




**Scheme 6.1:** Schematic representation of the catalyst preparation methods of Sn modified Pt/Mo/H-ZSM-5 zeolite catalysts, (a) co-impregnation method and (b) sequential impregnation.

## 6.3. Results and Discussion

### *6.3.1. Characterization Results*

The influence of the catalyst preparation method on the reducibility of molybdenum oxide species in tin modified Pt/Mo/H-ZSM-5 catalysts was investigated by hydrogen-TPR. The hydrogen TPR profiles of the tin modified Pt/Mo/H-ZSM-5 catalysts are presented in Figure 6.1.

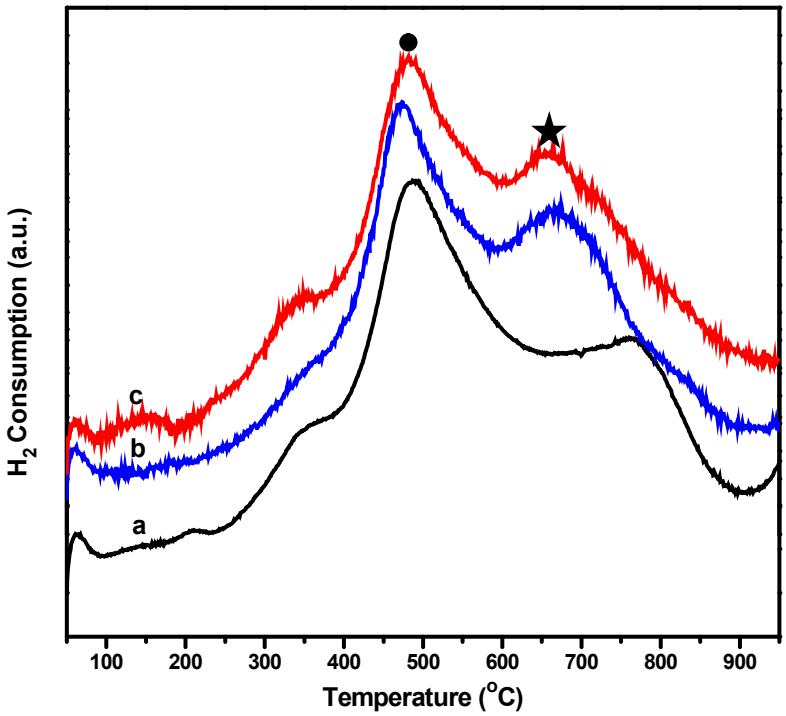



**Figure 6.1:** Hydrogen TPR profiles of tin modified Pt/Mo/H-ZSM-5 zeolite catalysts prepared by sequential and co-impregnation methods, (a) co-impregnated 0.2Sn-0.5Pt/2Mo/H-ZSM-5, (b) sequentially impregnated 0.2Sn/0.5Pt/2Mo/H-ZSM-5 and (c) 0.5Pt/0.2Sn/2Mo/H-ZSM-5.

The profile of the co-impregnated Pt/Mo/H-ZSM-5 catalyst shows two distinct reduction peaks at high reduction temperatures associated with the reduction of molybdenum oxide species. The first peak at 486 $^{o}$C (dot) is attributed to the reduction of $MoO_3$ to MoO and the second peak at 775 $^{o}$C (star) is attributed to the reduction of MoO to Mo metal [1-3]. The profiles of the sequentially loaded samples showed a decrease in the reduction temperature of the MoO to metallic molybdenum at 660 $^{o}$C. The reducibility of molybdenum species is mainly dependent

on the proximity of platinum particles to molybdenum species to facilitate the hydrogen spillover reaction. This suggests that in the sequentially impregnated samples there is a good molybdenum-platinum interaction and that the two metals are in proximity to each other, hence the platinum is able to enhance the reducibility of molybdenum oxide species.

The CO adsorption studies were employed to investigate the influence of catalyst preparation methods on the interaction between tin, platinum and molybdenum metal species. A high vacuum system with an IR cell which was coupled to a FT-IR spectrometer was used to measure the change on the surface of the catalysts as CO was introduced. The catalysts were prepared using co-impregnation and sequential impregnation methods. Mo/H-ZSM-5 was treated as the parent part of the catalysts; tin and platinum were loaded in different sequences for the sequentially impregnated catalysts.

Figure 6.2 shows the CO adsorption FT-IR spectra of the uncalcined 0.5Pt/2Mo/H-ZSM-5 and co-impregnated 0.2Sn-0.5Pt/Mo/H-ZSM-5 zeolite catalysts; measurements were performed at beam temperature.

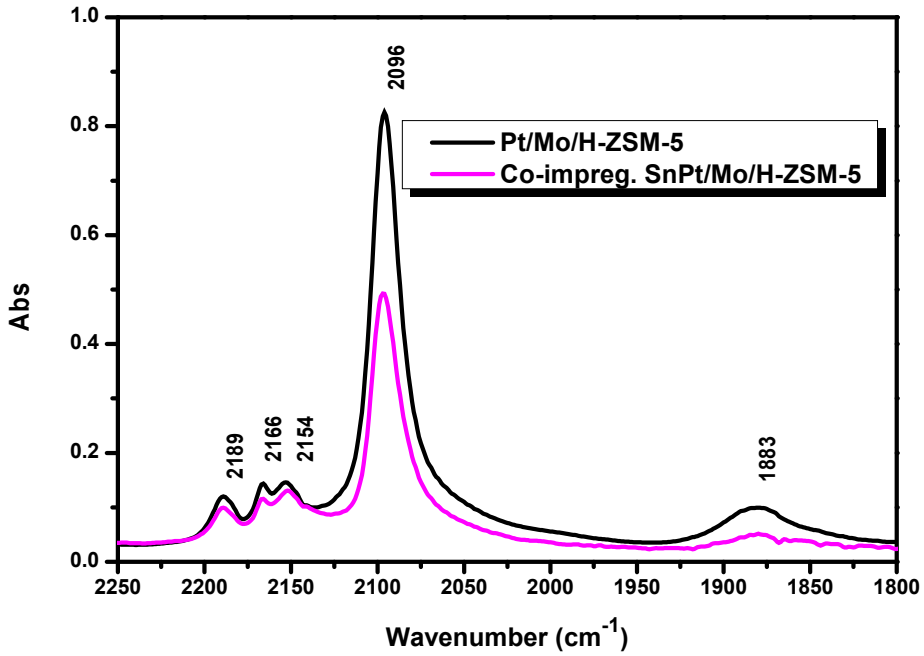



**Figure 6.2:** FTIR spectra of CO adsorbed on uncalcined 0.5Pt/2Mo/H-ZSM-5 and co-impregnated 0.2Sn-0.5Pt/2Mo/H-ZSM-5 zeolite catalysts.

Adsorption of CO on the un-calcined 0.5Pt/2Mo/H-ZSM-5 and co-impregnated 0.2Sn-0.5Pt/2Mo/H-ZSM-5 zeolite catalysts led to the appearance of five IR bands at 2189, 2166, 2154, 2096 and 1883 $cm^{-1}$ wavenumbers. The bands at 2189 and 2166 $cm^{-1}$ wavenumbers correspond to CO adsorbed on $Pt^{2+}$ associated with dicarbonyl complexes [4, 5] and the band at 2154 $cm^{-1}$ corresponds to the CO linearly bonded to $Pt^{2+}$ forming a monocarbonyl complex [6]. The band with high intensity at 2096 $cm^{-1}$ is due to CO bonded to $Pt^{1+}$ species. Upon addition of tin a significant decrease in the intensity of this band was observed which can be attributed to the electronic effects introduced by the presence of tin [7, 8]. The decrease in the intensity of the band at 1883 $cm^{-1}$ wavenumber is attributed to the decrease in the concentration of bridging CO species [9]. The presence of tin introduced a geometric effect which led to the surface dilution of platinum and this led to a decrease in the number of adjacent platinum atoms, and consequently a decrease in the number of bridged CO adsorbed molecules [10].

The effect of tin on the adsorption capacity of platinum in the calcined Sn-Pt modified Mo/H-ZSM-5 zeolite catalysts prepared by co-impregnation and sequential impregnation methods is shown in Figure 6.3. The catalysts were pressed into a wafer and mounted in a cell equipped with CaF windows. The catalysts were exposed to CO at beam temperature and CO adsorption was monitored by FT-IR spectroscopy. Figure 6.3 shows the spectra of CO adsorbed on 0.5Pt/2Mo/H-ZSM-5, co-impregnated 0.2Sn-0.5Pt/2Mo/H-ZSM-5, and sequentially impregnated 0.2Sn/0.5Pt/2Mo/H-ZSM-5 and 0.5Pt/0.2Sn/2Mo/H-ZSM-5 catalysts as the function of pressure.

When these samples are calcined prior to CO adsorption FT-IR studies, several IR bands which correspond to CO bonded to platinum species in high oxidation states observed (Figure 6.3). This suggests that during the calcination stage platinum species with low oxidation states were oxidized into platinum species in higher oxidation states. From the FT-IR profiles the band intensity of CO adsorbed on $Pt^{1+}$ decreased while the concentration CO bonded to $Pt^{2+}$ increased. Furthermore the formation of less stable $Pt^{3+}$-CO species was well pronounced with the presence of 2205 and 2173 $cm^{-1}$ bands (Figure 6.3(c)). The band that is associated with CO bonded to $Pt^{2+}$ species shifted from 2148 to about 2160 and 2155 $cm^{-1}$ upon addition of tin. This change might be due to the platinum-tin interaction. The bands at 2205 and 2169 $cm^{-1}$ correspond to $Pt^{3+}$-$(CO)_2$ species which tend to collapse at high CO coverage. The band at 2194 $cm^{-1}$ is associated with CO bonded on $Pt^{3+}$ species that forms a more stable monocarbonyl complex than the

germinal dicarbonyl complex [4, 11]. The presence of $Pt^{2+}$-CO species is shown by the appearance of bands at 2157 and 2148 $cm^{-1}$ which are associated with CO molecules forming germinal carbonyl species with $Pt^{2+}$ species [4-6]. We further observed the presence of $Pt^{1+}$-CO after calcination which matches the two bands at 2130 and 2108 $cm^{-1}$. These bands are associated with CO adsorbed on $Pt^{1+}$ that form a dicarbonyl complex. The band at 2080 $cm^{-1}$ is associated with CO adsorbed on the metallic platinum species on the surface of the catalyst [12]. A change in the intensity of the bands corresponding to CO adsorbed on $Pt^{1+}$ after calcination was noted. It was also observed that the intensity of these bands is low when compared with other bands (i.e. at 2157 and 2148 $cm^{-1}$ associated with $Pt^{2+}$-CO species). This suggests that during calcination $Pt^{1+}$ is oxidized to $Pt^{3+}$ and $Pt^{2+}$ species. However, for the catalyst prepared by the co-impregnation method no significant change on the intensity of the band at 2099 $cm^{-1}$, which corresponds to CO adsorbed on $Pt^{1+}$, was observed after calcination. This might be due to tin inhibiting the oxidation of $Pt^{1+}$ to high oxidation state platinum species. Thus, we observed less intense bands corresponding to $Pt^{2+}$ species. The spectra associated with the sequential impregnated catalyst (Seq(0.2Sn/0.5Pt)) showed a different trend when compared with the co-impregnated catalyst (Co-(0.2Sn-0.5Pt)) and the sequential impregnated catalyst (Seq(0.5Pt/0.2Sn)). The intensity of the band due to the CO linearly adsorbed on $Pt^{1+}$ species is high for the co-imp(0.2Sn-0.5Pt) and seq(0.5Pt/0.2Sn) catalysts but no band signifying the presence of $Pt^{1+}$ species was observed for the seq(0.2Sn/0.5Pt) catalyst. It is suggested that after successive calcination processes the platinum species become exposed and this led to full oxidation of $Pt^{1+}$ species in the seq(0.2Sn/0.5Pt) catalyst.

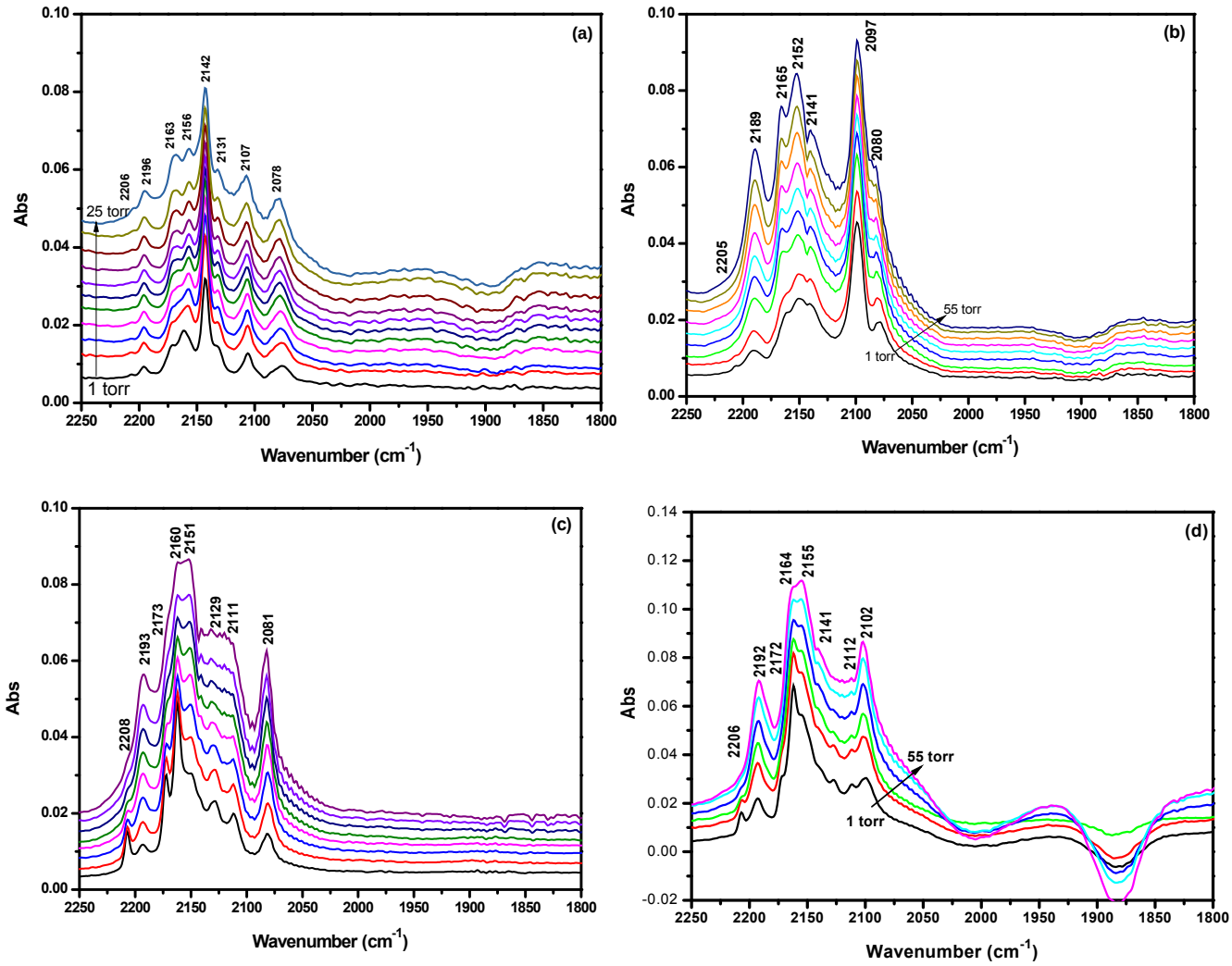



**Figure 6.3:** FTIR spectra of CO adsorbed of calcined Sn modified Pt/Mo/H-ZSM-5 zeolite catalysts, taken at different CO pressure after 15 minutes adsorption intervals. (a) 0.5Pt/2Mo/H-ZSM-5, (b) co-impregnated 0.2Sn-0.5Pt/2Mo/H-ZSM-5, (c) sequentially impregnated 0.2Sn/0.5Pt/2Mo/H-ZSM-5 and (d) 0.5Pt/0.2Sn/2Mo/H-ZSM-5.

Figure 6.4 shows the FT-IR spectra of CO adsorbed on the tin modified Pt/Mo/H-ZSM-5 zeolite catalysts reduced at 200 $^{o}$C for 1 hour. The spectral measurements were taken at beam temperature and the CO pressure was adjusted to 5 Torr. The FT-IR spectra of CO adsorbed on the reduced catalysts show bands at 2080 and 2085 cm$^{-1}$ for the Pt/Mo/H-ZSM-5 and co-impregnated Sn-Pt/Mo/H-ZSM-5 catalysts respectively. The bands correspond to CO molecules that are linearly bonded to the metallic platinum atoms. The shift in band position after addition of tin is associated with the electronic effects of tin on platinum surface atoms [13]. It is worth noting that for the sequential impregnated sample only gaseous CO was detected by the FT-IR

technique. This suggests that after reduction no platinum surface atoms are available for the adsorption of CO molecules. Arteaga et al.[12] reported that during the reduction step that tin oxide tends to spread over the surface of the catalyst and covers the surface platinum atoms. Another reason might be that during reduction a subsequent migration of tin took place leading to the formation of a mixed oxide layer that covered the surface platinum atoms (or Pt-Sn alloys) resulting in the platinum not being accessible to interact with CO [14].

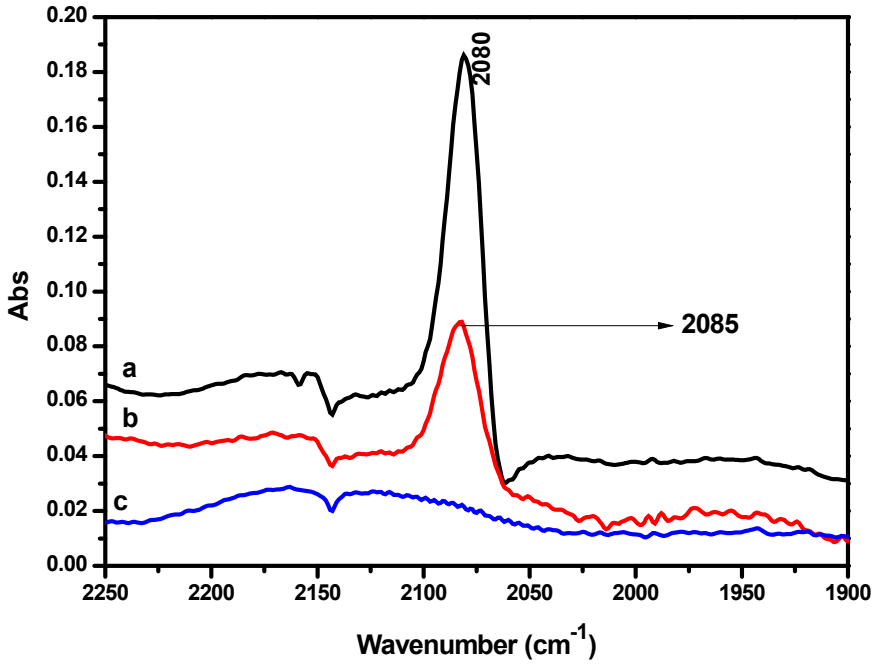



**Figure 6.4:** FT-IR spectra of CO adsorbed of reduced Sn modified Pt/Mo/H-ZSM-5 zeolite catalysts, taken at 5 Torr CO pressure. (a) 0.5Pt/2Mo/H-ZSM-5, (b) Co impregnated 0.2Sn-0.5Pt/Mo/H-ZSM-5, (c) Sequentially impregnated 0.2Sn/0.5Pt/2Mo/H-ZSM-5.

The XPS spectra of Pt 4f levels of the sequentially impregnated Sn/Pt/Mo/H-ZSM-5 catalyst in the calcined form and reduced form are shown in Figure 6.5 (a) and Figure 6.5 (b). The spectrum of the calcined form catalyst show two well defined peaks, a broad peak at higher binding energy (75.8 eV) corresponding to Pt $4f_{5/2}$ and the second peak at lower binding energy (74.4 eV) corresponds to Pt $4f_{7/2}$. The peak at lower binding energy is associated with platinum in the metallic state. After reducing the catalyst the peaks shifted to lower binding energies (i.e. 74.5 eV and 73.0 eV) and the intensities of the peaks decreased. The decrease in the peak intensity may be attributed to a decrease in the amount of detectable surface platinum which may

be covered by tin oxide species [15, 16]. This can also be due to the dilution of platinum surface atoms by the metallic tin species.

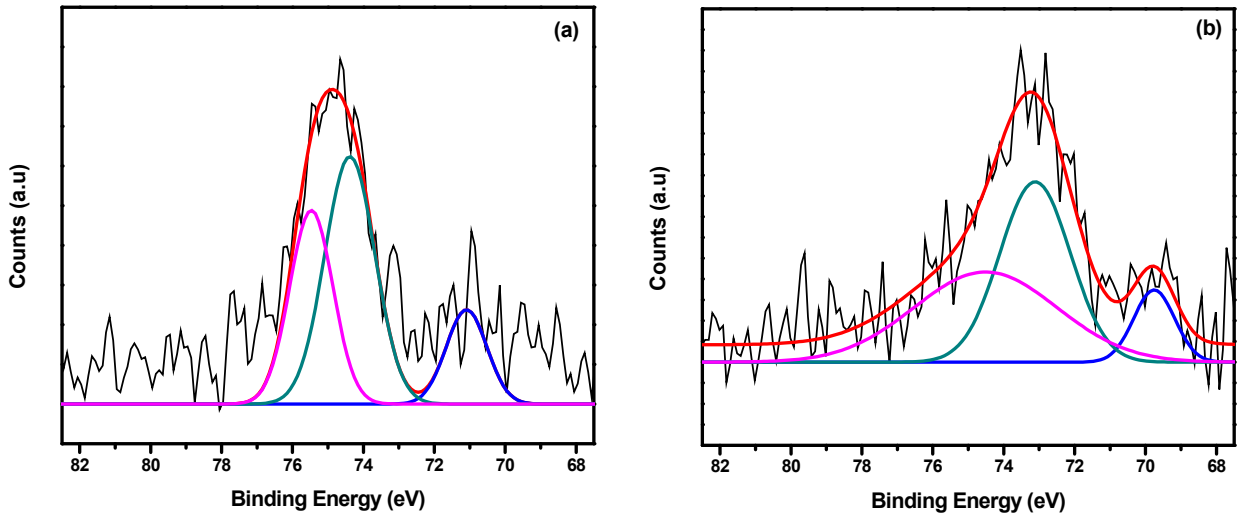



**Figure 6.5:** XPS spectra corresponding to the Pt 4f level of sequentially impregnated Sn/Pt/Mo/H-ZSM-5 catalyst, (a) calcined form and (b) reduced form.

The XPS spectra corresponding to Sn $3d_{5/2}$ levels of the calcined form and reduced form of Sn/Pt/Mo/H-ZSM-5 catalysts are shown in Figure 6.6(a) and Figure 6.6(b) respectively.

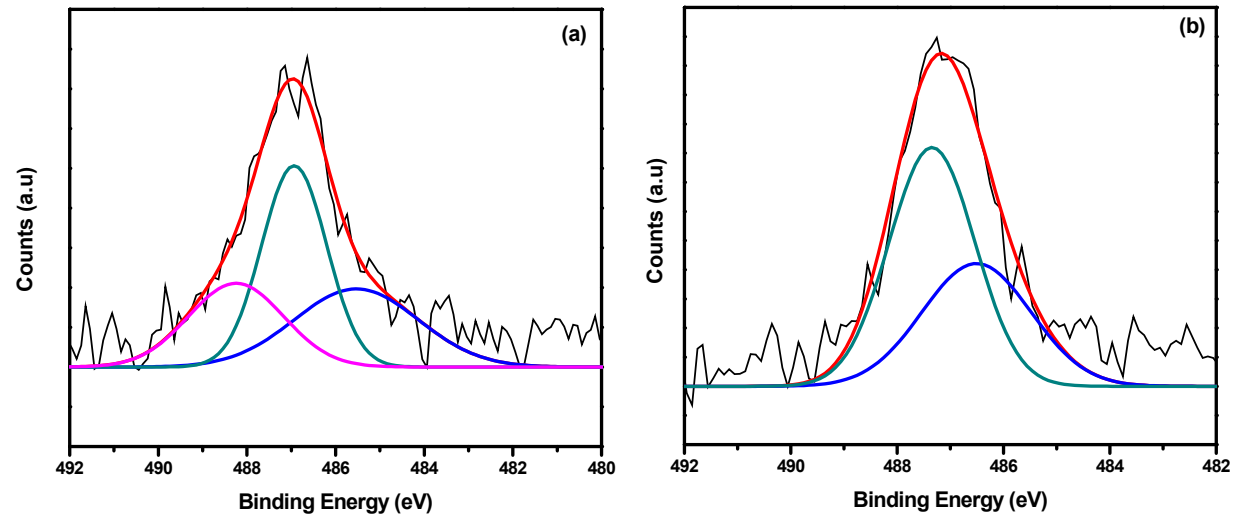



**Figure 6.6:** XPS spectra corresponding to the Sn 3d level of sequentially impregnated Sn/Pt/Mo/H-ZSM-5 catalyst, (a) calcined form and (b) reduced form.

The spectrum of the calcined form (Figure 6.6(a)) shows three peaks associated with Sn $3d_{5/2}$ components. The band at higher binding energy (488.2 eV) is attributed to the presence of $SnCl_2$ in the catalyst [14, 17]. The other two bands are associated with tin in different oxidation states, ca. 486.9 eV corresponds to $Sn^{2+}$ and $Sn^{4+}$, and ca. 485.5 eV is associated with tin in the metallic state. It is worth noting that the $Sn^{2+}$ and $Sn^{4+}$ species are characterized by one band as their binding energies are very close and it is difficult to differentiate between the two tin oxide species [16, 17]. Upon reduction the band associated with $SnCl_2$ disappeared and the intensity of the band at lower binding energy associated with metallic tin was increased. This suggests that the concentration of metallic tin species was increased and the probability of metallic platinum and metallic tin species was enhanced.

Table 6.1 shows the CO and metal dispersion calculated from the amount of probe molecules adsorbed on the metallic platinum surface atoms. The values were calculated based on the assumptions: (i) molybdenum and tin were CO inactive and (ii) the stoichiometric ratio between platinum and CO is 1. Experiments were carried out using the pulse dynamic chemisorption technique.

**Table 6.1:** Percentage metal dispersion and the amount of CO molecules adsorbed on the surface of platinum atoms in the tin modified 0.5Pt/2Mo/H-ZSM-5 zeolite catalysts.

| **Catalysts** | **CO uptake (µmol/g)** | **%$D_{CO}$** |
|---|---|---|
| 0.5Pt/2Mo/HZSM-5 | 7.35 | 28.67 |
| Co-imp(0.2Sn-0.5Pt) | 2.77 | 10.8 |
| Seq(0.5Pt/0.2Sn)/ | 1.43 | 5.58 |
| Seq(0.2Sn/0.5Pt | 0.33 | 1.41 |

Before chemisorption all the catalysts were reduced at 200 $^oC$ for 1 hour and pulse CO chemisorption was then performed at 50 $^oC$. The CO chemisorption results corroborate the FT-IR results observed in the figures above. Addition of tin led to a significant decrease in the amount of CO uptake. This may be attributed to a decrease in the number of surface platinum atoms available to adsorb CO molecules. During the reduction stage platinum surface atoms

interact with tin and form Pt-Sn alloys or the tin and molybdenum oxide migrate onto the external surface of the catalyst covering the platinum surface atoms [15]. It is also possible that the electron effects associated with tin contribute towards decreasing the biding energy of CO onto the platinum leading to a decrease in the CO uptake [18]. The decrease in the dispersion is not only due to an increase of platinum particle size but also due to the low amounts of CO adsorbed on the tin containing catalysts. The impregnation method seems to have a significant effect on the quantity of tin interacting with platinum and the amount of CO uptake. A low CO uptake might be indicative of high levels of tin forming a thin layer covering the platinum surface atoms [18, 19]. Catalysts prepared by a sequential impregnation method show low CO uptake. Addition of tin to the catalyst led to a rapid decrease in the amount of CO uptake, reaching 0.33 µmol/g for the seq(0.2Sn/0.5Pt) catalyst. This might suggest that surface platinum atoms are totally covered by a thin tin layer blocking the CO molecules from accessing platinum atoms.

Figure 6.7 shows the spectra for a single disc (0.2Sn/0.5Pt/2Mo/H-ZSM-5) which was subjected to *in-situ* successive reduction treatments before CO adsorption measurements. The disc was reduced at 200 $^{o}$C and oxidized at temperatures between 300 and 450 $^{o}$C. Each spectrum was taken at CO pressure of 5 Torr.

After each oxidation cycle, the sample was exposed to CO and spectra were taken at different CO pressures. The spectrum recorded after reducing the sample at 200 $^{o}$C showed broad bands (at 2162 and 2130 $cm^{-1}$) for gaseous CO. This indicates that CO was not adsorbed on the surface of the catalyst suggesting the absence of platinum surface atoms. This is attributed to the migration of tin and molybdenum oxide over the surface of the platinum atoms which blocked the CO molecules from interacting with the platinum atoms [14, 20]. The formation of Pt-Sn alloys will also decrease the platinum affinity for CO [21, 22]. Exposing the disc to oxidative condition at different temperatures (i.e. from 300 to 450 $^{o}$C) led to the appearance of two bands at 2169 and 2089 $cm^{-1}$ after CO adsorption. These bands are due to the adsorption of CO on $Pt^{2+}$ and metallic platinum species, respectively [5]. We suspect that during oxidation the layer covering the platinum surface atoms was removed when the sample was exposed to hydrogen. After reduction step the platinum atoms were subsequently exposed on the surface of the catalyst [10, 12]. Hence CO is adsorbed after exposing the sample to an oxygen environment at different

temperatures. However, it is worth noting that the intensity of the bands associated with CO adsorbed on metallic platinum decreased with an increase in the oxidation temperature. As the oxidation temperature was increased from 300 to 450 $^{o}$C a shift in band position to lower wavenumbers (i.e. red shifted) associated with the CO adsorbed on metallic platinum was observed. This is attributed to electronic effects associated with tin species which are in different oxidation states in the oxidation cycle.

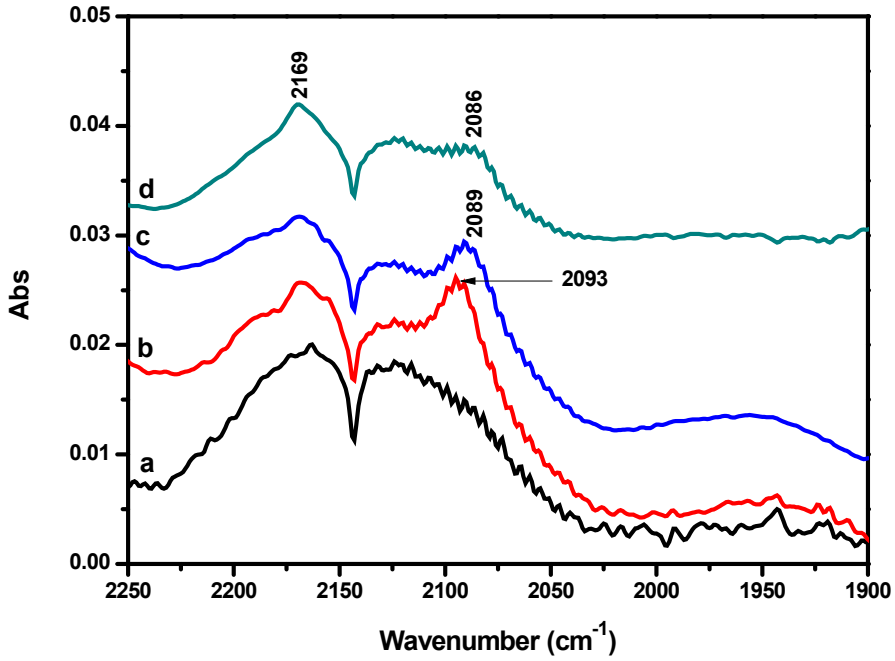



**Figure 6.7:** FT-IR spectra of CO adsorption on 0.2Sn/0.5Pt/2Mo/H-ZSM-5 zeolite catalyst which was reduced at 200 $^{o}$C and oxidized at different temperatures. (a) reduced, (b) oxidized 300 $^{o}$C, (c) 400 $^{o}$C and (d) 450 $^{o}$C.

### *6.3.2. Catalytic Results of MDA*

The effect of the catalyst preparation was further investigated using the MDA reaction at 700 $^{o}$C for 6 hours. The catalysts were firstly exposed to a methane gas mixture for 1 hour before monitoring the reaction by GC. The results of the catalytic activity of Sn modified Pt/Mo/H-ZSM-5 zeolite catalysts prepared using different methods are shown in Figure 6.8 below. The activity results show that the catalytic behavior is dependent on the preparation method. High methane conversions were observed for the first 15 minutes on-stream followed by a rapid

deactivation with increase in TOS. After 100 minutes on-stream the catalysts reached an equilibrium value. After 100 minutes on-stream, the methane conversion was only 8% for the tin free Pt/Mo/H-ZSM-5 zeolite catalyst. Addition of tin by co-impregnation led to a decrease in methane conversion to 6%. For a sequentially impregnated catalyst a significant drop in methane conversion was observed, with methane conversion being 5%.

As much as the presence of tin led to low methane conversions, high aromatic selectivity values were obtained for the tin modified Pt/Mo/H-ZSM-5 catalysts (Figure 6.9). Aromatic selectivities between 63 and 75% were observed with a 0.5Pt/2Mo/H-ZSM-5 catalyst. For the co-impregnated catalyst, aromatic selectivities between 65 and 90% were attained and the sequentially impregnated catalyst reached aromatic selecivities between 55 and 97%. From the aromatic selectivity plots, we observed a linear decrease in aromatic selectivity with increase in TOS and this may be attributed to catalyst deactivation. The catalyst deactivation is due to coke formation on the active sites and the Brønsted acid sites [23, 24]. The deactivation might also be due to the spreading of tin over surface platinum atoms and molybdenum carbides during the MDA reaction at 700 $^{o}$C [14]. This will lead to the exposure of less Brønsted acid sites and less $C_2$ intermediates being converted into aromatic compounds. There could also be a fewer number of platinum atoms to hydrogenate the carbonaceous deposits formed during the reaction. Hence a decrease in aromatic selectivity from 97 to 55% for the sequentially impregnated catalyst was observed.

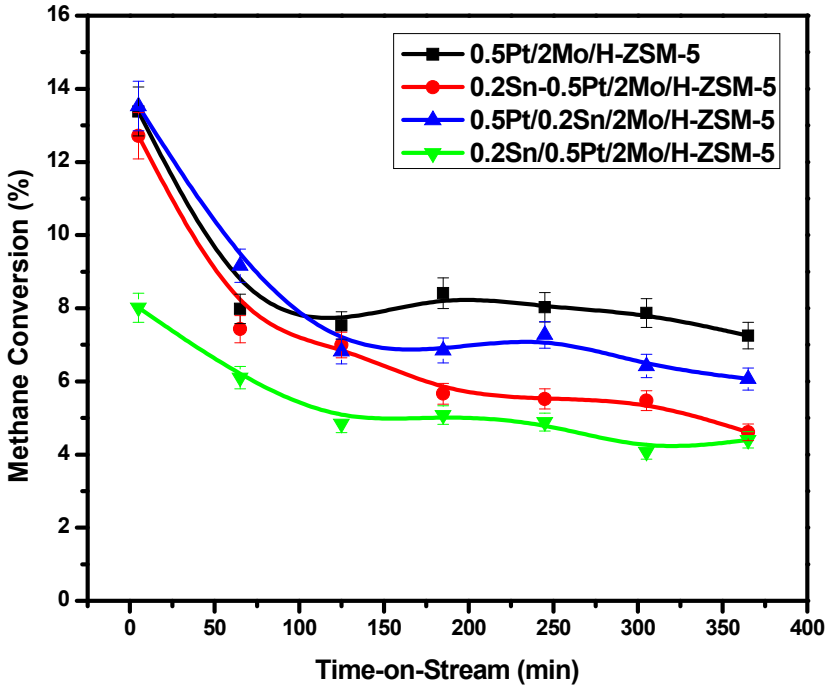



**Figure 6.8**: Catalytic conversion of methane over Sn doped Pt/Mo/H-ZSM-5 catalysts prepared using different impregnation methods.

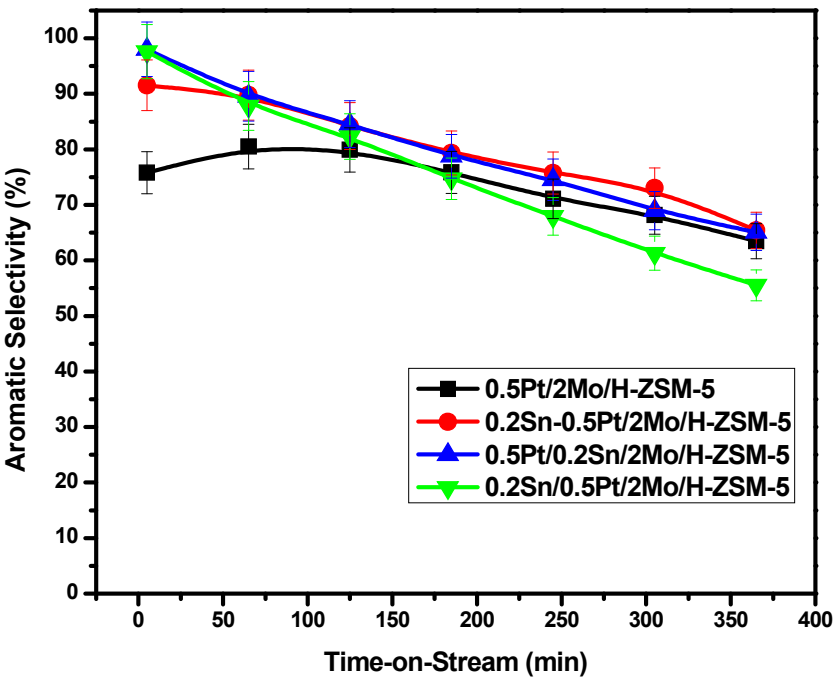



**Figure 6.9:** Percentage aromatic selectivity as a function of time-on-stream for tin doped Pt/Mo/H-ZSM-5 catalysts prepared using co-impregnation and sequential impregnation methods.

Results showing the effect of the catalyst preparation method on the product distribution of the MDA over tin modified Pt/Mo/H-ZSM-5 zeolite catalysts prepared by the co-impregnation and sequential impregnation methods are shown in Figure 6.10.

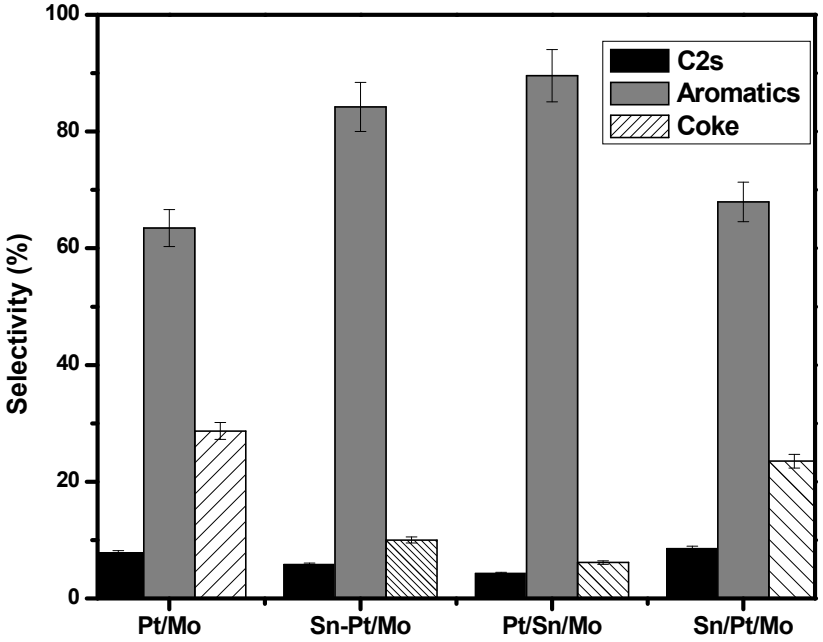



**Figure 6.10:** The effect of preparation method on the $C_2$ species, aromatics and coke selectivity during methane aromatization at 700 $^{o}$C taken at a methane conversion of 7%.

The catalyst prepared by the co-impregnation method produced a high aromatic selectivity (i.e. above 80%) and low coke selectivity (i.e. 12%). The aromatic selectivity for the sequential impregnated catalyst decreased to 65% while the selectivity towards coke was increased to 23%. From the CO chemisorption and FT-IR adsorption results it can be inferred that after reduction of the catalyst at 200 $^{o}$C no CO uptake was observed for the sequential impregnated catalyst. This was attributed to tin spreading over the catalyst and covering the surface platinum atoms. We suspect that during the MDA reaction the same effect takes place leading to a decrease in the number of platinum atoms available for the hydrogenation of the carbonaceous deposit. Hence, large amounts of coke are formed on the surface of the catalyst because there are fewer platinum atoms that react with the hydrogen produced to lower the coke levels accumulating on the surface of the catalyst. The catalytic activity and selectivity to coke are dependent on the catalyst preparation method and the amount of tin present on the external surface of the catalyst (blocking effect of tin on the platinum surface atoms).

A summary of the results of the effect of preparation method of tin modified Pt/Mo/H-ZSM-5 zeolite catalysts on the product distribution in the MDA reaction is shown in Table 6.2.

**Table 6.2:** Product selectivity of tin modified Pt/Mo/H-ZSM-5 prepared using co-impregnation and sequential impregnation methods taken at a methane conversion of 7%.

| Catalysts | Conversion (%) | Percentage Selectivity (%) | | | | | | Coke* (mg/g.cat) |
|---|---|---|---|---|---|---|---|---|
| | | C2s | Benzene | Toluene | Naphthalene | Aromatics | Coke | |
| Pt/Mo | 7.25 | 7.86 | 46.58 | 13.88 | 2.99 | 63.45 | 28.69 | 56.9 |
| Co-(PtSn) | 7.00 | 5.77 | 75.40 | 8.80 | 0.00 | 84.20 | 10.02 | 58.4 |
| Seq-(Sn/Pt) | 7.27 | 8.53 | 53.50 | 8.44 | 6.00 | 67.94 | 23.53 | 69.5 |
| Seq-(Pt/Sn) | 6.10 | 4.27 | 79.80 | 9.11 | 0.66 | 89.57 | 6.16 | 49.2 |

*Coke deposit analyzed by TGA.

Addition of tin to the Pt/Mo/H-ZSM-5 catalyst led to an increase in the total aromatic selectivity and a decrease in selectivity towards coke was observed. The major aromatic compound formed is benzene and its selectivity was enhanced by the presence of tin; the method of catalyst preparation has an effect on the product selectivity. The benzene selectivity of the co-impregnated catalyst was observed to be 75% and for the sequentially prepared catalysts different selectivities towards benzene were observed. This suggests that the sequence of adding Pt and Sn has an influence on the catalytic behavior towards product selectivity. The seq(Pt/Sn) catalyst showed good selectivity (79%) and while the seq(Sn/Pt) showed a benzene selectivity below 60%. This can be explained by referring to the CO adsorption FT-IR results after reduction. The CO adsorption results showed that after reduction no platinum surface atoms were available to interact with CO for the seq(Sn/Pt) catalyst but for the seq(Pt/Sn) catalyst a band at 2089 $cm^{-1}$ was observed. This signifies the availability of surface platinum atoms post reduction. It is suspected that when the catalysts are exposed to the MDA reaction at 700 $^{o}C$ the same effect is observed, as hydrogen is produced during the reaction. These results suggest that the selectivity towards benzene is mainly dependent on the availability of surface platinum atoms which play a crucial role in hydrogenating the bulk aromatic compounds formed during the MDA reaction [25, 26]. The naphthalene selectivity for seq(Sn/Pt) catalyst was high when compared with seq(Pt/Sn) catalyst. Selectivity towards the coke selectivity was 23% and 6.2% for the seq(Sn/Pt) and the seq(pt/Sn) catalysts, respectively. The coke selectivity for the

seq(Sn/Pt) catalyst is significantly higher when compared with other catalysts. The results indicate that the seq(Sn/Pt) catalyst favoured the formation of heavier aromatic compounds which were subsequently transformed into polyaromatic compounds and led to coke [27]. Hence a high coke selectivity for the seq(Sn/Pt) catalyst was observed. The decrease in the coke selectivity on the catalysts with tin loadings is due to the role of tin in facilitating the transfer of carbon deposits from the metallic species onto the support leading to the increase in the number of platinum atoms available for coke hydrogenation.

## 6.4. Summary

The influence of the preparation methods and the effects of tin on the CO adsorption and catalytic properties of platinum modified Mo/H-ZSM-5 were investigated. From the CO FT-IR adsorption spectra and CO chemisorption studies it can be concluded that the presence of tin decreased the adsorption capacity of the platinum surface atoms. However, the preparation methods and successive calcination treatments were shown to influence the location of both tin and platinum atoms. Catalyst prepared by the co-impregnation method showed a good platinum dispersion, better than found for the sequentially impregnated catalysts. This was attributed to the mobility of tin species which covered the platinum atoms on the surface of the catalyst as shown by the CO FT-IR profiles of the hydrogen treated catalysts.

The MDA reaction at 700 $^{o}$C was studied over Sn-Pt/Mo/HZSM-5 catalysts prepared by co-impregnation and sequential impregnation methods and compared to a Pt/Mo/H-ZSM-5 catalyst. Catalysts containing tin showed low activity towards the conversion of methane. Further, the formation of aromatic compounds was favoured. The co-impregnated and sequentially impregnated Pt/Sn catalysts showed high aromatic selectivity and low coke selectivity. The decrease in coke selectivity is mainly dependent on the availability of platinum sites for the hydrogenation of carbonaceous species. The order of sequentially loading platinum and tin has an effect on the electronic and structural properties of platinum. Hence different catalytic activities and aromatic selectivities were observed for the seq(Pt/Sn) and seq(Sn/Pt) catalysts.

## 6.5. Reference List

[1] M.W. Ngobeni, A.F. Carley, M.S. Scurrell, C.P. Nicolaides, *Journal of Molecular Catalysis A: Chemical*, **305** (2009) 40.

[2] H. Jiang, L. Wang, W. Cui, Y. Xu, *Catalysis Letters*, **57** (1999) 95.

[3] B. Liu, Y. Yang, A. Sayari, *Applied Catalysis A: General*, **214** (2001) 95.

[4] K. Chakarova, M. Mihaylov, K. Hadjiivanov, *Microporous and Mesoporous Materials*, **81** (2005) 305.

[5] K. Chakarova, M. Mihaylov, K. Hadjiivanov, *Catalysis Communications*, **6** (2005) 466.

[6] P. Kubanek, H.W. Schmidt, B. Spliethoff, F. Schüth, *Microporous and Mesoporous Materials*, **77** (2005) 89.

[7] F.B. Passos, D.A.G. Aranda, M. Schmal, *Journal of Catalysis*, **178** (1998) 478.

[8] J. Llorca, N. Homs, J. León, J. Sales, J.L.G. Fierro, P. Ramirez de la Piscina, *Applied Catalysis A: General*, **189** (1999) 77.

[9] K. Taniya, H. Jinno, M. Kishida, Y. Ichihashi, S. Nishiyama, *Journal of Catalysis*, **288** (2012) 84.

[10] G.J. Arteaga, J.A. Anderson, C.H. Rochester, *Science*, **58** (1999) 189.

[11] K. Chakarova, E. Ivanova, K. Hadjiivanov, D. Klissurski, H. Knözinger, *Physical Chemistry Chemical Physics*, **6** (2004) 3702.

[12] G.J. Arteaga, J.A. Anderson, S.M. Becker, C.H. Rochester, *Journal of Molecular Catalysis A: Chemical*, **145** (1999) 183.

[13] J. Llorca, N. Homs, J. Araña, J. Sales, P. Ramírez de la Piscina, *Applied Surface Science*, **134** (1998) 217.

[14] Z. Paál, A. Wootsch, D. Teschner, K. Lázár, I.E. Sajó, N. Győrffy, G. Weinberg, A. Knop-Gericke, R. Schlögl, *Applied Catalysis A: General*, **391** (2011) 377.

[15] J. Ruiz-Martínez, A. Sepúlveda-Escribano, J.A. Anderson, F. Rodríguez-Reinoso, *Catalysis Today*, **123** (2007) 235.

[16] J. Ruiz-Martínez, F. Coloma, A. Sepúlveda-Escribano, J.A. Anderson, F. Rodríguez-Reinoso, *Catalysis Today*, **133–135** (2008) 35.

[17] B.K. Vu, M.B. Song, I.Y. Ahn, Y.-W. Suh, D.J. Suh, W.-I. Kim, H.-L. Koh, Y.G. Choi, E.W. Shin, *Applied Catalysis A: General*, **400** (2011) 25.

[18] C. Xu, B.E. Koel, *Surface Science*, **304** (1994) L505.

[19] M.T. Paffett, S.C. Gebhard, R.G. Windham, B.E. Koel, *The Journal of Physical Chemistry*, **94** (1990) 6831.

[20] M.A. Pereira da Silva, R.A. MelloVieira, M. Schmal, *Applied Catalysis A: General*, **190** (2000) 177.

[21] A.D. Ballarini, C.G. Ricci, S.R. de Miguel, O.A. Scelza, *Catalysis Today*, **133–135** (2008) 28.

[22] J.C. Serrano-Ruiz, A. Sepúlveda-Escribano, F. Rodríguez-Reinoso, *Journal of Catalysis*, **246** (2007) 158.

[23] H. Liu, S. Yang, J. Hu, F. Shang, Z. Li, C. Xu, J. Guan, Q. Kan, *Fuel Processing Technology*, **96** (2012) 195.

[24] J.-P. Tessonnier, B. Louis, S. Rigolet, M.J. Ledoux, C. Pham-Huu, *Applied Catalysis A: General*, **336** (2008) 79.

[25] A.K. Aboul-Gheit, A.E. Awadallah, S.M. El-Kossy, A.-L.H. Mahmoud, *Journal of Natural Gas Chemistry*, **17** (2008) 337.

[26] Y. Shu, Y. Xu, S.-T. Wong, L. Wang, X. Guo, *Journal of Catalysis*, **170** (1997) 11.

[27] B. Weckhuysen, M. Rosynek, J. Lunsford, *Catalysis Letters*, **52** (1998) 31.

# Chapter 7

# Dehydroaromatization of Methane over Mn/H-ZSM-5 Zeolite Catalysts

## 7.1. Introduction

Methane has been successfully activated and converted into aromatic compounds by various metal modified zeolite catalysts. Molybdenum and tungsten in their carbide form are regarded as the most active metals for dehydroaromatization of methane under non-oxidative conditions. The thermal properties of both metals supported on H-ZSM-5 were studied and W/H-ZSM-5 zeolite catalyst was found to be a good catalyst for methane activation at reactions temperatures above 750 $^{o}$C. Ledoux et al. [1] studied the properties of Mo and W and in their carbide forms and compared them with the properties of platinum. Based on their results they concluded that the catalytic properties of a W/H-ZSM5 catalyst should be similar to that of a Mo/H-ZSM5 catalyst in its ability to activate $CH_4$.

A comparison of Mo and W based catalysts, revealed that W-based catalysts can be active at reaction temperature of 800 $^{o}$C and give a methane conversion that is twice as high as that of a Mo-based catalyst operating at reaction temperature of 700 $^{o}$C [2-4]. Zhang et al. [5]studied the MDA reaction over W/H-ZSM-5 zeolites catalysts; in their work they reported high methane activity and good heat-resistance of the catalyst. At a reaction temperature of 800 $^{o}$C methane conversions of about 20% and high benzene selectivity were obtained without loss of tungsten through sublimation. Though high methane conversions were obtained with W/H-ZSM-5 based catalysts, formation of coke on the surface of the active sites was still unavoidable leading to catalytic deactivation with time-on-stream. Xiong et al. [4, 6] and Zeng et al. [7] explored the

effect of promoters such as La, Li, Mn and Zn on the catalytic performance of W/H-ZSM-5 and W-$H_2SO_4$/H-ZSM-5 zeolite catalysts for the MDA reaction at 800 $^oC$. They reported that the presence of these promoters improved the catalytic activity and stability. This was attributed to the ability of each metal to generate medium strength acid sites and to enhance the reducibility of tungsten oxide species in the catalyst.

From the list of promoters it was noted that manganese oxide species possessed good catalytic activity in the oxidative coupling of methane [8]. Lunsford et al. [9, 10] compared the catalytic behaviour of $Na_2WO_4$-$SiO_2$, $Na_2WO_4$-Mn/MgO, and $NaMnO_4$/MgO catalysts for the oxidative coupling reaction. Their study showed that the Na-O-Mn catalyst component was the active matrix of the catalysts. The Mn was the active site and Na played a role of a structural and chemical promoter while W enhanced the stability of the catalyst. Malekzadeh et al. [11] found that manganese oxides enhanced the number of charge carriers between the catalyst surface and the methane leading to a good interaction between methane molecules and the active sites. Furthermore, Ji and co-workers [12, 13] suggested that both Na-O-W and Na-O-Mn species are active sites in the $Na_2WO_4$-Mn/$SiO_2$ catalyst, with W on the surface of the catalyst enhancing the catalytic activity. Marczewski and Marczewska [14] studied the activation of methane under non-oxidative environment over Na-MnOx supported on $SiO_2$ and H-ZSM-5 catalysts. They successfully showed the transformation of methane into heavy hydrocarbons at 700 $^oC$ and obtained a methane conversion of 6% from a 3.4%Na-10%Mn/$SiO_2$-H-ZSM-5 catalyst.

With limited research conducted on MDA over manganese modified H-ZSM-5 zeolite catalysts we therefore undertook a study of the MDA reaction over a Mn/H-ZSM-5 zeolite catalysts prepared by the incipient impregnation method. Different studies were performed to explore the influence of manganese species on the MDA reaction. In this chapter we focused on the effect of range of parameters on the catalytic performance and product selectivity of Mn/H-ZSM-5 on the MDA reaction. Parameters included: the reaction temperature, the manganese precursor, addition of tungsten as promoter, manganese loading and the use of noble metals. The catalytic properties of Mn/H-ZSM-5 were studied using XRD, $H_2$-TPR, $NH_3$-TPD and BET surface area

measurements techniques. The amount of coke deposited after the MDA reaction was quantified by TGA measurements.

## 7.2. Experimental

### 7.2.1. Catalysts Preparation

The preparation of Mn/HZSM-5 catalysts involved the incipient wetness impregnation of H-ZSM-5 with an aqueous solution of manganese nitrate $Mn(NO_3)_2$, $MnCl_3$ and $KMnO_4$ precursors. The samples were dried at 120 $^oC$ and then calcined at 500 $^oC$ for 6 hours. A series of tungsten modified Mn/H-ZSM-5 zeolite catalysts were prepared by a sequential impregnation method using manganese nitrate ($Mn(NO_3)_2$) and ammonium paratungstate (ATP) ($(NH_4)_{10}W_{12}O_{41}\cdot 5H_2O$) salts as metal precursors. The Mn loading was kept constant and the W loading was varied between 0.5 and 1.5 wt% loading. Subsequently, the samples were dried at 120 $^oC$ overnight and calcined at 500 $^oC$ for 6 hours.




**Scheme 7.1:** Schematic representation of catalyst preparation methods.

## 7.3. Results and Discussion

### *7.3.1. Effect of Reaction Temperature*

The effect of reaction temperature on the catalytic activity of Mn/H-ZSM-5 catalyst was investigated to obtain the optimum reaction temperature at which aromatization of methane over Mn/H-ZSM-5 catalyts can be studied. The Mn/H-ZSM-5 catalyst was prepared by incipient impregnation of H-ZSM-5 with an appropriate concentration of $Mn(NO_3)_2$ to attain a 2 wt% loading and calcined at 500 $^oC$ for 6 hours. The results below show the effect of reaction temperature on the catalytic stability of a Mn/H-ZSM-5 catalyst studied between 700 and 850 $^oC$, with a metal loading of 2 wt%.

The results of the effect of reaction temperature on the catalytic performance of Mn/H-ZSM-5 zeolite catalysts are shown in Figure 7.1. Catalysts were exposed to methane for 6 hours under a desired reaction temperature. The results below suggest that conversion of methane into aromatics is dependent on the reaction temperature. Wang et al. [15] studied the aromatization of methane over a Mo/H-ZSM-5 zeolite catalyst at 700 $^oC$ and observed methane conversions of about 14%. From our studies of MDA over Mn/H-ZSM-5 catalysts, we observed methane conversion between 1 and 2.5% at 700 $^oC$. As the reaction temperature was increased to 750 and 800 $^oC$, methane conversions of about 4% were obtained. A further increase of reaction temperature to 850 $^oC$ led to an increase in methane conversion with an initial conversion of 9% followed by a subsequent decrease in methane conversion reaching a steady state conversion below 6%. This decrease in catalytic activity with TOS can be attributed to an increase in the coke formation rate at high temperatures. Coke formed during the MDA reaction anchors on the active sites; it also blocks the pore and channels of the zeolite catalyst. The low methane conversions observed at lower reaction temperature suggests that the manganese oxide species are not as active for the initiation of methane aromatization and as they are exposed to methane at higher reaction temperatures the oxide species are transformed into carbides and/or oxy-

carbides which are considered to be the main catalyst species to activate methane into reactive intermediates [16].

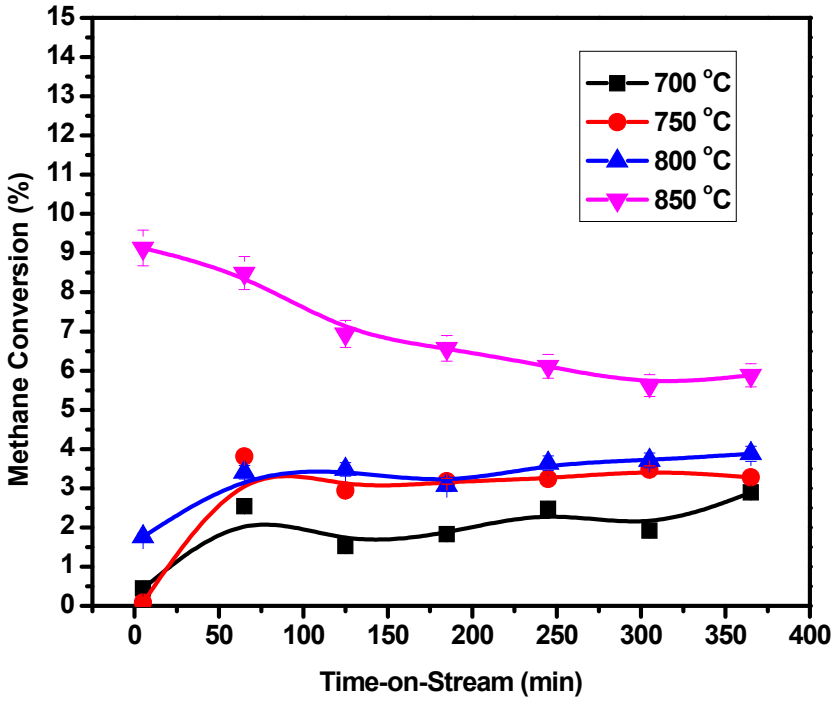



**Figure 7.1:** MDA catalytic activity of 2%Mn/H-ZSM-5zeolite catalyst taken at different reaction temperatures between 700 and 850 $^{o}$C for 6 hours on-stream.

Figure 7.2 shows the effect of reaction temperature on the catalytic performance of 2Mn/H-ZSM-5 catalyst taken at 5, 185, 365 minutes on-stream. For the TOS of 5 minutes there is an exponential increase in methane conversion with increase in reaction temperature. When the TOS was increased the catalytic performance of 2%Mn/H-ZSM-5 dropped from exponential growth to a somewhat near-linear growth behaviour. However, the methane conversion still increased with increase in reaction temperature. At reaction temperatures of 750 and 800 $^{o}$C the catalyst was stable reaching an equilibrium conversion of 3.5%. When the reaction temperature was kept at 850 $^{o}$C a decrease in methane conversion was observed with increase in TOS. This decrease is methane conversion is attributed to catalyst deactivation caused by coke deposits formed on active sites during the MDA reaction.

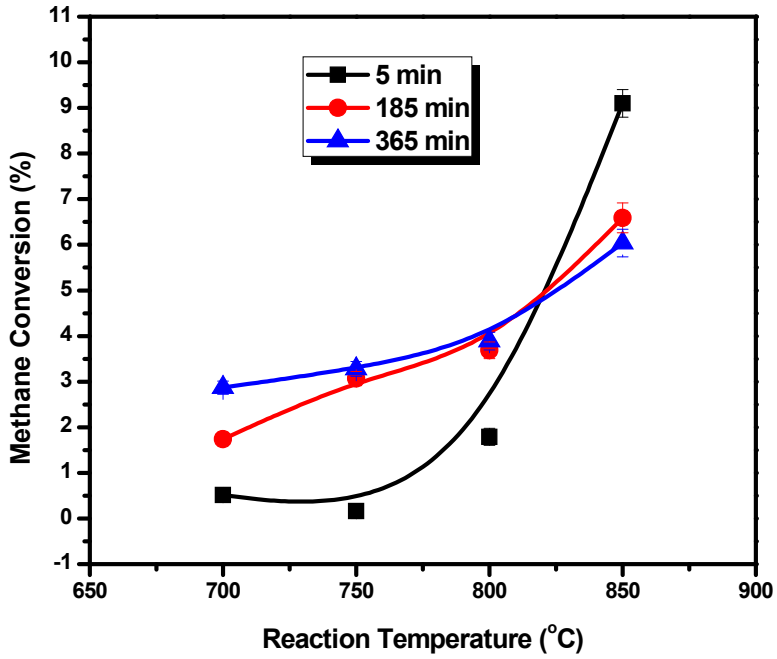



**Figure 7.2:** The catalytic conversion as the function of reaction temperature over the 2Mn/H-ZSM-5 catalysts at TOS of 5, 185 and 365 minutes.

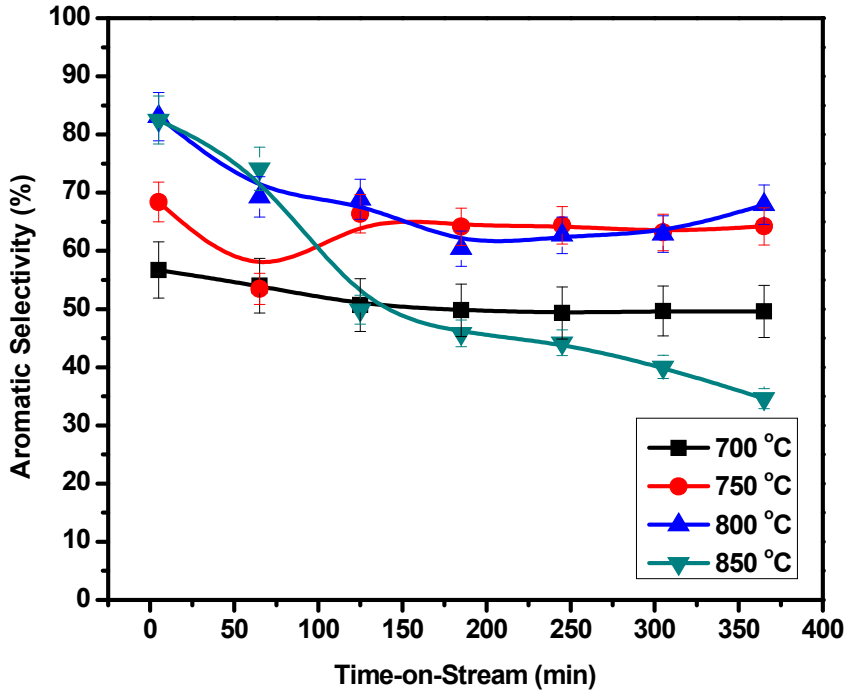



**Figure 7.3:** Aromatic selectivity versus TOS plot of 2Mn/H-ZSM-5 catalyst taken at different reaction temperatures.

The results of the influence of reaction temperature on the aromatic selectivity of Mn/H-ZSM-5 catalyst are shown in Figure 7.3 above. At 700 $^{o}$C we observed a stable aromatic selectivity slightly above 50%. An increase in reaction temperature to 750 and 850 $^{o}$C led to an increase in the initial aromatic selectivity to 68% and 84% respectively. The high aromatic selectivity observed for the reactions performed at high reaction temperatures (i.e. 750-850 $^{o}$C) in an initial stages (first 60 minutes on-stream) of the reaction is due to the shortening of the induction period as the reaction temperature was increased from 700 to 850 $^{o}$C [16-18]. This was followed by a gradual decrease in aromatic selectivity with increase in time-on-stream, which then leveled off at 65% after a TOS of 125 minutes. For a reaction temperature of 850 $^{o}$C, an initial aromatic selectivity of 84% was observed followed by a linear decrease with time-on-stream reaching a minimum of 35%. The dramatic decrease in aromatic selectivity is probably related to the coke formation that is favoured at higher reaction temperatures.

The product distribution results of 2%Mn/H-ZSM-5 catalyst taken at different reaction temperatures are presented in Figure 7.4.

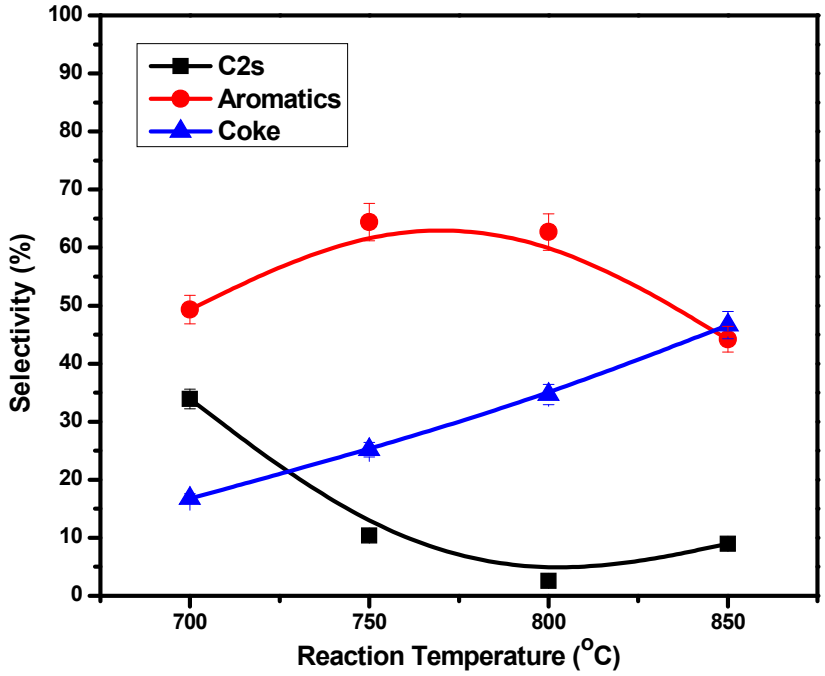



**Figure 7.4:** The effect of reaction temperature on the product distribution of methane aromatization over 2%Mn/H-ZSM-5 catalyst at time-on-stream of 245 minutes.

The $C_{2s}$ selectivity decreased with reaction temperature and a simultaneous increase in the aromatic selectivity, indicating that the aromatization process is favoured at high reaction temperatures. The selectivity to aromatics increased with increase in reaction temperature reaching an optimum of 65% at 750 and 800 $^{o}$C. A further increase in the reaction temperature to 850 $^{o}$C yielded to a decrease in the aromatic selectivity. The selectivity to coke showed a linear increase with reaction temperature. This shows that the selectivity for aromatics and coke are dependent on each other, and that the formation of coke is more favoured at temperatures above 800 $^{o}$C than the formation of aromatic compounds.

The effect of reaction temperature on formation of coke during MDA over the Mn/H-ZSM-5 zeolite catalysts was further investigated by TGA in order to obtain the amounts of coke formed and the coke stability under an oxygen atmosphere. Figure 7.5(a) and Figure 7.5(b) shows the TGA and DTG profiles of Mn/H-ZSM-5 catalysts which were exposed to MDA reaction at different reaction temperatures.

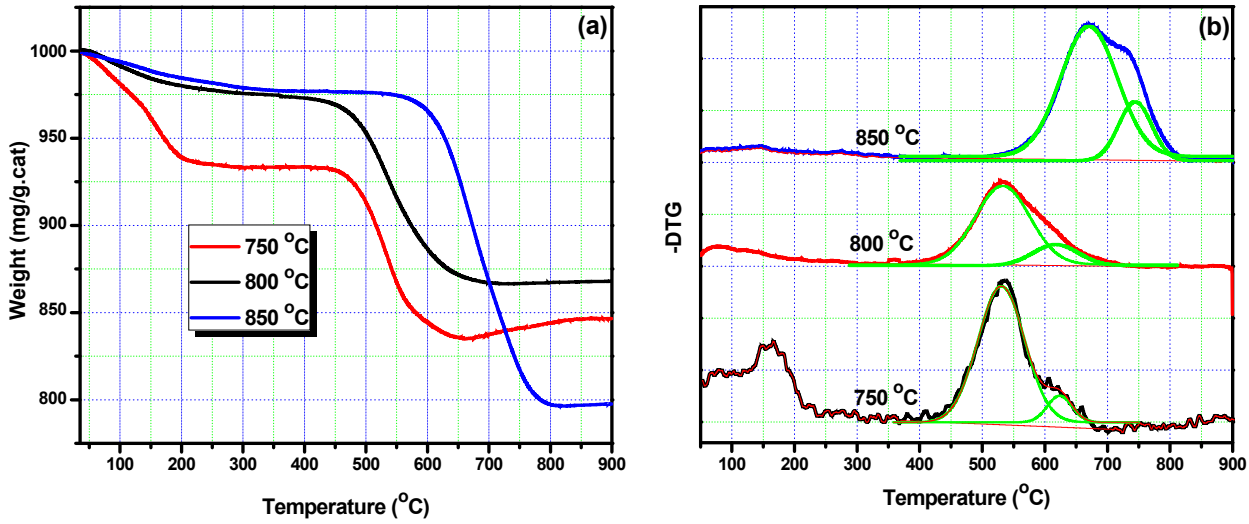



**Figure 7.5:** TGA (a) and DTG (b) profiles of coked Mn/H-ZSM-5 catalysts after MDA reaction at different reaction temperatures.

The TGA profiles show a weight loss which is attributed to decomposition of coke formed during the MDA reaction at different reaction temperatures. An increase in the amount of coke

deposit was observed with an increase in reaction temperature. The amount of coke deposited on Mn/H-ZSM-5 catalyst at 750 $^{o}$C reaction temperature was 100 mg as the reaction temperature was increase to 850 $^{o}$C the amount of coke reached values close to 200 mg (Table 7.1). This suggests that the rate of coke formation is mainly dependent on the reaction temperature.

**Table 7.1:** TGA and DTG results of coked Mn/H-ZSM-5 zeolite catalysts after MDA reaction studied at different reaction temperatures.

| **Temperature ($^{o}$C)** | **Amount of Coke (mg/g cat.)** | **Decomposition Temperature ($^{o}$C)** | **Decomposition Temperature ($^{o}$C)** |
|---|---|---|---|
| 750 | 99.8 | 536 | 603 |
| 800 | 107.6 | 540 | 611 |
| 850 | 183.5 | 666 | 730 |

The DTG profiles presented in Figure 7.5(b) exhibited two well defined oxidation peaks which are attributed to the decomposition of different carbon species formed during the MDA reaction. The peak at lower decomposition temperature is associated with the decomposition of carbon formed on the manganese, which might have led to the formation of manganese carbide or oxycarbide [16]. The peak at a higher decomposition temperature is due to the decomposition of carbonaceous species formed on the support which is associated with Brønsted acid sites. There was not much change in the decomposition temperature of carbon associated with both the metal and Brønsted acid sites for the reactions performed at 750 and 800 $^{o}$C. For the reaction performed at 850 $^{o}$C, we observed an increase in the decomposition temperature of carbon associated with manganese and carbon deposited on Brønsted acid sites. The decomposition temperature associated with oxidation of carbon on manganese increased to 666 $^{o}$C and that of carbon deposited on Brønsted acid sites was 730 $^{o}$C. This increase in the decomposition temperature of different carbon species with increase in reaction temperature of MDA is attributed to a change in thermal stability of the carbon species. This indicates that increasing the reaction temperature favours the formation of more stable and graphitic carbon on the Brønsted acid sites.

### *7.3.2. The Effect of Manganese Precursor*

The effect of manganese precursor was studied to investigate the effect of the counter ion on the catalytic performance of Mn/H-ZSM-5 in the MDA reaction. Three different manganese precursors (i.e. $Mn(NO_3)_2$, $MnCl_2$ and $KMnO_4$) were used to impregnate H-ZSM-5 to attain a 2 wt.% loading and the catalysts were calcined at 500 $^oC$ for 6 hour. The MDA reaction was performed at 800 $^oC$, with a methane/argon mixture flowing at 13 mL/min under atmospheric pressure.

The influence of the manganese precursor on the reducibility of Mn/H-ZSM-5 catalysts is shown in Figure 7.6.

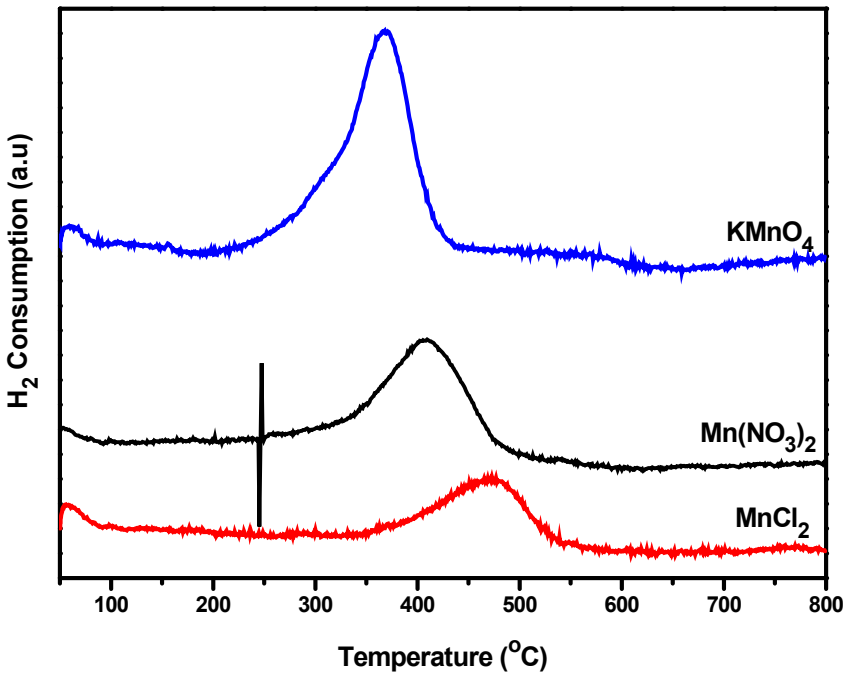



**Figure 7.6:** TPR profiles of Mn/H-ZSM-5 catalysts impregnated with different manganese precursors (i.e. $Mn(NO_3)_2$, $MnCl_2$ and $KMnO_4$).

The reduction profiles of Mn/H-ZSM-5 catalysts illustrate that the presence of the counter ion has an effect on the reducibility of manganese oxide species. The reduction temperatures manganese species in the Mn/H-ZSM-5 catalysts prepared from $MnCl_2$ and $Mn(NO_3)_2$ solutions quite high (478 and 409 $^oC$) as compared to $KMnO_4$ catalyst (170 $^oC$). The decrease in the reduction temperature of manganese oxide may attributed to presence of $K^+$ ions in the $KMnO_4$ acting as promoters [19].

The results of the of manganese precursor on the catalytic performance and aromatic selectivity of Mn/H-ZSM-5 zeolite catalysts as a function time-on-stream are shown in Figure 7.7 and Figure 7.8 respectively. Catalysts impregnated with $Mn(NO_3)_2$ and $MnCl_2$ showed good catalytic stability with methane conversion being maintained between 4 and 6%. However, for $KMnO_4$ impregnated catalysts underwent a rapid deactivation with increase in TOS reaching a minimum methane conversion of 4% after 185 minutes on-stream. This rapid deactivation may be ascribed to the poising effect of potassium ions.

The effect of the counter ions was more pronounced on the aromatic selectivity of Mn/H-ZSM-5 zeolite catalysts (Figure 7.8). For the $Mn(NO_3)_2$ impregnated catalyst we observed good and stable aromatic selectivity between 60 and 70%. This suggests that the nitrate ion have no effect on the catalytic activity and aromatic selectivity as they decompose during the calcinations stage of the catalyst preparation. A decrease in aromatic selectivity with increase in TOS was observed when $MnCl_2$ was used as a precursor. Aromatic selectivity below 20% was observed for the $KMnO_4$ catalysts. This is attributed to a decrease in concentration of Brønsted acid sites caused by the presence of potassium ions. The Brønsted acid sites are responsible for transforming $C_2$ hydrocarbons into aromatic compounds.

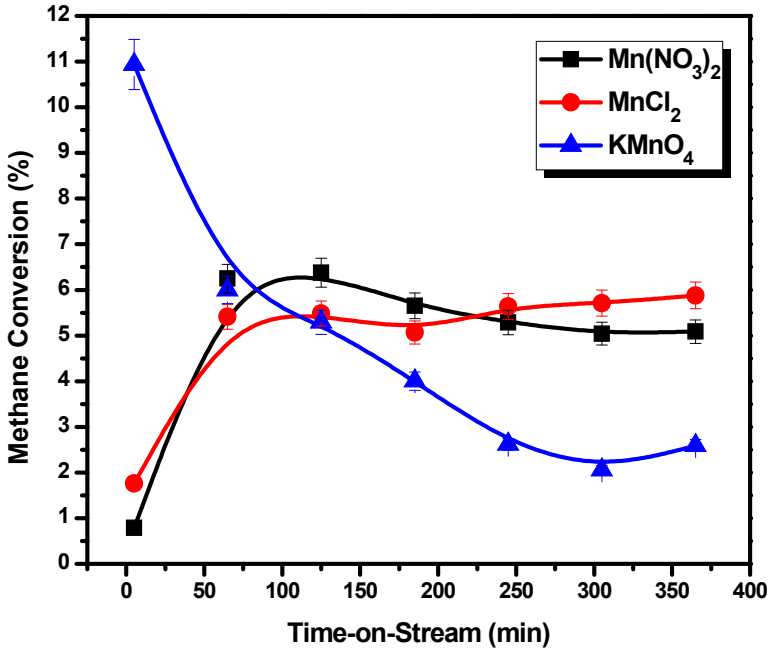



**Figure 7.7:** The catalytic conversion of methane of Mn/H-ZSM-5 zeolite catalysts impregnated with different manganese precursors (i.e. $Mn(NO_3)_2$, $MnCl_2$ and $KMnO_4$), taken at 800 $^oC$ for 6 hours.

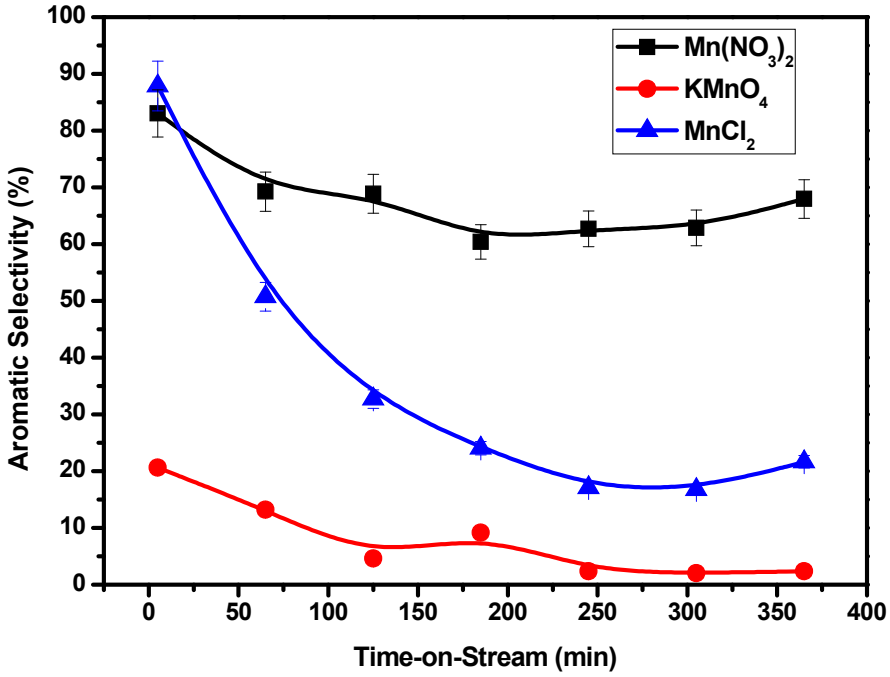



**Figure 7.8:** The effect manganese precursor on the aromatic selectivity of Mn/H-ZSM-5 zeolite catalysts.

Figure 7.9 shows the effect of the counter ions on the product distributions of the Mn/H-ZSM-5 catalysts prepared from different manganese precursors for MDA reaction at 800 $^{o}$C after 245 minutes on-stream.

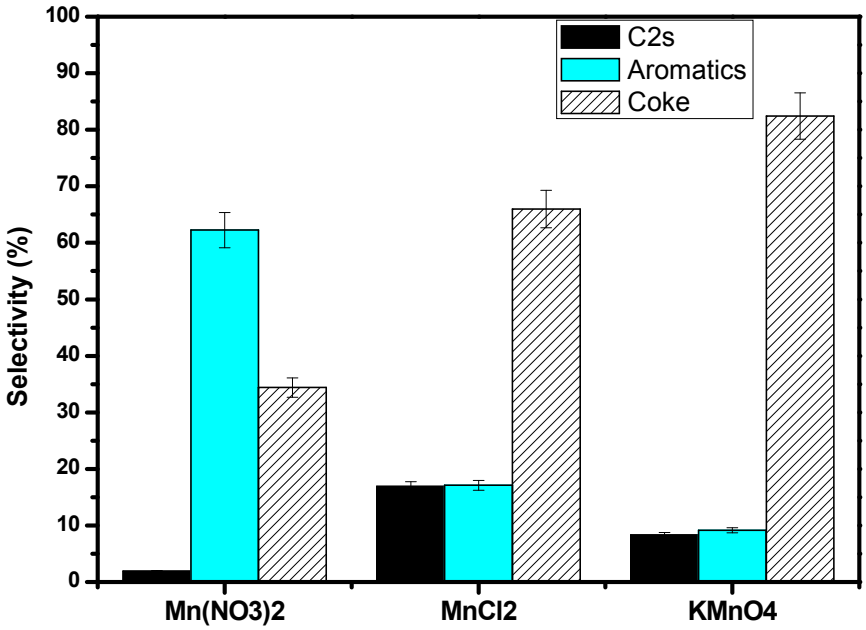



**Figure 7.9:** The effect manganese precursor on the product distribution of Mn/H-ZSM-5 catalysts for methane conversion at 800 $^{o}$C after TOS of 245 minutes.

Comparing the product selectivity of these catalysts we observe that the catalyst prepared from $Mn(NO_3)_2$ precursor was superior when compared to both $MnCl_2$ and $KMnO_4$ catalysts. Aromatic selectivity of about 60% was obtained with low selectivity towards carbonaceous deposits. This may be attributed to the low decomposition temperature associated with nitrate complexes. However, when $MnCl_2$ and $KMnO_4$ were used we observed a decrease in the aromatic selectivity with a concurrent increase of coke selectivity. Selectivity towards coke was above 60% for the $MnCl_2$ catalyst and for $KMnO_4$ catalysts we observed coke selectivity of 85%. This suggests that the $K^+$ ions act as catalyst poisons for the MDA reaction leading to high formation of carbonaceous deposit. We suspect that during impregnation an ion exchange takes place between the zeolitic proton and $K^+$ ions leading to a decrease in Brønsted acid sites. Brønsted acid sites are known to be responsible for converting $C_2$ intermediates in to aromatic compounds. If the concentration of Brønsted acid sites is insufficient to transform $C_2$ into

aromatic compounds this will result in the $C_2$ intermediates being transformed into carbonaceous deposits. Hence, we observed a high coke selectivity and low aromatic selectivity for the $KMnO_4$ catalysts.

### *7.3.3. Effect of Manganese Loading*

The effect of manganese loading on the catalytic activity of Mn/H-ZSM-5 zeolite catalyst for the MDA reaction was studied at 800 $^oC$. The Mn/H-ZSM-5 with different metal loadings (i.e. between 0 and 10 wt.% Mn loading) were prepared by an incipient wetness impregnation method and calcined at 500 $^oC$. The effect of manganese loading on the nitrogen adsorption (BET) surface areas and pore volumes of these catalysts are presented in Table 7.2.

**Table 7.2**: The effect of manganese loading on the surface area and pore volume of Mn/H-ZSM-5 catalyst prepared using $Mn(NO_3)_2$ manganese source.

| Mn Loading (wt.%) | BET Surface Area ($m^2/g$) | Pore Volume ($cm^3/g$) |
|---|---|---|
| 0 | 392 | 0.247 |
| 2 | 386 | 0.239 |
| 4 | 383 | 0.203 |
| 6 | 381 | 0.205 |
| 10 | 358 | 0.195 |

From the summarized nitrogen adsorption results presented above we observe that increasing the manganese loading leads to a decrease in surface area and pore volumes of the Mn/H-ZSM-5 zeolites catalysts. The BET surface area and pore volume decreased from 392 to 358 $m^2/g$ and 0.247 to 0.195 $cm^3/g$, respectively with the increase in manganese loading. Such decrease in surface area and pore volume is attributed to the pore blockage caused by manganese oxide species formed on the mouths of the pores [20].

The XRD patterns of the impregnated Mn/H-ZSM-5 zeolite catalysts are shown in Figure 7.10 below. It can be observed that XRD patterns show no extra features for the patterns of manganese loaded H-ZSM-5 catalysts when compared to the parent H-ZSM-5. This implies that the structure of H-ZSM-5 zeolite is well preserved during impregnation and even with the increased manganese loading. It worth noting that when the manganese loading was increased the intensities of the peaks at 2θ angle between 23 and 25$^{o}$ decreased, suggesting that addition of manganese may decreases the crystallinity of H-ZSM-5 zeolite.

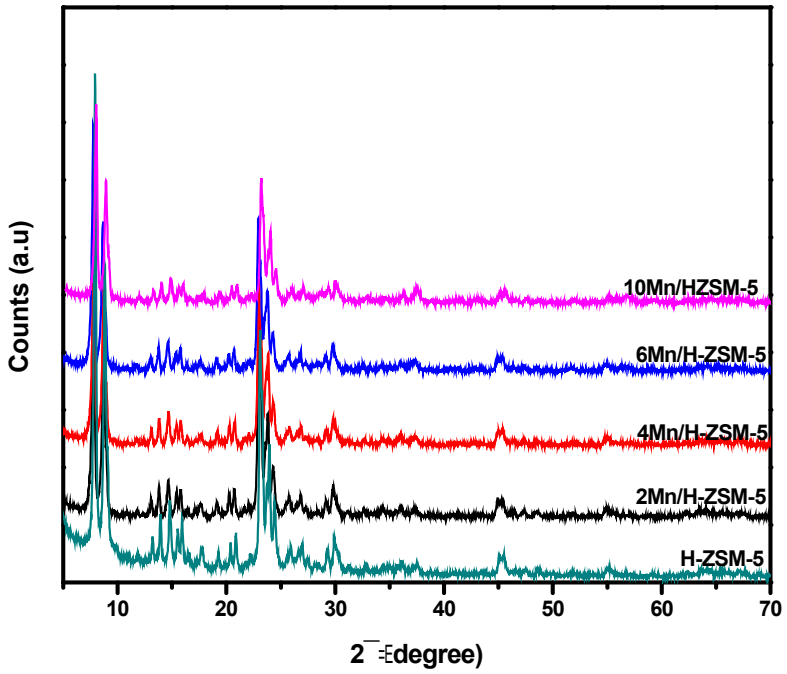



**Figure 7.10:** The XRD patterns of Mn/H-ZSM-5 zeolite catalysts of different manganese loadings.

The hydrogen temperature programmed profiles of bulk $MnO_2$ and Mn/H-ZSM-5 zeolite catalysts with different manganese loadings are shown in Figure 7.11(a) and Figure 7.11(b) respectively. The profile of the bulk manganese catalyst shows two well defined reduction steps, with the first reduction step at 360 $^{o}$C and second reduction step at 430 $^{o}$C. It is worth noting that the intensity of the first reduction step is much greater than the intensity of the second reduction step. Several authors [21-23] have reported on the reduction of supported manganese catalysts. They described the reduction of manganese oxide as successive reduction process (from $MnO_2$

→ $Mn_2O_3$ → $Mn_3O_4$ → MnO). Boot et al.[24] and Kapteijn at al [25] studied the reduction of supported manganese oxide catalysts prepared from $Mn(NO_3)_2$ solution. In their results they revealed that both $MnO_2$ and $Mn_2O_3$ species are reduced to $Mn_3O_4$ in one step without an intermediate transformation step, followed by the reduction of $Mn_3O_4$ to MnO. The first reduction peak is attributed to the hydrogen consumption during the transformation of $MnO_2$ and $Mn_2O_3$ species to $Mn_4O_3$ species and the second reduction peak at 427 $^oC$ is associated with the reduction of $Mn_2O_3$ and $Mn_3O_4$ species to of MnO [26, 27].

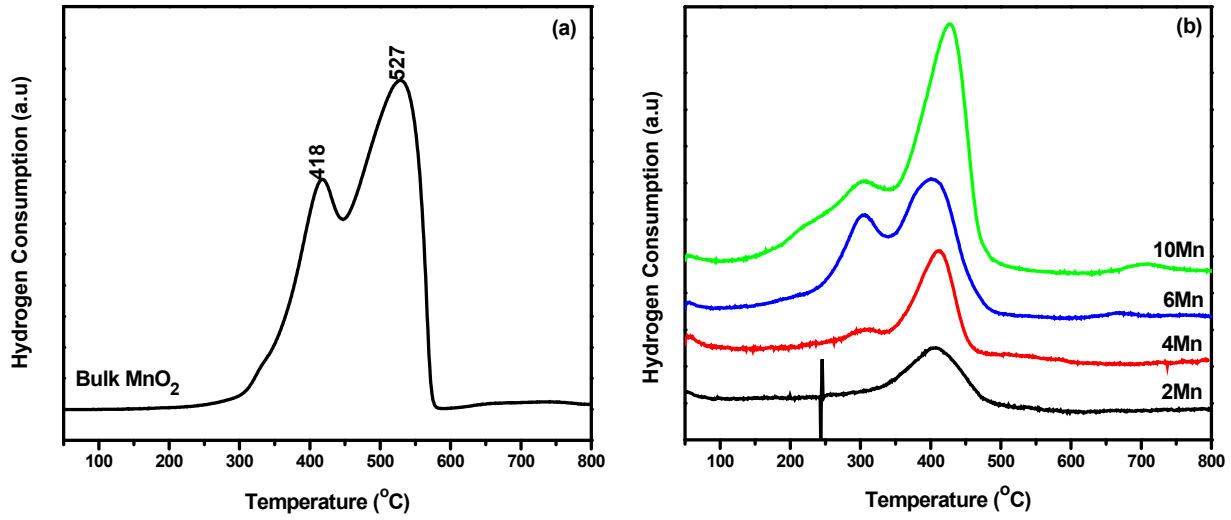



**Figure 7.11:** TPR profiles of bulk $MnO_2$ and Mn/H-ZSM-5 zeolite catalysts with different manganese loadings prepared by incipient impregnation method.

The TPR profiles of supported Mn/H-ZSM-5 zeolite catalysts are different from the profile of the bulk manganese oxide. From the TPR profile of 2Mn/H-ZSM-5 we only observed a broad reduction peak with the reduction process starting at 250 $^oC$. A lower degree of reduction is due to lack of accessibility of $Mn_xO_y$ species at low Mn loadings as manganese oxide species are located inside the channels and pores of the zeolite. As manganese loading was increased two well defined peaks were observed and the reduction started at lower reduction temperatures (i.e. 130 $^oC$ for 10Mn/H-ZSM-5 catalyst). The increase in reducibility with increase in manganese loading can be attributed to the presence of manganese oxide species on the external surface of the zeolite which are more easily accessible and readily reduced.

The influence of manganese loading on the concentration of acid sites was studied by ammonia TPD. Figure 7.12 show the profiles of the parent H-ZSM-5 and manganese modified H-ZSM-5 zeolite catalysts.

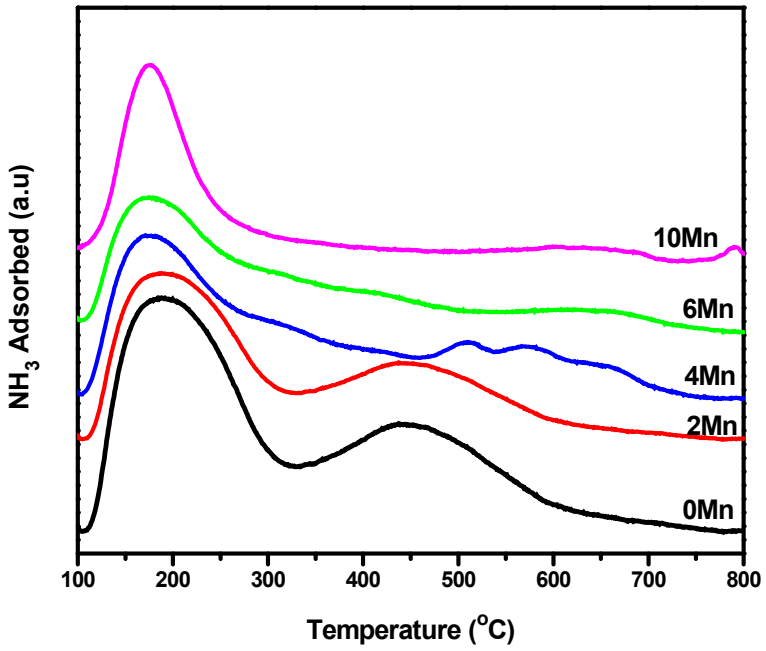



**Figure 7.12:** $NH_3$-TPD profiles of the parent H-ZSM-5 and Mn/H-ZSM-5 catalysts with different manganese loadings.

The TPD profile of the H-ZSM-5 shows two desorption peaks at 182 and 440 $^oC$, which are attributed to desorption of ammonia from different acid sites. The peak appearing at lower desorption temperature is due to desorption of weakly bonded ammonia molecules from the Lewis acid sites and the second peak at higher desorption temperature is associated to desorption of ammonia molecules that were strongly bonded to Brønsted acid sites [28-30]. Addition of 2 wt.% of manganese led to the decrease in intensity of the HT (440 $^oC$) peak and thus the peak was suppressed when the manganese loading was further increased. The intensity of the LT (182 $^oC$) peak was also decreased when manganese loading was above 2 wt.%. These results show that addition of manganese onto H-ZSM-5 decreases the concentration of both Brønsted and Lewis acid sites. This suggests that during impregnation there is an exchange taking place between $Mn^{2+}$ and $H^+$ of the H-ZSM-5 zeolite which led to suppression of Brønsted acid sites.

The results of the effect of manganese loading on the catalytic performance on MDA reaction was investigated (800 $^{o}$C for 6 hours) and the results are presented in Figure 7.13. The catalytic conversion of methane initially increased with the addition of manganese attaining a maximum of 8% conversion at a manganese loading of 4 wt.%. An increase in methane conversion observed upon addition of manganese is attributed to the presence of manganese oxycarbide species generated during an induction period in the MDA reaction. These oxycarbide species are responsible for initiating the MDA reaction. A decrease in methane conversion was observed when the manganese loading was more than 4 wt.% and may be attributed to a decrease in the concentration of the H-ZSM-5 Brønsted acid sites which are occupied by the manganese species in the zeolite channels as shown by the $NH_3$-TPD profiles (Figure 7.12). The decrease in the BET surface areas and the pore volumes (Table 7.2) suggest that high manganese loading led to manganese species being dispersed on the surface of H-ZSM-5 covering the active sites and blocking the pores of the H-ZSM-5 zeolite. This may also contribute in the decrease in activity of the catalysts for the MDA reaction.

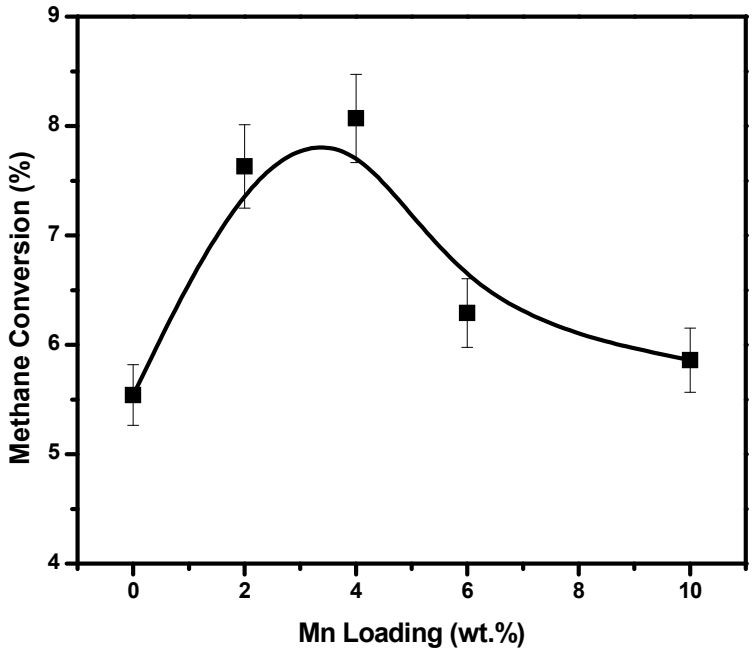



**Figure 7.13:** The effect of manganese loading on methane conversion over Mn/H-ZSM-5 catalyst at 800 $^{o}$C, taken at TOS of 125 min.

The influence of manganese loading on the catalytic stability of Mn/H-ZSM-5 catalysts was investigated for 6 hours on-stream. Catalysts with a manganese loading between 0 and 10 wt% loading were subjected to MDA (800 $^{o}$C); results are shown in Figure 7.14. These results show an increase in methane conversion for first 60 minutes on-stream followed by a decrease in methane conversion with increase in TOS. This decrease can be attributed to the deactivation of the catalysts associated with the deposition of coke on the active sites of catalysts rendering them inactive. The manganese free H-ZSM-5 catalyst showed low methane conversion. However, good catalytic stability relative to TOS was observed for H-ZSM-5 when compared to the manganese containing catalysts. For catalysts with low manganese content (2 and 4 wt%) a steady decrease in conversion with TOS was observed. However, for catalysts with high manganese loading, i.e. 6 and 10 wt% there is a rapid decrease in methane conversion (from 6.5% to 3%) with increase in TOS. These observations may be attributed to the agglomeration of manganese oxide species in the H-ZSM-5 channels which led to the blockage of zeolite pores.

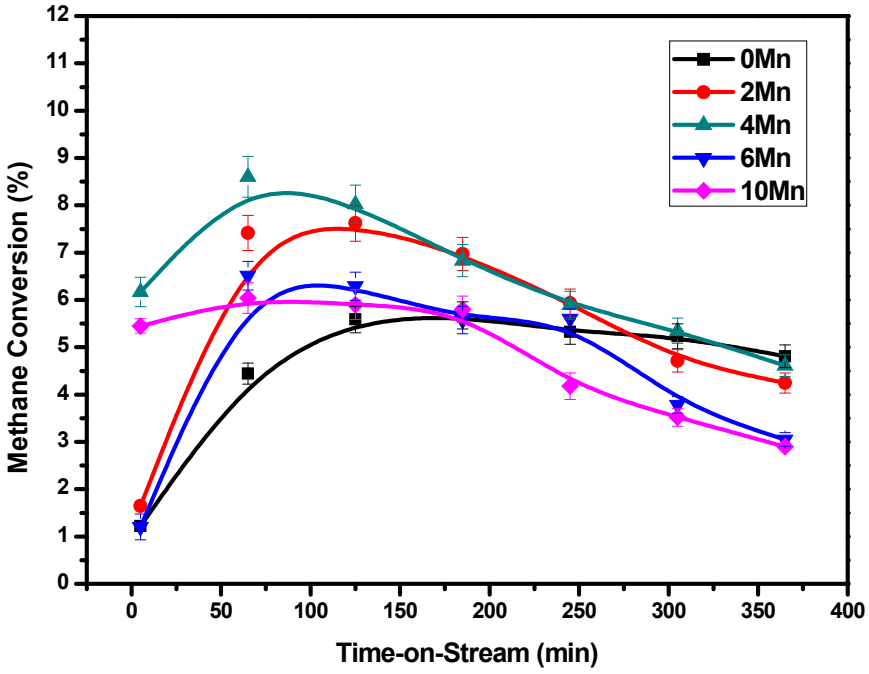



**Figure 7.14:** The catalytic conversion of methane of Mn/H-ZSM-5 zeolite catalysts with different manganese loading as the function of time-on-stream with reaction temperature set at 800 $^{o}$C.

The effect of manganese loading on the product selectivity towards C2s, aromatics and coke in the MDA reaction at 800 $^{o}$C was compared at 6% methane conversion, as shown in Figure 7.15.

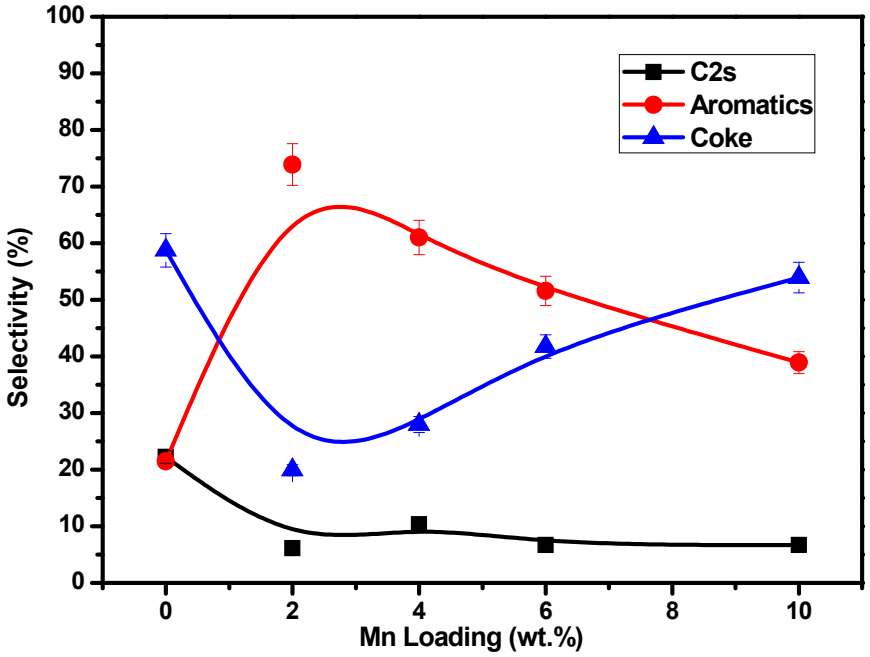



**Figure 7.15:** The effect of manganese loading the C2s, aromatics and coke selectivity from MDA over Mn/H-ZSM-5 at 800 $^{o}$C taken at isoconversion of 6%, for a TOS of 245 minutes.

And effect of manganese loading on the product distribution (i.e. C2s, benzene, toluene, naphthalene and coke) is presented in Table 7.3. The selectivity towards C2s was observed to be 21% for the manganese free H-ZSM-5 catalyst and upon addition of manganese there was a significant decrease reaching values between 6 and 10%. The selectivity to aromatics varied between 51 and 74% with 2 wt.% loaded catalyst giving the optimum selectivity of 74%. The major aromatic product formed is benzene. We observed a significant increase in benzene selectivity when the H-ZSM-5 zeolite catalyst was impregnated with manganese, with a benzene selectivity of 52% for 2 wt% loaded catalyst being the highest value attained. However, a noticeable decrease in benzene selectivity was observed with increase in manganese loading. This decrease in benzene selectivity was compensated for an increase in naphthalene and toluene selectivity as the manganese loading increased. The increase in manganese loading favoured the formation of heavy aromatic compounds. Hence high coke selectivity was observed for the 10 wt% loaded catalyst. The selectivity to coke was between 20 and 41% that when the manganese

loading was increased. This may be attributed to a change in the pore structure due to pore blockage by manganese oxide species at high manganese loading.

**Table 7.3:** The effect of manganese loading on the product selectivity of Mn/H-ZSM-5 zeolite catalysts for MDA at 800 $^{o}$C , taken at 6% methane conversion.

| Mn Loading (wt.%) | Conversion (%) | Percentage Product Selectivity | | | | | |
|---|---|---|---|---|---|---|---|
| | | C2s | Benzene | Toluene | Naphthalene | Aromatics | coke |
| 0 | 6.33 | 19.8 | 21.5 | 0 | 0 | 21 | 58.7 |
| 2 | 5.93 | 6.2 | 52.47 | 14.6 | 6.8 | 73.9 | 19.5 |
| 4 | 5.80 | 10.2 | 43.2 | 11.1 | 7.5 | 61.7 | 28.0 |
| 6 | 5.95 | 6.5 | 41.4 | 6.3 | 9.1 | 56.8 | 36.5 |
| 10 | 5.60 | 6.7 | 33.2 | 6.4 | 11.4 | 50.93 | 40.5 |

The influence of manganese loading on the amounts and nature of the deposited carbonaceous material during the MDA reaction (800 $^{o}$C for 6 hours on-stream) was investigated by a thermal analysis technique. The TGA and DTG profiles of Mn/H-ZSM-5 zeolite catalysts with different manganese loadings are shown in Figure 7.16(a) and Figure 7.16(b), respectively.

The TGA results corroborate the coke selectivity results presented in Table 7.4. From the coke selectivity results we observed a high selectivity to coke for H-ZSM-5 catalysts without manganese and a decrease in coke selectivity was observed upon manganese loading. A similar trend is observed when coked catalysts were subjected to TGA measurements under oxidative conditions. The amount of carbonaceous deposits for the H-ZSM-5 catalyst was found to be 121 mg per gram of catalyst and a decrease was observed when manganese was loaded; cokes levels of 87 mg per gram of catalysts for 2 and 4 wt.% manganese loadings were measured. However, an increase in carbonaceous deposits was observed for catalysts with high manganese loadings. The high amounts of carbonaceous deposits for catalysts with higher manganese loadings can be attributed to pore blockage leading to an alteration of the pore structure. The shape selectivity character of H-ZSM-5 is compromised and this leads to heavy aromatic compounds being trapped in the cages of the zeolite. The heavy aromatic compounds trapped in the zeolite cages

will further react to form coke. Hence high amounts of carbonaceous deposits for 6 and 10 wt% loaded Mn/H-ZSM-5 catalysts were observed.

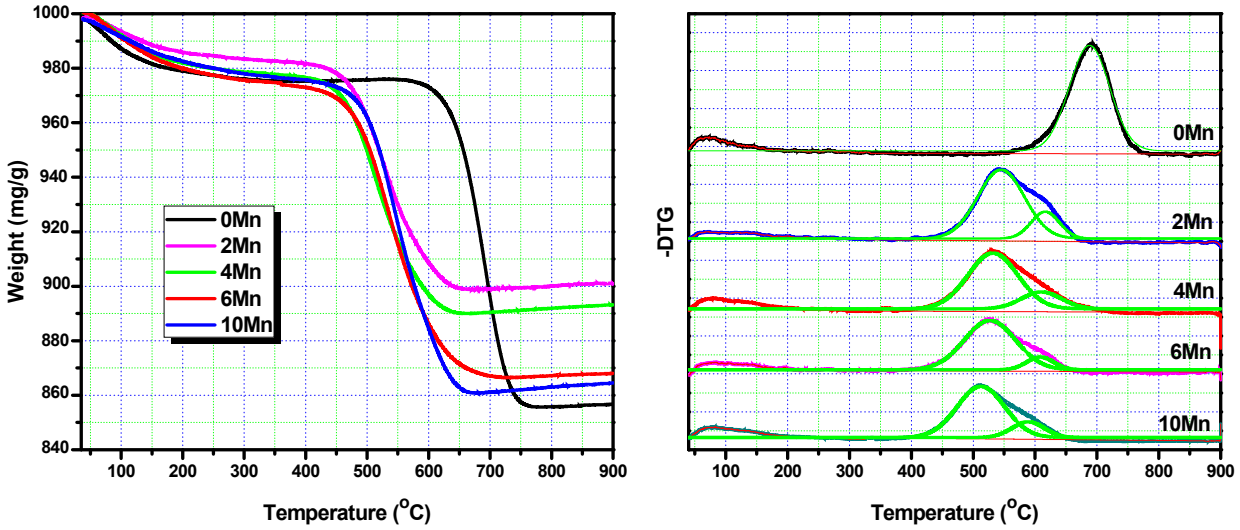



**Figure 7.16:** TGA (a) and DTG (b) profiles of coked Mn/H-ZSM-5 zeolite catalysts with different manganese loadings that were used for MDA reaction at 800 °C for 6 hours on-stream.

**Table 7.4:** Summarized TGA and DTG results of coked Mn/H-ZSM-5 zeolite catalysts with different manganese loadings after MDA reaction at 800 °C for 6 hours on-stream.

| Mn Loading (wt%) | Amount of Coke (mg/ g cat.) | Decomposition Temperature (°C) | Decomposition Temperature (°C) |
|---|---|---|---|
| 0 | 120.7 | - | 692 |
| 2 | 87.2 | 541 | 619 |
| 4 | 86.4 | 534 | 621 |
| 6 | 107.3 | 524 | 615 |
| 10 | 116.0 | 510 | 591 |

The DTG profiles reveal the nature of carbonaceous material deposited on the Mn/H-ZSM-5 zeolite catalysts. The DTG profile of the H-ZSM-5 catalyst exhibited one peak at higher decomposition temperature (i.e. 692 °C) which is associated with carbon formed on the Brønsted acid sites. For the manganese loaded H-ZSM-5 catalysts we observed two peaks, one at lower decomposition temperature which is associated with carbon formed on metal species and other

peak at high decomposition temperature. Upon addition of manganese we observed a decrease in decomposition temperature associated with Brønsted acid sites. This might be due to the presence of the metal catalyzing the oxidation of carbon. As the manganese loading was increased the high temperature position peak shifted to lower temperatures and the peak intensity also decreased, suggesting that the amount of carbon deposited on the Brønsted acid sites decreased with increase in manganese loading. These results showed that the rate of catalyst deactivation is dependent on manganese loading and the aromatic selectivity is dependent on the number of Brønsted acid sites available during the MDA reaction.

### *7.3.4. Effect of Tungsten on the MDA Reaction*

The influence of tungsten on the catalytic stability of the Mn/H-ZSM-5 zeolite catalysts in the MDA reaction was investigated at 800 $^{o}$C for 6 hours on-stream. Catalysts with different tungsten loadings, between 0.5 and 1.5 wt%, were prepared by an impregnation method and calcined at 500 $^{o}$C.

Figure 7.17 shows the results of the effect of tungsten loading on the catalytic performance of Mn/H-ZSM-5 catalysts with different tungsten loadings in the MDA reaction. It is evident that the addition of tungsten to the Mn/H-ZSM-5 zeolite catalyst lowered the catalytic activity. The methane conversion was decreased from 6% to 4% upon addition of tungsten. However, the tungsten modified catalysts still showed catalytic stability with increase in time-on-stream, as tungsten is known to be thermally stable at high MDA reaction temperatures.

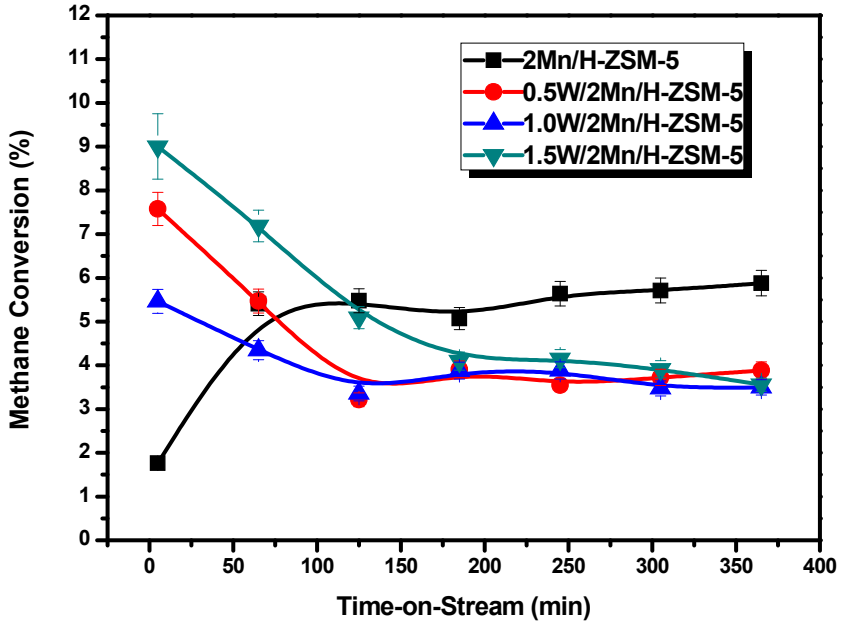



**Figure 7.17:** The effect of tungsten on the catalytic conversion and stability of Mn/H-ZSM-5 zeolite catalysts for MDA reaction at 800 $^{o}$C.

The results of the effect of tungsten loading on the product selectivity towards $C_{2s}$, aromatics and coke in the MDA reaction (800 $^{o}$C taken after 245 minutes on-stream) are shown in Figure 7.18 below. The selectivity towards aromatics for tungsten free 2Mn/H-ZSM-5 zeolite catalysts was 74% and upon addition of tungsten we observed a linear decrease in the aromatic selectivity and a simultaneous increase in coke selectivity with increase in tungsten loading. An aromatic selectivity of 41% was obtained for the 0.5wt.% tungsten loaded Mn/H-ZSM-5 catalyst. As the tungsten loading was increased to 1.5 wt.% a decrease in selectivity was observed reaching an aromatic selectivity of 12%. An increase in tungsten loading resulted into an increase in selectivity towards coke reaching values as high as 74% for tungsten loading of 1.5 wt.%. These results suggest that the presence of tungsten suppressed the formation of aromatic compounds and favoured the formation of carbonaceous deposits.

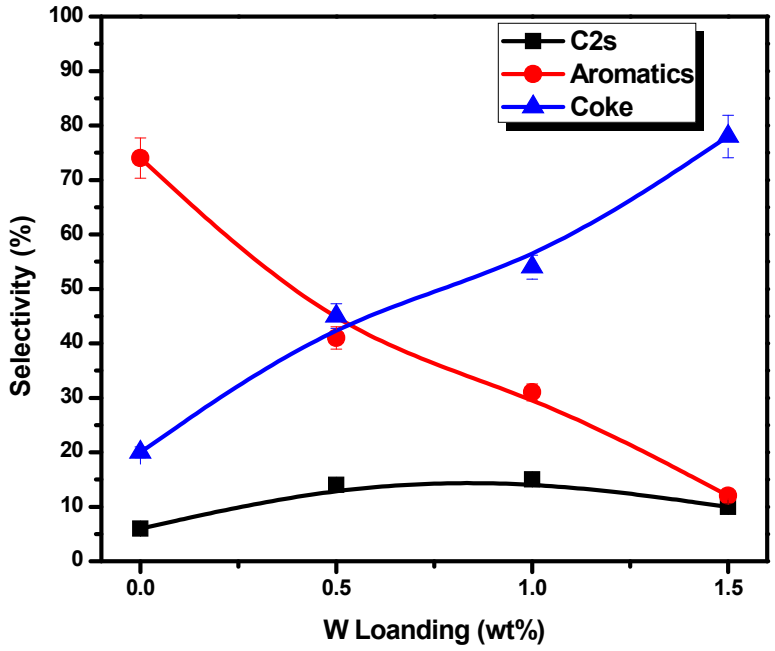



**Figure 7.18:** The effect of tungsten loading on the catalysts product distribution of Mn/H-ZSM-5 for MDA reaction at 800 $^{o}$C taken after 245 minutes on-stream.

Table 7.5 shows the effect of tungsten loading on the product distribution of the Mn/H-ZSM-5 zeolite catalyst evaluated after 245 minutes on-stream. .

**Table 7.5:** The effect of tungsten loading on the product selectivity of Mn/H-ZSM-5 zeolite catalysts for MDA reaction at 800 $^{o}$C taken after 245 minutes on stream.

| W Loading (wt.%) | Conversion (%) | Percentage Product Selectivity | | | | | |
|---|---|---|---|---|---|---|---|
| | | C2s | Benzene | Toluene | Naphthalene | Aromatics | Coke |
| 0 | 5.6 | 5.2 | 53.7 | 11.6 | 7.9 | 73.2 | 19.6 |
| 0.5 | 3.5 | 14.3 | 25.0 | 6.7 | 9.3 | 41.0 | 44.7 |
| 1.0 | 3.9 | 15.3 | 16.3 | 4.1 | 10.1 | 30.5 | 54.2 |
| 1.5 | 4.2 | 10.1 | 4.2 | 1.3 | 6.5 | 12.0 | 77.3 |

The results show that benzene is the major product formed during the MDA reaction. However, we observed a decrease in benzene and toluene selectivity with increased tungsten loading. The

benzene produced over the tungsten free Mn/H-ZSM-5 catalyst was 54% and this reduced upon addition of tungsten reaching 4.2% for the 1.5 wt.% tungsten loaded Mn/H-ZSM-5 catalyst. The selectivity towards toluene was between 12 and 1%, with 12% being associated with catalysts containing 0 wt.% tungsten and 1% assigned to the catalyst containing a high tungsten loading. The noticeable decrease in benzene and toluene selectivity is accounted for by a stable increase in both $C_{2s}$ and naphthalene selectivity. The increase in tungsten loading favoured the formation of heavy aromatic compounds which are further transformed into carbonaceous deposits leading to high coke selectivity. High selectivity towards $C_{2s}$ with increase in tungsten loading may be attributed to a decrease in the concentration of the Brønsted acid sites caused by an increase in metal content.

The effect tungsten loading on the amounts and nature of the coke deposits during the MDA reaction at 800 $^{o}$C for 6 hours on-stream was investigated by thermal analysis technique. The TGA and DTG profiles of Mn/H-ZSM-5 zeolite catalysts with different tungsten loadings are shown in Figure 7.19(a) and Figure 7.19(b), respectively.

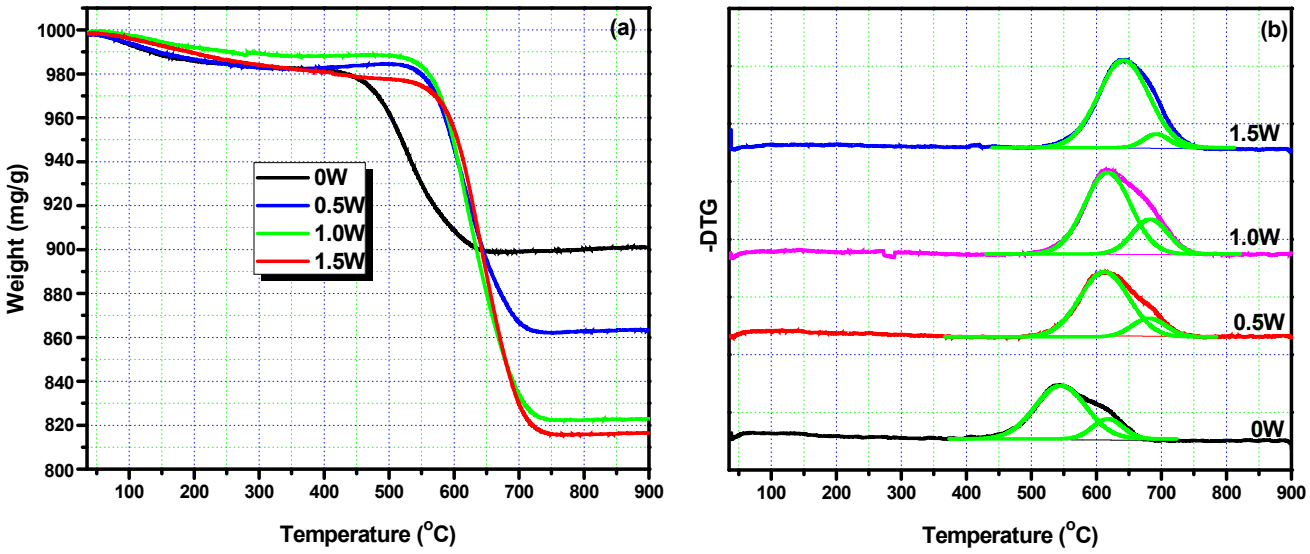



**Figure 7.19:** TGA (a) and DTG (b) profiles of coked tungsten modified Mn/H-ZSM-5 zeolite catalysts with different tungsten loadings that were used for MDA reaction at 800 $^{o}$C for 6 hours on-stream.

The selectivity results revealed that addition of tungsten led to an increase in coke selectivity towards coke. These results are in agreement with the TGA results. The TGA measurements of coked samples after the MDA reaction showed an increase in the coke deposits with increase in tungsten loading. The amount of coke deposited onto tungsten free 2Mn/H-ZSM-5 was 87 mg per gram of catalyst. Upon addition of tungsten an increase of 50 and 100% of coke deposits was observed. For the 0.5 wt.% tungsten loading a coke deposit of 122 mg/g.cat reaching 166 and 163 mg/g.cat for the 1 and 1.5 wt.% tungsten loaded catalysts was observed.

**Table 7.6:** Summarized TGA and DTG results of coked tungsten modified 2Mn/H-ZSM-5 zeolite catalysts with different tungsten loadings after MDA reaction at 800 $^{o}$C for 6 hours on-stream.

| W Loading (wt%) | Amount of Coke (mg/ g cat.) | Decomposition Temperature ($^{o}$C) | Decomposition Temperature ($^{o}$C) |
|---|---|---|---|
| 0 | 87.2 | 541 | 619 |
| 0.5 | 122.2 | 605 | 682 |
| 1.0 | 166.4 | 610 | 684 |
| 1.5 | 163.6 | 637 | 697 |

The DTG profiles exhibited two decomposition peaks, one at low temperature and the other at high temperature. Depending on the position of the decomposition temperature one can clearly differentiate the nature of the carbonaceous deposits that form on the catalyst. The decomposition temperatures for tungsten free 2Mn/H-ZSM-5 catalysts were lower compared with the tungsten modified loaded catalysts. This suggests that addition of tungsten enhances the stability of carbonaceous deposits formed on metal species and Brønsted acid sites. The decomposition temperatures associated with the carbonaceous deposits formed on the metal species increased from 541 to 637 $^{o}$C with increase in tungsten loading. This increase in decomposition temperature may be attributed to a difference in the metal carbide species formed during the MDA reaction. The second decomposition peak at high temperature is associated with deposition of polyaromatic carbon on the Brønsted acid sites also shifted to higher temperatures (619 to 697 $^{o}$C) as the tungsten loading was increased. It is worth noting that the intensity of the peak associated with polyaromatic carbon on the Brønsted acid sites decreased

with increase in tungsten loading. The decrease in the intensity of high temperature decomposition peak can be attributed to a decrease in the formation rate of polyaromatic compounds on the Brønsted acid sites of H-ZSM-5. This suggests that an increase in tungsten loading led to a decrease in the concentration of Brønsted acid sites and more carbonaceous deposits were formed on the metal species (i.e. both manganese and tungsten).

### *7.3.5. Addition Effect of Noble Metals of the MDA Reaction over a W/Mn/H-ZSM-5 Catalyst*

A comparison study was performed to investigate the influence of other noble metals on the MDA reaction over a W/Mn/H-ZSM-5 zeolite catalyst. A catalyst with low selectivity towards aromatic compounds and high coke selectivity was chosen to clearly observe the effect of noble metals on the product selectivity and on the total amounts of coke deposited by TGA. Platinum and ruthenium were chosen as the metals of interest. These noble metal catalysts were prepared by impregnation of 1.5W/2Mn/H-ZSM-5 with 0.5 wt.% of the noble metal. Catalysts were calcined at 500 $^{o}$C for 6 hours. The MDA reaction was performed at 800 $^{o}$C for 6 hours. Prior to the reaction the catalysts were treated with nitrogen at 800 $^{o}$C for 1 hour and exposed to methane for 60 minutes.

Figure 7.20 shows the influence of noble metal on the catalytic performance of 1.5W/2Mn/H-ZSM-5 catalyst for the MDA reaction at 800 $^{o}$C for 6 hour on-stream. Following an induction period of 60 minutes, in the first 60 minutes on-stream methane conversions of 9% and 7% were obtained for the 1.5W/2Mn/H-ZSM-5 catalyst. Upon addition of platinum an improvement in the catalytic activity was observed. Methane conversions of 12% and 10% were obtained in the first 60 minutes on-stream. This was followed by a rapid decrease in methane conversion with increase in TOS. A similar catalytic behaviour was observed upon addition of ruthenium; however, low methane conversions (i.e. 7% and 5%) were obtained when compared with the platinum catalyst. It is worth noting that all three catalysts reached equilibrium methane conversions that are between 4 and 5%.

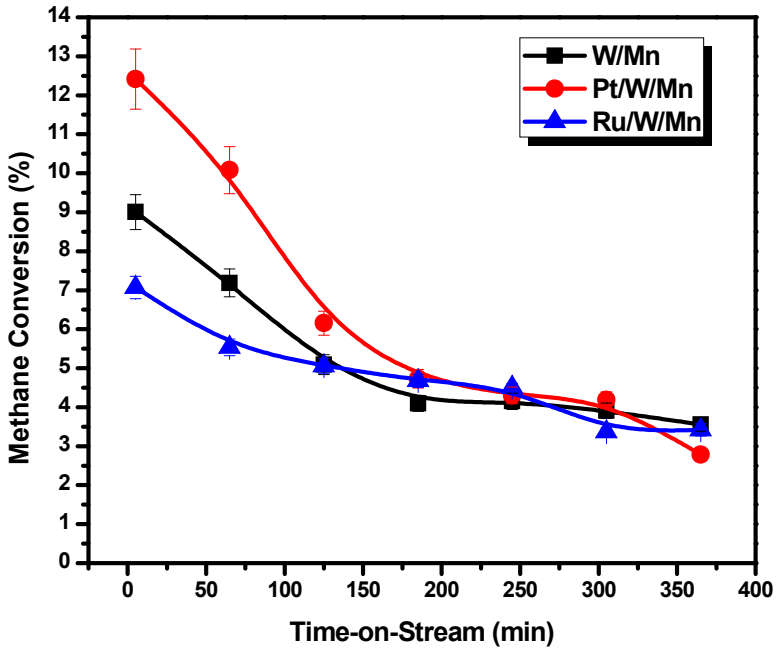



**Figure 7.20:** The catalytic conversion of methane as a function of time-on-stream over noble metal modified 2Mo/H-ZSM-5 zeolite catalysts with a of 0.5 wt.% loading of the noble metal

The effect of noble metals on the product distribution towards hydrocarbon formation of the 1.5W/2Mn/H-ZSM-5 catalysts are shown in Table 7.7. The product selectivities of these catalysts were compared at similar methane conversion (4%) taken after 245 minutes on-stream.

**Table 7.7:** Comparison results of the effect of noble metals on the MDA reaction and product selectivity taken at 4% methane conversion after 245 minutes on-stream.

| Catalyst | Conversion (%) | Percentage Product Selectivity | | | | | |
|---|---|---|---|---|---|---|---|
| | | C2s | Benzene | Toluene | Naphthalene | Aromatics | Coke |
| W/Mn | 4.2 | 10.1 | 4.2 | 1.3 | 6.5 | 12.0 | 77.9 |
| Pt/W/Mn | 4.2 | 7.4 | 40.7 | 12.2 | 2.4 | 55.3 | 37.3 |
| Ru/W/Mn | 4.5 | 12.6 | 33.6 | 8.6 | 3.5 | 45.7 | 41.7 |

From the results presented above it is clear that addition of a noble metal onto the W/Mn/H-ZSM-5 catalyst significantly influenced the product distribution. The presence of platinum and

ruthenium enhanced the catalyst capabilities by producing aromatic compounds and suppressing coke formation during the MDA reaction at 800 $^{o}$C. Addition of platinum and ruthenium led to an increase in the aromatic selectivity to 55% and 46% respectively. The coke selectivity for the W/Mn catalyst was 77% and upon addition of noble metals a decrease in coke selectivity was observed. Coke selectivities of 37% and 42% were obtained for the Pt/W/Mn and Ru/W/Mn catalysts respectively while the selectivity towards naphthalene was below 5%. The suppression of naphthalene formation is attributed to the ability of noble metals to catalyze the hydrogenolysis of heavy aromatic compounds [31].

The ability of ruthenium and platinum to reduce the amount of coke deposit during MDA reaction was investigated using TGA measurements under oxidative conditions. The TGA and DTG profiles of 1.5W/2Mn/H-ZSM-5, 0.5Pt/1.5W/Mn/H-ZSM-5 and 0.5Ru/1.5W/Mn/H-ZSM-5 zeolite catalysts are shown in Figure 7.21(a) and Figure 7.21(b), respectively.

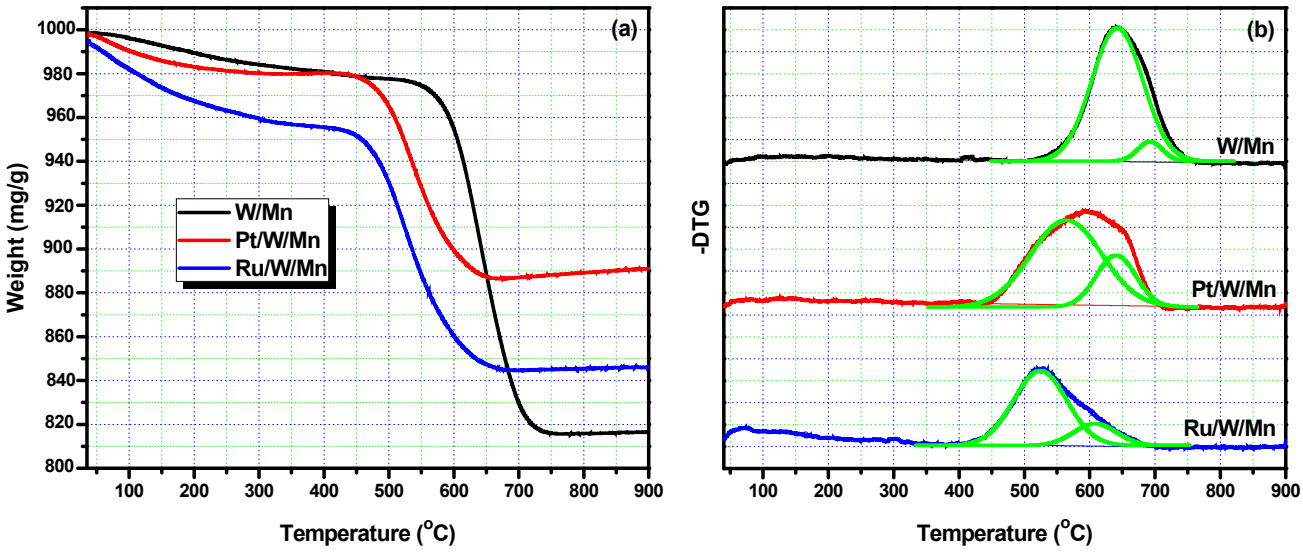



**Figure 7.21:** TGA (a) and DTG (b) profiles of coked tungsten modified Mn/H-ZSM-5 zeolite catalysts with various tungsten loadings after for the MDA reaction at 800 $^{o}$C for 6 hours on-stream.

**Table 7.8:** Summarized TGA and DTG results of coked tungsten modified 2Mn/H-ZSM-5 zeolite catalysts with different tungsten loadings after the MDA reaction at 800 $^{o}$C for 6 hours on-stream.

| W Loading (wt%) | Amount of Coke (mg/ g cat.) | Decomposition Temperature ($^{o}$C) | Decomposition Temperature ($^{o}$C) |
|---|---|---|---|
| W/Mn | 164 | 637 | 697 |
| Pt/W/Mn | 95 | 562 | 639 |
| Ru/W/Mn | 113 | 521 | 610 |

The TGA results substantiate the coke selectivity results presented in Table 6.8 above. The total amount of coke deposited on the noble metal promoted W/Mn/H-ZSM-5 catalysts was lower than that formed on the W/Mn/H-ZSM-5 catalyst. The amount of coke deposited on the Pt/W/Mn catalyst was somewhat lower (95 mg/g) than that deposited on the Ru/W/Mn catalyst (113 mg/g). The total amount of coke deposited on a noble metal promoted W/Mn/H-ZSM-5 catalysts was reduced by 42% for the platinum catalyst and by 31% for the ruthenium catalyst. This can be attributed to platinum possessing a higher hydrogenation activity than ruthenium. The DTG profile of W/Mn exhibited two decomposition peaks, a low decomposition temperature peak (637 $^{o}$C) and a higher decomposition temperature paek (697 $^{o}$C), which are associated with carbon in the metal carbide matrix and carbon deposited on the Brønsted acid sites respectively. Addition of the noble metal decreased the thermal stability of the coke deposit. The decomposition temperature of carbon associated with the metal carbide matrix shifted to lower temperatures, 562 $^{o}$C for platinum and 521 $^{o}$C for ruthenium. A similar trend was observed for the peaks associated with carbon deposited on the Brønsted acid sites. The decomposition temperature decreased from 697 $^{o}$C to 639 $^{o}$C for the platinum promoted catalyst and to 610 $^{o}$C for the ruthenium promoted catalyst. The decrease in the thermal stability of the coke deposited on the noble metal promoted catalyst can be attributed to the decrease in the carbon to hydrogen ratio caused by the hydrogenation of carbon formed during the MDA reaction. The presence of a noble metal may also catalyze the oxidation of carbon during TGA measurements.

## 7.4. Summary

The MDA reaction was successfully studied over a Mn/H-ZSM-5 catalyst at different reaction temperatures. The methane conversion increased linearly with increase in reaction temperature from 700 to 850 $^{o}$C. The selectivity towards aromatic compounds of about 65% was attained for the reactions performed at 750 and 800 $^{o}$C. An increase in coke selectivity with increase in reaction temperature also followed a linear trend. The total amount of coke deposit increased to 200 mg/g for the reaction performed at 850 $^{o}$C. Coke deposition was thermally favoured at high reaction temperature (i.e 850 $^{o}$C).

The use of different manganese precursors to prepare Mn/H-ZSM-5 catalysts had an effect on both catalytic behaviour and product distribution. High catalytic activity was obtained for the catalysts prepared from $Mn(NO_3)_2$ and $MnCl_2$ salts. The product distribution was however significantly different. When $Mn(NO_3)_2$ catalyst was used the selective towards aromatic compounds was enhanced while $MnCl_2$ catalyst was more selective toward coke. The use of $KMnO_4$ lowered the methane conversion and high coke selectivity was observed.

The effect of manganese loading was studied at 800 $^{o}$C and optimum catalyst activity was obtained at 2 and 4 wt.% manganese loadings. An aromatic selectivity above 70% and coke selectivity of 20% were obtained for the 2 wt.% loaded catalyst. An increase in manganese loading led to rapid deactivation which is due to the formation of coke deposits on active sites. An increase in coke selectivity was observed with increase in manganese loading.

Addition of tungsten onto 2Mn/H-ZSM-5 decreased the methane conversion and the catalysts were found to be fairly stable with increase in TOS. An increase in tungsten loading favoured the formation of coke while the aromatic selectivity decreased linearly with tungsten loading. The total amount of coke deposit for the 1.5 wt.% tungsten loaded catalyst was 164 mg/g which translated to an 88% increase of coke formed on the catalyst.

The promotional effect of platinum and ruthenium were tested using the most coke selective W/Mn/H-ZSM-5 catalyst. Addition of platinum and ruthenium increased the aromatic selectivity from 12% to 55% and 46% respectively. Benzene selectivities of 42% and 33% were obtained for the noble metal promoted W/Mn/H-ZSM-5 catalysts. A reduction in the total amount of coke was achieved for the platinum promoted catalyst (42%) and for the ruthenium promoted catalyst (31%). The presence of a noble metal favoured the formation of aromatic compounds and suppressed the formation of coke.

## 7.5. Reference List

[1] M.J. Ledoux, P.H. Cuong, J. Guille, H. Dunlop, *Journal of Catalysis*, **134** (1992) 383.

[2] W. Ding, G.D. Meitzner, D.O. Marler, E. Iglesia, *Journal of Physical Chemistry B*, **105** (2001) 3928.

[3] W.P. Ding, S. Li, G.D. Meitzner, E. Iglesia, *Journal of Physical Chemistry B*, **105** (2001) 506.

[4] Z.-T. Xiong, L.-L. Chen, H.-B. Zhang, J.-L. Zeng, G.-D. Lin, *Catalysis Letters*, **74** (2001) 227.

[5] C.L. Zhang, S. Li, Y. Yuan, W. Zhang, T. Wu, L.W. Lin, *Catalysis Letters*, **56** (1998) 207.

[6] Z.-T. Xiong, H.-B. Zhang, G.-D. Lin, J.-L. Zeng, *Catalysis Letters*, **74** (2001) 233.

[7] J.L. Zeng, Z.T. Xiong, H.B. Zhang, G.D. Lin, K.R. Tsai, *Catalysis Letters*, **53** (1998) 119.

[8] V.B. Y. Amenomiya, M. Goledzinowski, J. Galuszka, *Catalysis Reviews-Science and Engineering*, **32** (1990) 163.

[9] D.J. Wang, M.P. Rosynek, J.H. Lunsford, *Journal of Catalysis*, **155** (1995) 390.

[10] S. Pak, J.H. Lunsford, *Applied Catalysis A: General*, **168** (1998) 131.

[11] A. Malekzadeh, A. Khodadadi, M. Abedini, M. Amini, A. Bahramian, A.K. Dalai, *Catalysis Communications*, **2** (2001) 241.

[12] S.-F. Ji, T.-C. Xiao, S.-B. Li, C.-Z. Xu, R.-L. Hou, K.S. Coleman, M.L.H. Green, *Applied Catalysis A: General*, **225** (2002) 271.

[13] S. Ji, T. Xiao, S. Li, L. Chou, B. Zhang, C. Xu, R. Hou, A.P.E. York, M.L.H. Green, *Journal of Catalysis*, **220** (2003) 47.

[14] M. Marczewski, H. Marczewska, *Reaction Kinetics and Catalysis Letters*, **53** (1994) 33.

[15] L. Wang, L. Tao, M. Xie, G. Xu, J. Huang, Y. Xu, *Catalysis Letters*, **21** (1993) 35.

[16] P.L. Tan, C.T. Au, S.Y. Lai, *Catalysis Letters*, **112** (2006) 239.

[17] D. Ma, Y. Shu, M. Cheng, Y. Xu, X. Bao, *Journal of Catalysis*, **194** (2000) 105.

[18] H. Jiang, L. Wang, W. Cui, Y. Xu, *Catalysis Letters*, **57** (1999) 95.

[19] F. Buciuman, F. Patcas, J. Zsakó, *Journal of Thermal Analysis and Calorimetry*, **61** (2000) 819.

[20] J. Wang, M. Kang, Z. Zhang, X. Wang, *Journal of Natural Gas Chemistry*, **11** (2002) 43.

[21] L.M. Gandía, M.A. Vicente, A. Gil, *Applied Catalysis A: General*, **196** (2000) 281.

[22] R. Lin, W.-P. Liu, Y.-J. Zhong, M.-F. Luo, *Applied Catalysis A: General*, **220** (2001) 165.

[23] F. Arena, T. Torre, C. Raimondoa, A. Parmalianac, S. Sperone, S.A. Messina, L. Studi, P.A. Moro, *Physical Chemistry Chemical Physics*, **3** (2001) 1911.

[24] L.A. Boot, M.H.J.V. Kerkhoffs, B.T. van der Linden, A.J. van Dillen, J.W. Geus, F.R. van Buren, *Applied Catalysis A: General*, **137** (1996) 69.

[25] F. Kapteijn, A.D. Vanlangeveld, J.A. Moulijn, A. Andreini, M.A. Vuurman, A.M. Turek, J.M. Jehng, I.E. Wachs, *Journal of Catalysis*, **150** (1994) 94.

[26] D. Delimaris, T. Ioannides, *Applied Catalysis B: Environmental*, **84** (2008) 303.

[27] W. Gac, *Applied Catalysis B: Environmental*, **75** (2007) 107.

[28] F. Lónyi, J. Valyon, *Thermochimica Acta*, **373** (2001) 53.

[29] F. Lónyi, J. Valyon, *Microporous and Mesoporous Materials*, **47** (2001) 293.

[30] K.F.M.G.J. Scholle, A.P.M. Kentgens, W.S. Veeman, P. Frenken, G.P.M. Van der Velden, *Journal of Physical Chemistry*, **88** (1984) 5.

[31] R. Kojima, S. Kikuchi, H. Ma, J. Bai, M. Ichikawa, *Catalysis Letters*, **110** (2006) 15.

# Chapter 8

# General Conclusions

## 8.1. Conclusions

The MDA reaction was investigated over platinum modified Mo/H-ZSM-5 catalysts which were pre-carbided at 750 $^{o}$C. The influence of platinum on the surface properties of molybdenum was studied using a CO adsorption FT-IR technique and CO chemisorption. The results showed that addition of platinum to the Mo/H-ZSM-5 catalysts led to Mo species adsorbing CO molecules. The FT-IR spectra showed two bands at 2162 and 2174 $cm^{-1}$ for the platinum modified catalysts before and after reductions which are attributed to CO adsorbed on $Mo^{4+}$ species, respectively. The shift in band position from 2162 to 2174 $cm^{-1}$ is due to a Mo-Pt interaction. The band associated with CO molecules adsorbed on molybdenum carbide species was not observed. This may be due to the oxidation of molybdenum carbide in the catalysts as the catalysts were carbided in an *ex-situ* setup.

The influence of platinum on the catalytic performance and product selectivity of Mo/H-ZSM-5 catalysts for the MDA reaction at 700 $^{o}$C was studied. Catalysts with platinum loadings between 0.5 and 2 wt.% were prepared by an incipient impregnation method. The presence of platinum led to a slight decrease in methane conversion. As the platinum loading increased the methane conversion decreased and the catalytic stability increased with TOS during the MDA reaction. Aromatic selectivities above 90% were obtained with catalysts containing low platinum loadings (0.5 and 1.0 wt.%), with benzene being the most prominent product. A decrease in coke selectivity and coke deposits was noted with the platinum modified Mo/H-ZSM-5 zeolite catalyst.

A comparative study was performed to compare platinum with other noble metals (ruthenium and palladium). Our results show that addition of noble metals does significantly affect the methane conversion and the catalytic stability was enhanced. The ruthenium promoted catalyst proved to be superior in terms of catalytic performance, with a higher methane conversion obtained than found for platinum promoted and palladium promoted Mo/H-ZSM-5 catalysts. Benzene selectivity of about 60% was obtained for ruthenium and palladium promoted Mo/H-ZSM-5 catalysts and the total aromatic selectivity was maintained at 90%. A decrease in coke selectivity was observed for the noble metal promoted Mo/H-ZSM-5 zeolite catalysts. The decrease in coke selectivity is attributed to the hydrogenation character possessed by a noble metal which helps in hydrogenating any carbonaceous deposits formed on the surface of the active sites during the MDA reaction. TGA results showed a total reduction of 50% by weight of carbon deposited on promoted Mo/H-ZSM-5 catalysts.

In Chapter 5 and 6 studies focused on the MDA reaction at 700 $^{o}$C over tin modified Pt/Mo/H-ZSM-5 zeolite catalysts. The effect of different catalyst preparation methods (i.e. co-impregnation and sequential impregnation methods) was also investigated. The CO FT-IR adsorption and CO chemisorption techniques were used to investigate the influence of the effect of the preparation method on the catalytic performance of tin modified Pt/Mo/H-ZSM-5 and in order to understand the interaction between tin and platinum before the catalytic reaction. Catalysts prepared by the co-impregnation method showed a good platinum dispersion, better than found for the sequentially impregnated catalysts. The co-impregnated and sequentially impregnated Pt/Sn catalysts showed high aromatic selectivity and low coke selectivity. The decrease in coke selectivity is mainly dependent on the availability of platinum sites for hydrogenation of carbonaceous species. The order of sequentially loading platinum and tin has an effect on the electronic and structural properties of platinum as shown by XPS and FT-IR studies. Hence different catalytic activities and aromatic selectivities were observed for the seq(Pt/Sn) and seq(Sn/Pt) catalysts. From the CO FT-IR adsorption spectra and CO chemisorption studies it can be concluded that the presence of tin decreased the adsorption capacity of the platinum surface atoms. However, the preparation methods and successive calcination treatments were shown to influence the location of both tin and platinum atoms in the catalyst.

In Chapter 7 a study of the MDA reaction was carried out at 800 $^{o}$C over manganese modified H-ZSM-5 zeolite catalysts prepared by incipient wetness impregnation method. The effect of a number of parameters on the catalytic performance and product selectivity was investigated, such as reaction temperature, manganese precursor, tungsten as promoter, manganese loading and use of noble metals.

The study of the effect of reaction temperature showed that the methane conversion increased linearly with increase in reaction temperature from 700 to 850 $^{o}$C. The selectivity towards aromatic compounds (of about 65%) was attained for the reactions performed at 750 and 800 $^{o}$C. An increase in coke selectivity with increase in reaction temperature followed a linear trend. The TGA results revealed that the total amount of coke deposited increased with increase in reaction temperature. The total amount of coke formed on the catalyst for the reaction performed at 850 $^{o}$C was 200 mg/gcat. Formation of coke on the catalyst is thermally favoured.

The use of different manganese precursors to prepare Mn/H-ZSM-5 catalysts had an effect on both the catalytic behaviour and the product distribution. High catalytic activities were obtained for the catalysts prepared from $Mn(NO_3)_2$ and $MnCl_2$ salts. But the product distribution was significantly different, with the $Mn(NO_3)_2$ catalyst being more selective towards aromatic compounds while the $MnCl_2$ catalyst was more selective toward coke. The use of $KMnO_4$ lowered the methane conversion and high coke selectivity was observed. The effect of manganese loading was studied at 800 $^{o}$C and an optimum catalyst activity was obtained at 2 and 4 wt.% manganese loadings. The aromatic selectivity above 70% and coke selectivity of 20% were obtained for 2 wt.% loaded catalyst. An increase in manganese loading led to rapid catalyst deactivation which is due to the formation of coke deposits on the active sites. An increase in coke selectivity was observed with an increase in manganese loading.

Some preliminary studies were performed to establish if tungsten could be used as a promoter in the Mn/H-ZSM-5 catalyst for the MDA reaction. The effect of tungsten on the catalytic activity of Mn/H-ZSM-5 catalysts and its ability to reduce the amount of coke formed during the reaction was investigated. Addition of tungsten onto 2Mn/H-ZSM-5 decreased the methane conversion

from 6 to 4% but the catalysts were fairly stable with increase in TOS. The formation of coke was highly favoured over the aromatic compounds. Selectivity towards coke was above 50% and this was confirmed by TGA results which showed a coke deposit of 164 mg/g.cat. This was calculated to be an 88% increase in coke deposits when tungsten was used a promoter.

The promotional effect of noble metals was investigated using the most coke selective W/Mn/H-ZSM-5 catalyst. The presence of a noble metal favoured the formation of aromatic compounds and suppressed the formation of coke Upon addition of platinum and ruthenium the aromatic selectivity increased from 12% to 55% and 46% respectively. A reduction in the total amount of coke deposit on the platinum promoted catalyst was 42% and for ruthenium promoted catalyst was 31%.

The MDA reaction under non-oxidative condition over metal modified H-ZSM-5 zeolite was successfully studied. Molybdenum modified H-ZSM-5 catalyst showed good catalysts activity at 700 $^{o}$C and high aromatic selectivity were achieved. The catalyst activity of manganese modified H-ZSM-5 catalysts is dependent of the reaction temperature, with low conversions (i.e. below 3%) at 700 $^{o}$C and high conversions (i.e. 7%) at 850 $^{o}$C. Formation of coke on both Mo/H-ZSM-5 and Mn/H-ZSM-5 zeolite catalysts is still a dominant problem. Addition of noble metals helps in reducing the total amount of coke deposit. Molybdenum remains as the suitable metal for methane activation as the reaction can be performed at reaction temperatures below 800 $^{o}$C.

## 8.2. Recommendations

Possible future work that could be pursued includes:

- Using a zeolite with mesoporous and microporous characters into to reduce the resident time for aromatic compounds forming during the MDA reaction without benzene selectivity.

- Extensive study on the spent catalysts to understand the interaction of platinum, tin and molybdenum during the reaction. The location of tin or platinum in Mo/H-ZSM-5 can also be studied using other techniques (i.e. XANES and EXAFS).
- Characterizing of carbonaceous deposits formed during the MDA reaction.